AN ADAPTIVE MAXIMUM LIKELIHOOD RECEIVER FOR RAYLEIGH FADING CHANNELS

AN ADAPTIVE MAXIMUM LIKELIHOOD RECEIVER FOR RAYLEIGH FADING CHANNELS

By

WAYNE CECIL DAM, B.Eng. (Engineering Physics) McMaster University.

A Thesis
Submitted to the School of Graduate Studies
in Partial Fulfilment of the Requirements
for the Degree
Master of Engineering

McMaster University
© Copyright by Wayne Cecil Dam, September 1990

McMASTER UNIVERSITY LIBRARY

MASTER OF ENGINEERING (1990)	MCMASTER UNIVERSITY
(Electrical & Computer Engineering)	Hamilton, Ontario

TITLE:	An Adaptive Maximum Likelihood Receiver for Rayleigh Fading Channels
AUTHOR:	Wayne Cecil Dam B.Eng. (Engineering Physics) McMaster University.
SUPERVISOR:	Dr. Desmond P. Taylor
NUMBER OF PAGES:	x, 140

Abstract

The purpose of this thesis is to develop a practical receiver for Rayleigh fading channels, which does not exhibit the error floor found for conventional receivers in this channel. A model of a general time and frequency-selective channel is developed, and the optimal receiver structure for a time-selective channel is derived for general signalling. The theoretical performance of a standard and maximum likelihood receiver is analyzed for the case of M-ary differential phase shift keying. A recursive, channel adaptive version of the optimal receiver is derived, and through simulation, its performance is compared to theoretical expectations . Results indicate that such a receiver will reduce the receiver error floor several orders of magnitude at typical channel signal-to-noise ratios.

Acknowledgement

I wish to thank Dr. Taylor for allowing me the opportunity to work on this thesis; his insights and suggestions were invaluable in its conception and completion. I would also like to thank the students and staff of the CRL for the many discussions that helped bring this work together. Thanks to my parents and family, who have given me their steady support and encouragement throughout. And finally to Pamela, of course, for everything.

Contents

List of Figures

List of Tables

Chapter 1

Introduction

1.1 General Introduction

The traditional communications channel that is first studied by communications engineers, and customarily used as a measure against all other channels for performance, is the additive white Gaussian noise (AWGN) channel. This model of a channel can then be extended by assuming the additive noise is coloured, or that the channel has a time-invariant frequency response. The corresponding optimal receivers may then be derived, either by appealing to intuition (e.g. spectral whitening), or through a more rigorous maximum likelihood derivation. Examples are found in Wozencraft and Jacobs [1] and Van Trees [2].

This analysis assumes completely deterministic signalling waveforms, which allows the conventional signal space interpretation of reception. Although a signal source always transmits deterministic signals, there exist channels which, in addition to the AWGN, will transform the signal itself into a random Gaussian process [3]. A further extension to signal reception then is the detection and estimation of *stochastic Gaussian signals* in additive Gaussian noise. The information used to modulate the original signals will be seen to impart a structure to the second order statistics of the received process. This is just a generalization of the AWGN or whitened coloured noise case, where the information in the received random process is contained in the mean, or first order statistics. The mobile communications channel, with its time-selective fading, is an example of this type of channel.

In practice, however, receivers used with this channel are conventional receivers designed to be optimal for the AWGN channel. Although these receivers have the advantage of simplicity, they also exhibit undesirable performance characteristics when used in the fading channel, which are not found in the AWGN channel. The random modulation of the signal by the channel, when viewed as a continuous random process, induces a limit of performance in the conventional receiver. As the transmitted signal-to-noise power ratio is increased, the receiver error rate tends to level out to a constant value, or floor, above a certain SNR, typically at 10^{-2}–10^{-3} error rates and at SNR's usually found in the mobile channel. This limitation found in conventional receivers seriously restricts the use of the mobile channel for data transmission, and in fact, it is barely acceptable for digital voice communications.

The mobile communications channel has recently given a new emphasis on non-AWGN channels. Although mobile radio has existed almost from the very beginning of radio technology [4], it is only within the last decade that practical digital modulation schemes have been considered for widespread commercial application. With the rapidly expanding mobile cellular and future mobile satellite services [5, 6], there is expected to be greater emphasis on compensating for the channel impairments found in these applications. A common viewpoint, however, is that the error floor is an inherent characteristic of the fading channel. Based on previous work in this area, we will show that this is not entirely accurate. Just as the error floor due to inter-symbol interference in a frequency-selective channel may be substantially lowered by suitable adaptive compensation, an analogous approach may be applied to random time-selective fading channels.

1.2 Background

This section gives a general historic survey of work on communications in fading channels. In this thesis, we will concentrate on receivers for purely random time-selective fading. Channels may also exhibit a second form of fading which is randomly frequency-selective, with both types often found in conjunction. The term "fading channel" alone should be *understood* as being vague, and does not fully define the characteristics of the channel.

Although the attention on mobile communications channels is fairly recent, effort into understanding fading and its effects on communications has been an active area for several decades. The original motivation for the study of fading channels occurred in the 1950's as the military came to increasingly rely on long distance radio, via ionospheric and tropospheric scatter, for digital data communications. The boom in space exploration during the 1960's, with the required global network of transceivers, also greatly increased the need for reliable data communications between distant points [7]. As well, countries with distant and isolated regions of population such as Canada, required reliable long distance radio communications.

The physics of transmission through scattering media was well understood at this time, and there existed a large number of propagation studies characterizing the statistics of the channels [3, 8]. Moreover, communications through the AWGN channel had also been put on a firm mathematical, and intuitively elegant foundation with the idea of signal space, as discussed in Arthurs and Dym [9], and it would be expected that the fading channel would soon also be put on such a footing. However, no consistent approach to fundamentally understanding communications through fading channels can really be said to have developed; at least not at the same level as the AWGN channel.

The simplest analysis of communications in time-selective fading makes the assumption of "fast fading", i.e. the amplitude and phase of the random channel modulation is assumed to be zero mean, complex Gaussian random variable, $\tilde{a}$, which is constant over each symbol and independent from symbol to symbol. The average probability of symbol error for a conventional receiver is just the probability of error conditioned on the random multiplicative factor, $P[\mathcal{E} \mid \tilde{a}]$, averaged over all possible values of $\tilde{a}$ [10]. i.e.

$$\begin{aligned} P[\mathcal{E}] &= \overline{P[\mathcal{E} \mid \tilde{a}]} \\ &= \int_{\tilde{a}} P[\mathcal{E} \mid \tilde{a}] p(\tilde{a})\, d\tilde{a} \end{aligned}$$

where $p(\tilde{a})$ is the probability density function of complex random variable $\tilde{a}$, $d\tilde{a}$ is a differential area in the complex plane, and the integral is performed over the entire complex plane. Evaluating this for the case of binary orthogonal signalling gives the error expression,

$$P[\mathcal{E}] = \frac{1}{2 + \overline{E}_s/\mathcal{N}_0}$$

where $\overline{E}_s$ is the average received signal energy, and $\mathcal{N}_0/2$ is the full bandwidth AWGN power spectral density.

This inverse relation of symbol error probability with SNR for fast Rayleigh fading is in contrast to the negative exponential relation for AWGN. However, the inverse relation is seen to bottom out in an error floor in practical systems, implying that the assumptions made in this analysis are too restrictive and simplistic. Physical channels will modulate the transmitted signal with a *continuous* complex Gaussian process, where there is correlation of the process across symbol intervals. This is loosely known as "slow", or "correlated fading".

Note that there is some confusion in the literature on the terminology used to describe time-selective fading channels, with the terms "fast" and "slow" fading seeming to be almost interchangeable. In this work we will consistently refer to a narrow bandwidth fading process as being slower and more correlated than a process with a relatively broader bandwidth. Thus, the model of the previous process is considered fast since its sampled values are independent from symbol to symbol, and the jumps in value are completely unrestrained. Introducing correlation between the symbol intervals will slow the rate of change of the process between samples, and the fading is considered to be slower, with the magnitude of the transitions between symbols more restrained by the process' narrow band characteristics. This can be seen in Figure 2.3 of the next chapter, which shows the trajectory of a simulated complex channel process in time. It was generated by filtering a zero mean, complex white Gaussian noise sequence with a filter corresponding to a channel process's power spectrum. If the filter bandwidth were narrowed, the trajectory would not loop around the time axis as violently, and would be more correlated between samples. As the filter bandwidth is broadened, the higher frequency components introduced into the process spectrum would create much faster twisting of the process in time, and the process would be less correlated between samples.

One of the first clear analysis of correlated fading was done by Voelcker [11] for differential binary and four phase shift keying using conventional differential receivers. However, for simplicity he used an assumption intermediate between fast fading and a full continuous fading process. He assumed that the process was still a constant, zero mean, complex Gaussian random variable in each symbol interval, but was correlated between symbol intervals. The process was characterized by a single parameter, $\rho = R(T)$, representing the correlation of the fading process between symbol intervals. Here $R(\cdot)$ is the correlation function of the actual fading process, and T is the symbol period. He derived formulae for the error floors for both types of signalling using conventional receivers, and for the optimal combining of an arbitrary number of independently received signals, i.e. diversity.

Several papers by other authors followed, notably by Bello and Nellin [12], Lindsey [13], and Hingorani [14], with similar assumptions on the fading process, but with more complete analysis. As well, the "duality" between random time and frequency selectivity [15], and the optimization of transmission rates for channels that were jointly time and frequency-selective was examined [16].

During this time people were also examining fading channels at a slightly more general and theoretical level, using the maximum likelihood approach to analyzing the transmission of information through random channels. This was spurred as much by developments in radar and sonar signal detection as it was from the communications field, although each area is dealing with the same physical problems of delay and Doppler spread of signals[17].

In 1960, Kailath [18] published a classic paper that fully defined the random channel in discrete form, and examined the various configurations of optimal receivers for the channel. The ideas in this paper were then extended by others to transmitted reference systems for binary signalling [19, 20, 21], where a second transmitted signal (e.g. a pilot tone) is used to form an estimate of the channel state. This additional information is then used to perform optimal demodulation of the information bearing signal. Although these derivations used the full covariance matrix for the fading process, as opposed to Voelcker's truncated form, they gave no evaluation of the error performance.

An interesting paper by Walker [22] extended this analysis for the case of a binary DPSK system using a transmitted reference phase. He considered the full structure of the fading process, which clearly cannot be represented by a single parameter, such as ρ, by using the Karhunen-Loéve expansion of the received random process over one symbol period. This continuous time analysis is in contrast to the discrete time approach, although a discrete set of random variables, the eigenfunction coefficients, is still used in the calculations. In addition, he assumed that the cross-correlation, R_{tr}, of the process between the transmitted and reference symbols was $R_{tr}(\tau) = \rho R(\tau)$. Although his ρ was the correlation between the frequency bands of the transmitted and reference signals, this can also be considered as $\rho = R(T)$ for a DPSK system. That is, it is a measure of the correlation between adjacent symbol intervals. The covariance function across two symbol intervals is thus assumed to have the form:

$$R_2(\tau) = \left\{ \begin{array}{lll} R(\tau) & ; & |\tau| < T \\ \rho R(|\tau| - T) & ; & T < |\tau| < 2T \end{array} \right\} \tag{1.1}$$

Two important consequences of Walker's work are:

- The full statistical structure of the Gaussian fading process is used to analyze the performance of a conventional DPSK receiver.

- An optimal receiver structure for this particular fading covariance function is derived which does not exhibit an error floor.

Suboptimal receivers using only a limited set of eigenvalues and eigenfunctions of the K - L kernel can be designed which will exhibit a greatly reduced error floor over a conventional receiver. Walker's analysis, however, assumed full prior knowledge of the channel statistics, and required the calculation of the K - L expansion within the receiver. In addition, (1.1) will generally have a discontinuity at delay $\tau = T$, and tends to be a poor approximation to a physical process having a continuous correlation function.

The continuous time maximum likelihood approach was also examined by others, [23, 17]. However, virtually all of these analyses examined only the case of binary signalling, and solutions to the resulting integral equations were analytically tractable only for special forms of the channel covariance function, again assumed to be completely known. The performance evaluation of these systems generally required bounding techniques. Although of significant theoretical interest, this work did not lend itself directly to practical real time application.

During the early seventies, a Kalman filtering approach to transmission through fading channels was taken [24, 25], where complete prior knowledge of the statistics of the additive and multiplicative noise processes was again assumed. Their simulations using pure amplitude modulation gave excellent results, with reduction of the error floor of $\sim 10^{-1}$ to the 10^{-4} limit of the simulation. However, when the noise and fading statistics were unknown and the filter parameters were simply fixed, performance was significantly degraded. Including simple estimators of the fading process' mean and the additive noise variance improved the performance somewhat, but as the authors point out, any practical implementation would require some form of estimator of the fading statistics. As well, no theoretical analysis of the optimal and suboptimal performance of the receiver was provided.

A pair of papers in the mid-80's re-examined the general case of receivers in time and frequency-selective fading [26, 27], using a more modern development and analysis of the discrete problem in matrix form. Barrett [28] recently published a concise letter describing the discrete maximum a posteriori binary receiver for Rayleigh fading channels. He also provides a method for calculating the binary error performance of general quadratic form receiver structures, operating in a channel with a given channel correlation matrix. Essentially, the optimal receiver forms the log likelihood decision variables,

$$\ell_i = -\mathbf{z}^H \mathbf{K}_m^{-1} \mathbf{z}; \quad m = 0, 1 \tag{1.2}$$

where $\mathbf{K}_m$ is the covariance matrix of the channel, assuming symbol i was transmitted, and $\mathbf{z}$ is the received data vector. His analysis explicitly shows a fundamental relationship between the fading statistics and the receiver structure, with respect to the error performance.

Recently, Lodge and Moher [29, 30] have examined a maximum likelihood receiver for continuous phase modulation (CPM) in Rayleigh fading channels. They consider a multi-symbol, sequence estimation approach, where only a few samples per symbol are taken, but a string of several symbols are considered simultaneously in determining the received message. As well, they give an interesting interpretation of the optimal receiver as minimising a process prediction error in forming its decisions. Although they state that the receiver may be made adaptive, they provide simulation results only for a receiver that has been optimally preset for a specific channel. As well, no theoretical performance evaluation is given.

The discrete maximum likelihood formulations of the receivers discussed by the above [18, 19, 20, 21, 22, 23, 17, 26, 27, 28, 29, 30] all involve equations similar to Equation (1.2). The limitation to actually implementing these receiver structures has been the required estimation of the channel statistics. This thesis will examine the efficient estimation of the channel's fading and additive noise statistics, and the integration of these estimates into a maximum likelihood receiver structure. The behaviour and limitations of a particular adaptive implementation will be examined, as well as the theoretical evaluation of the conventional and optimal receiver's performance.

1.3 Scope of Thesis

Chapter 2 of this thesis will give an overview of the physical origin of fading communications channels, including both time and frequency-selectivity. A detailed statistical and analytical description of fading channels will then be given. The application of the Karhunen-Loéve expansion to random processes will be reviewed, and its discrete form briefly examined.

In Chapter 3, the theory of maximum likelihood receivers for random fading channels will be briefly surveyed using both continuous and discrete time formulations.

In Chapter 4, the extension of Walker's analysis [22] to conventional and optimal M-ary DPSK receivers sampled data will be discussed. Barrett's [28] analysis of fading channels will be extended from binary to general complex symbols, including a specular (Rician) component. The theoretical results will then be discussed and an interpretation of the effective operation of the optimal receiver on the received channel process presented. In addition, a geometrical view of a receiver operating in a fading channel is suggested.

Chapter 5 will describe a real time, channel-adaptive implementation of the maximum likelihood receiver, using decision feedback. The results of a simulation for a constant amplitude M-ary DPSK will be presented and compared to theory.

Chapter 6 will summarize the results from this thesis and suggest possible future study, both theoretical and applied.

Chapter 2

Modelling General Fading Channels

In this chapter the physical assumptions used in modeling fading channels are described, and a statistical model for the general time and frequency-selective fading channel is developed. The channel scattering function and its relation to a tapped delay line model of the channel will also be examined. The interrelationships between the shape and extent of the two-dimensional scattering function and the signalling waveforms will be briefly discussed, as will the Karhunen-Loéve description of random processes and its application to fading channels.

As mentioned previously, simply describing a channel as fading is incomplete and requires a much more specific characterization. The effect the channel has on the transmitted, digitally modulated waveform, in terms of symbol dispersion and random modulation, depends on both the duration of the digital symbols and the rate of variation in the channel fading process. A particular channel may exhibit various forms and degrees of fading depending on the signals transmitted through it. Rather than developing the completely general fading channel at once, it will be described first as completely time-selective, with frequency-selective behaviour treated as a natural extension.

2.1 Pure Time Selective Fading

In an idealized sense, the channel can be imagined as many point reflecting particles, which could really be clouds of ionized atoms and molecules in the upper atmosphere, or buildings

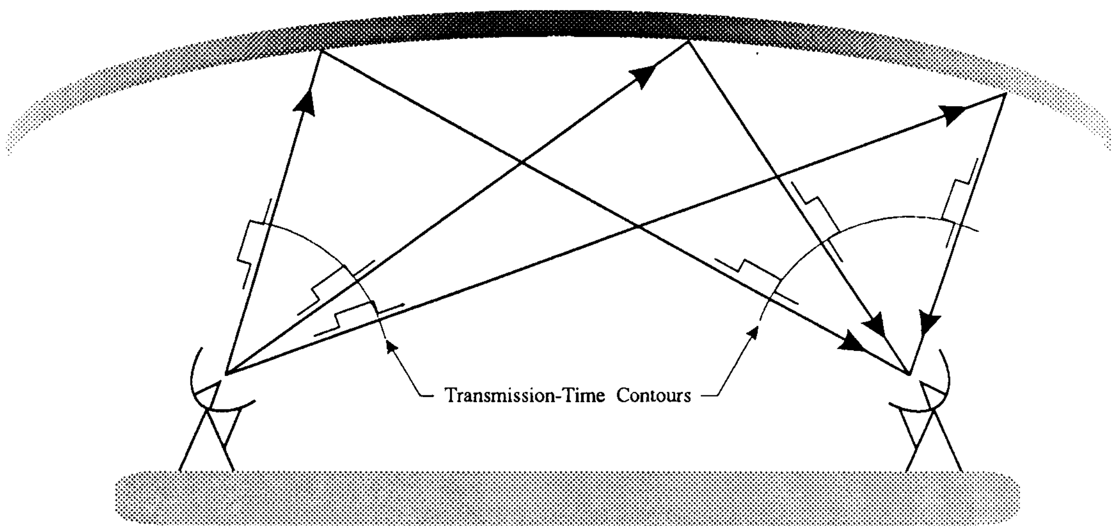

Figure 2.1: Physical model of a time-selective fading channel.

and vehicles in a city. This is illustrated in Figure 2.1. It is assumed here, however, that the propagation time through the reflecting layer is much less than the duration of one symbol, and the overall delay via reflection by the layer is identical for all points in the layer. That is, on the time scale of a symbol, the particles appear as a thin quasi-reflecting sheet in the shape of a section cut from an ellipsoid. This physical configuration does not directly correspond to the case of mobile channels, but the important point is that the greatest difference in delay, over the entire set of particles, is negligible compared to a data symbol period, but significant compared to the carrier wavelength. This assumption will be relaxed later for the case of frequency-selective fading. Note it is assumed here that there is no direct, unscattered path from the transmitter to the receiver, so that we will be dealing with the case of Rayleigh rather than Rician fading. An unscattered, deterministic signal component in the received signal may be included straightforwardly in the final model, and will be excluded here.

Each reflecting particle will introduce a delay $T_j(t)$ in the received signal about some nominal propagation delay, which, without loss of generality, may be set to zero. This delay will be taken here to be the average delay time of all the scattering paths from the layer.

Note that the individual delays themselves are a function of time because of the motion of the particles. Under the assumption that the particles will not move significantly during a symbol period, a linear expansion of the unknown delay function about the nominal time $t = 0$, gives[1]

$$T_j(t) = \tau_j + \dot{\tau}_j t \tag{2.1}$$

where τ_j is the initial delay at t equal to zero, and $\dot{\tau}_j$ is the rate of change of the delay with respect to time, which is proportional to the relative radial velocity of the particle. From the previous assumptions, we must have τ_j and $\dot{\tau}_j$ small, such that $T_j(T) = \tau_j + \dot{\tau}_j T \ll T$.

The transmitted signal, $s(t)$, is assumed to be a general complex envelope modulated carrier, with the carrier frequency, ω_o, much greater than the bandwidth of the complex envelope, $u(t)$,

$$s(t) = u(t)e^{i\omega_o t} \tag{2.2}$$

Using the delay in (2.1), the received signal from scatterer j has the form,

$$r_j(t) = \rho_j u(t - \tau_j - \dot{\tau}_j t)e^{i\omega_o(t-\tau_j-\dot{\tau}_j t)} \tag{2.3}$$

where ρ_j is the unknown real reflectivity of the particle. However, since the delay T_j is assumed to be much less than a symbol period, the envelope $u(t)$ will not vary appreciably from its delayed version, $u(t - T_j(t))$, as it is scattered from the j'th particle, and the delay may be ignored for this portion of the expression. Defining $\omega_j = \dot{\tau}_j\omega_o$ as the Doppler shift due to the relative motion between the receiver and the scattering particle, the received signal can be written in the form,

$$r_j(t) = u(t)\rho_j e^{-i\omega_o\tau_j}e^{i(\omega_o-\omega_j)t} \tag{2.4}$$

Taking this to baseband, where for simplicity we neglect to relabel $r(t)$, we have the received complex envelope from the j'th scatterer,

$$\begin{aligned} r_j(t) &= u(t)\rho_j e^{-i\omega_o\tau_j}e^{-i\omega_j t} && (2.5)\\ &= u(t)\tilde{\rho}_j e^{-i\omega_j t} && (2.6)\end{aligned}$$

where $\tilde{\rho}_j \equiv \rho_j e^{-i\omega_o\tau_j}$ is an unknown complex constant value. Thus, the j'th component of the baseband received signal is simply the original signal envelope, modulated by a scaled

[1]Assuming a zeroth order approximation results in "fast fading", which will be a special case of the present analysis. For an example see Wozencraft and Jacobs[1]. Higher order expansions apparently do not offer any more advantages for the model[3].

complex sinusoid, with a frequency given by the Doppler frequency ω_j. The constant $\tilde{\rho}_j$ may be taken to be a random variable with some unknown distribution. For a given Doppler frequency ω_j, then, the sinusoid $\tilde{\rho}_j e^{-i\omega_j t}$ is a random process in time. By summing over all the scattered signals, the total base band received signal may then be written as,

$$r(t) = u(t) \sum_j \tilde{\rho}_j e^{-i\omega_j t} \tag{2.7}$$

$$\equiv u(t)a(t) \tag{2.8}$$

where $a(t)$ is *defined* as the channel fading process.

It is seen that the complex received baseband waveform, $r(t)$, is just the transmitted complex envelope, $u(t)$, modulated by a sum of complex sinusoids, each with an unknown frequency ω_j and complex amplitude $\tilde{\rho}_j$. This sum itself represents a randomly time varying waveform, $a(t)$, which, in (2.7), is decomposed explicitly into its frequency components. Picking a particular frequency, ω_k, from the virtually infinite set of frequencies in the waveform, and summing over all $|\tilde{\rho}_j|^2$, such that $j = k$, will give the power in the waveform represented by frequency ω_k. If the frequency range of the process is divided into bins of size 2Δ, then this may be written as a power spectral density function, where the total power in each bin is divided by the bin size. That is,

$$\sigma(f) \equiv \frac{1}{2\Delta} \sum_{\{j|(f-\Delta)<\omega_j/(2\pi)<(f+\Delta)\}} \overline{|\tilde{\rho}_j|^2} \tag{2.9}$$

where $\sigma(f)$ is the power spectral density, as a function of frequency, averaged over all possible realizations of the channel process. As well, the complex amplitude of the resultant sinusoid with frequency ω_k will be given by,

$$\sum_{\{j|\omega_j=\omega_k\}} \tilde{\rho}_j \tag{2.10}$$

Although the statistical distribution of the complex scalars $\tilde{\rho}_j$ is unknown, it is reasonable to assume on physical grounds that they are statistically independent. Then, by the central limit theorem [1], the distribution of their sum will be a complex Gaussian random variable, and each term of the sum in (2.7) for $a(t)$ is a complex Gaussian random process. Thus, the modulating waveform, $a(t)$, being the sum of Gaussian random processes, is itself a Gaussian random process. The correlation function of $a(t)$ is given by,

$$R_a(t,\tau) = \overline{a(t)a^*(\tau)} \tag{2.11}$$

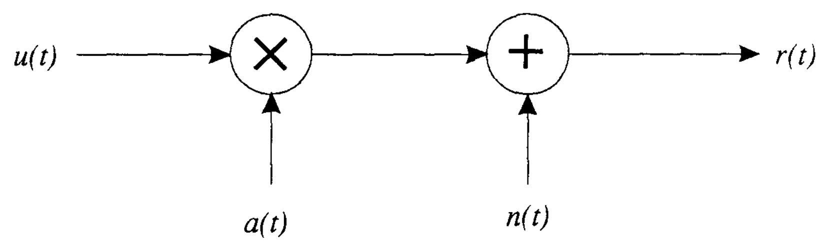

Figure 2.2: Single tap baseband model of a time-selective fading channel with additive noise.

$$= \overline{\sum_l \tilde{\rho}_l e^{-i\omega_l t} \sum_m \tilde{\rho}_m^* e^{i\omega_m \tau}} \quad (2.12)$$

$$= \sum_l \sum_m \overline{\tilde{\rho}_l \tilde{\rho}_m^* e^{-i(\omega_l t - \omega_m \tau)}} \quad (2.13)$$

$$= \sum_l \overline{|\tilde{\rho}_l|^2} e^{-i\omega_l (t-\tau)} \quad (2.14)$$

$$\equiv R_a(t-\tau) \quad (2.15)$$

where in the last line we have assumed the scatterers are independent, and we are summing over each individual particle. The channel process is seen to be stationary. However, this means that the correlation function of $a(t)$ is also the Fourier transform of its power spectral density, as given by the Wiener-Khintchine relation [31]. That is,

$$R_a(t-\tau) = \mathcal{F}_f\{\sigma(f)\} \quad (2.16)$$

$$= \int_f \sigma(f) e^{-2\pi i f(t-\tau)}\, df \quad (2.17)$$

Assuming there are enough particles so that f may be treated as continuous, it is seen that the integral of (2.17) is identical to the sum of (2.15) to within an arbitrary scaling, via the definition (2.9).

The correlation function of the total received signal, $r(t)$, can be similarly expanded to give,

$$R_r(t,\tau) = u(t)u^*(\tau) \int_f \sigma(f) e^{-2\pi i f(t-\tau)}\, df \quad (2.18)$$

$$= u(t)u^*(\tau) R_a(t-\tau) \quad (2.19)$$

where $R_a(\cdot)$ is the autocorrelation function of the channel fading process derived previously. As well, the mean of $a(t)$, being simply the sum of sinusoids, is seen from (2.8) to be zero.

The received signal from the scattering channel may then be described in baseband as the transmitted envelope modulated by a stationary zero mean Gaussian process, $a(t)$, as shown in Figure 2.2. The autocorrelation function $R_a(t-\tau)$, or equivalently the power spectrum, $\sigma(f)$, completely characterizes the channel. The width of the power spectrum, and, through the Fourier transform, its autocorrelation function, is determined by the largest Doppler shift present in the scattering media. For the case of the mobile channel, the greatest Doppler shift is due mainly to the vehicle motion, and occurs when the vehicle is moving directly toward or away from an oncoming radio wave. The Doppler shift will be determined by the vehicle's velocity and the frequency of transmission. We have, for vehicle velocity, v, and carrier wavelength, λ,

$$f_d = \frac{v}{\lambda} \tag{2.20}$$

For a vehicle velocity of say 50 km/h and 30 cm wavelength (at a carrier frequency of 10^9 Hz), $f_d \approx 50$ Hz. The fading modulation will typically have a narrow bandwidth compared to that of the baseband signal.

Figure 2.3 (a) shows a simulated complex Gaussian time- selective fading process as a function of time, where the fading time-bandwidth product is 0.08 and 4 samples per symbol are taken. This is typical of the mobile channel. The process was generated by filtering a sequence of independent, unit-variance complex Gaussian random variables. Based on the FIR filter coefficients used, the variance of the filtered process is 1.6812e-2. Note that a Rician or deterministic component of the signal may be included in this model, and simply shifts the mean of the process away from the origin. This occurs, for example, in a mobile satellite system with shadowing [32]. Although this shift is itself a function of time, i.e. it will trace out a trajectory of its own in time, in practical situations it changes very slowly compared to the symbol rate.

Figure 2.4 (a) and (b) show the magnitude and phase of the process respectively, illustrating the extreme magnitude nulls, and rapid phase shifts that are periodically experienced. The phase plot includes the received phase decision boundaries for BDPSK signalling for a relative comparison with the channel's phase modulation. Figure 2.3 (b) gives a view of the process projected down the time axis onto the real and imaginary plane with the symbol intervals shown. As the real and imaginary components of the sampled Gaussian process are independent Gaussian random variables, the time averaged density

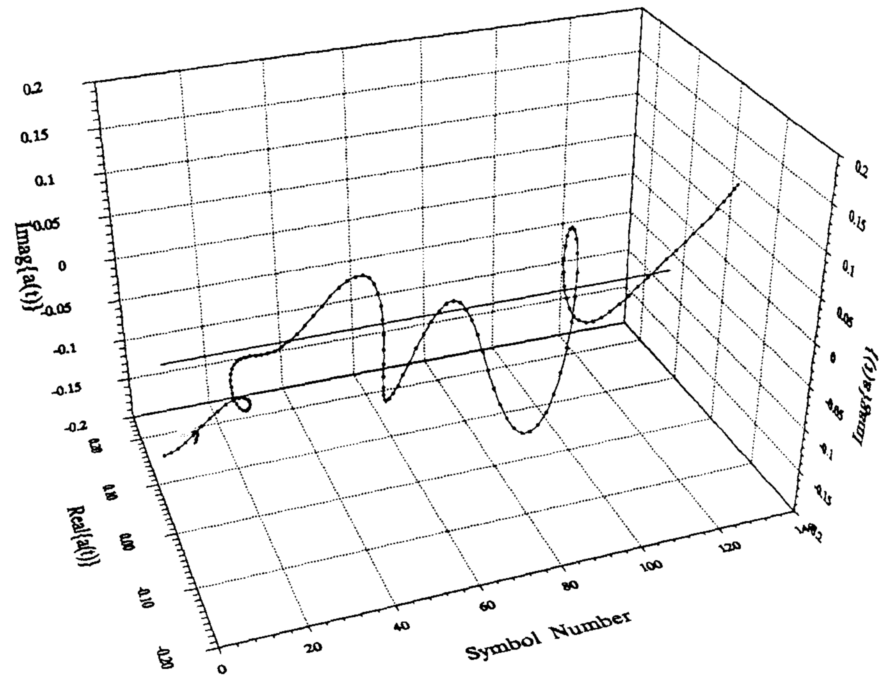

(a)

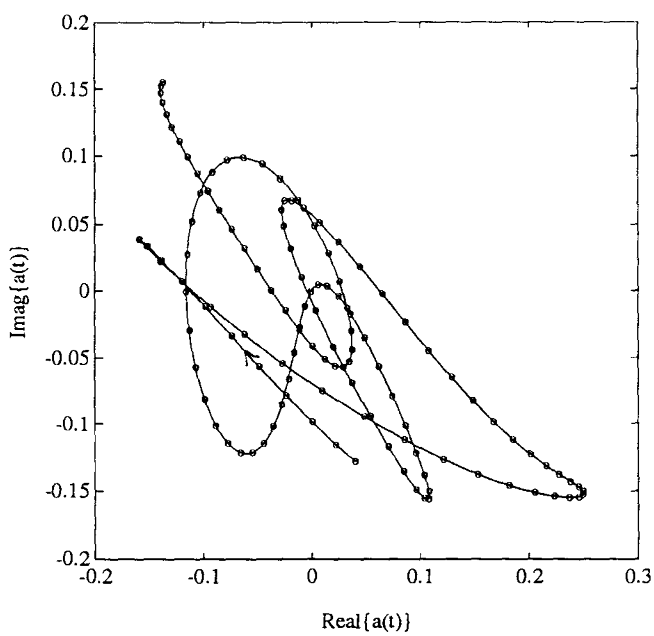

(b)

Figure 2.3: An example complex Gaussian fading process (a) in perspective view, and (b) projected down the time axis onto the complex plane. Symbol intervals are indicated.

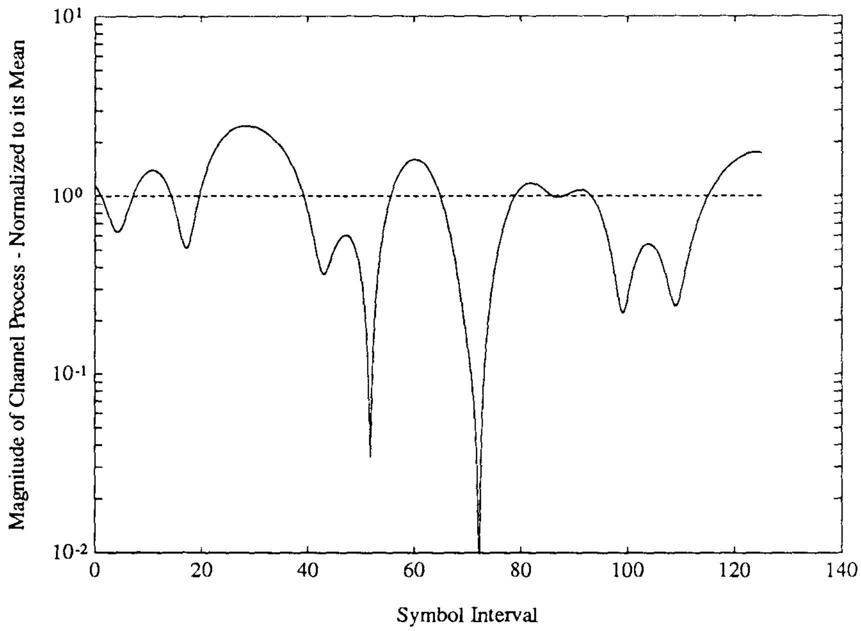

(a)

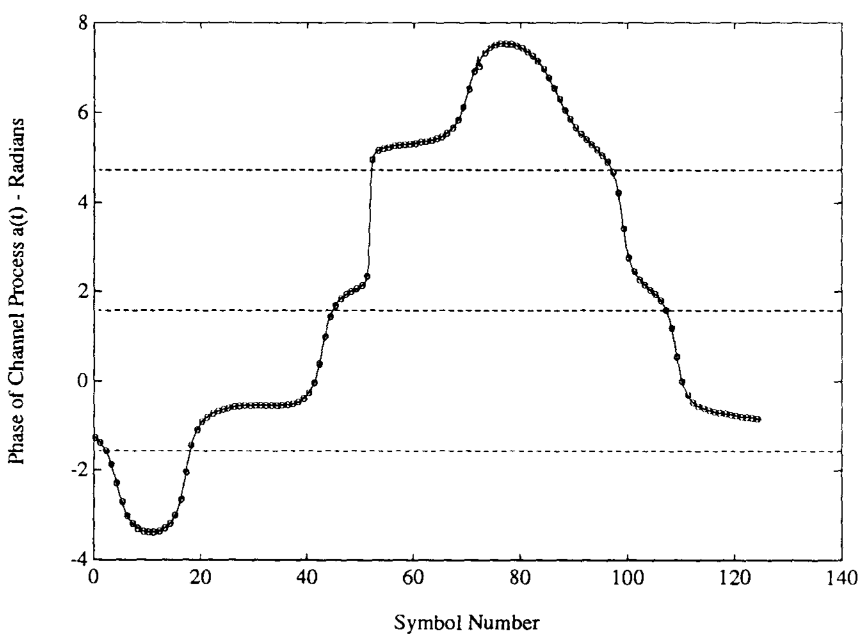

(b)

Figure 2.4: (a) Magnitude and (b) phase of the fading process of a complex Gaussian fading process. Symbol intervals are indicated in (b).

function of the projection is a two-dimensional Gaussian distribution, with the two component variances equal to the received signal power. The magnitude of time samples of the two-dimensional process will then be Rayleigh distributed, and the phase will have a uniform distribution. This is why time-selective fading is often referred to as Rayleigh fading.

It is seen that the "slow fading" approximation, where the phase and amplitude is reasonably constant over a symbol interval, is almost always valid. However, during the occasional rapid excursions of the signal, the receiver is virtually guaranteed to make errors. Intuitively, the approximate periodicity of these excursions means the guaranteed error will occur at a fairly fixed rate, generating a fundamental error rate independent of the additive noise. From techniques developed later in this thesis, a BDPSK receiver operating in the channel of Figure 2.3 would experience an error floor rate of 3.13e-3, or one error in every 320 symbols. The phase swing involved in such an error event is seen occurring at about the 50'th symbol. Without knowledge of the fading process's statistics, and the use of some kind of predictive compensation of the random channel modulation, a conventional receiver will inherently experience an error floor in its performance curve.

2.2 Time and Frequency Selective Fading

In the previous section, it was assumed that the scattering media incurred delays of the transmitted signals on the order of the period of the carrier, with no measurable delay distortion of the symbol waveform, $u(t)$. However, if the transmitted symbol rate is high enough, the range of propagation delays of the scattering layer may become comparable to the symbol period. The previous section's analysis may then be extended by assuming a multilayered media. Each individual layer will scatter the signal independently of the others, producing separate realizations of the modulating random processes, $a_k(t)$, and each will have a characteristic layer delay, τ_k, where the delay is now comparable to the symbol period. The variable k is used to index the layers, and will approximate a continuum in the limit as the layer separation approaches zero. The received signal is seen to be the sum of the individual layers' signals, $r_k(t)$, each delayed by τ_k. We have,

$$
\begin{aligned}
r(t) &= \sum_k r_k(t) && (2.21) \\
&= \sum_k r(t-\tau_k) && (2.22)
\end{aligned}
$$

$$= \sum_k u(t-\tau_k)a_k(t) \tag{2.23}$$

Note that the random process, $a_k(t)$, was not shifted in time since stationary Gaussian random process' are equivalent under an arbitrary time translation. That is, the statistics of $a_k(t-\tau_k)$ are the same as $a_k(t)$, and are given by $R_k(\Delta t) = \overline{a_k(t)a_k^*(t+\Delta t)}$. If we consider a sampled data system, this may be written in discrete time form,

$$r(i) = \sum_{k=0}^{M} a_k(i)u(i-k) \tag{2.24}$$

where k corresponds to the delay index, i to the time, and M is the number of layers considered. This may be viewed as a tapped delay line filter, where each tap gain, $a_k(\cdot)$, is an independent zero mean, complex Gaussian random process, with the correlation function, $R_k(\Delta t)$, given above, and a tap delay, $\Delta\tau$, given by the difference in delays between adjacent media layers.

This is seen to correspond to the continuous time filter equation,

$$r(t) = \int_\tau a(\tau,t)u(t-\tau)\,d\tau \tag{2.25}$$

where t is the time variable, τ is the delay, and $a(\tau,t)$ is the time variant impulse response of the channel. This response is a random process in the time variable, t, with the delay τ, effectively indexing the individual, time-selective fading processes from the scattering media. The impulse response is the output response of the channel, at time t, to an impulse input to the channel τ seconds before t. These two methods of representing the general fading channel are shown in Figure 2.5. For bandlimited signals, the delays are the inverse of the Nyquist sampling rate for the baseband signal.

The tap autocorrelation function may be formally written as,

$$R_a(\tau,\Delta t) \equiv \sum_{k=0}^{M} \delta(\tau-\Delta\tau\cdot k)R_k(\Delta t) \tag{2.26}$$

where $\Delta\tau$ is a delay increment. For infinite bandwidth signals, we let $\Delta\tau \to 0$ such that $R_a(\tau,\Delta t)$ approaches a continuous function. The function $R_a(\tau,\Delta t)$ represents the autocorrelation function of the channel in time at a constant delay of τ. This is usually represented by the *channel scattering function*, $\sigma(\tau,f)$, which is the *power spectrum* of the random Gaussian tap weight process existing at a delay of τ,

$$\sigma(\tau,f) = \mathcal{F}_{\Delta t}\{R_a(\Delta t,\tau)\} \tag{2.27}$$

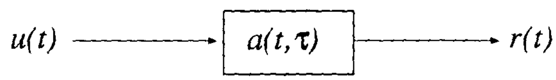

(a)

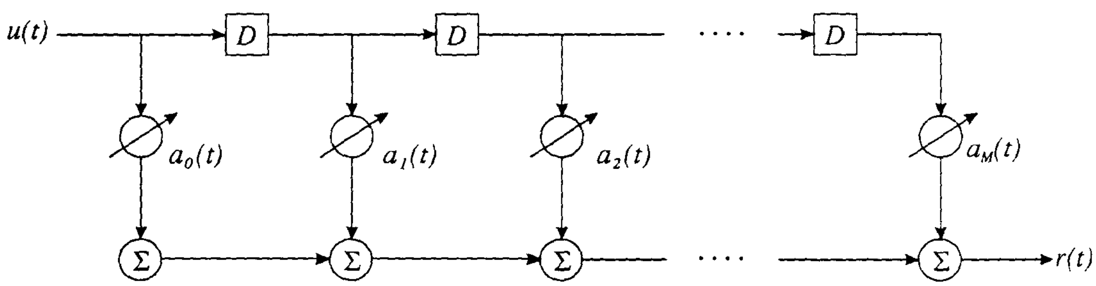

(b)

Figure 2.5: Model of a time and frequency-selective fading channel. (a) Continuous time-variant channel impulse model, (b) tapped delay line model. The tap delays, D, correspond to $\Delta\tau$ in the text.

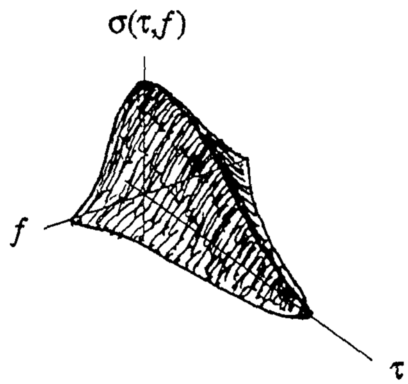

Figure 2.6: Two-dimensional scattering function of a time and frequency-selective fading channel.

where $\mathcal{F}_{\Delta t}$ is the Fourier transform with respect to the time variable. An example of a scattering function is shown in Figure 2.6. This tapped delay line model of the fading channel, where each multiplicative tap is an independent random Gaussian process, has a great deal of intuitive appeal for visualizing the effect of a general fading channel on a signal.

2.3 Pure Frequency Selective Fading

In Section 2.1.1 we started with a purely time-selective fading channel, and then extended it in Section 2.1.2 to include frequency selectivity. We may now specialize our general model again to the case of a purely frequency-selective channel, also known as "time-flat" or "time-dispersive". Its scattering function is given by,

$$\sigma(\tau, f) = \sigma(\tau)\delta(f) \tag{2.28}$$

as shown in Figure 2.7. This type of channel may be interpreted as a series of taps, each with a delta function power spectral density, i.e. a constant DC bias. The tap with a delay τ_o has a power $\sigma(\tau_o)$, and is an independent complex Gaussian random variable with variance $\sigma(\tau_o)$. In effect, $\sigma(\tau)$ is the ensemble averaged, impulse power response of the channel. The Rummler fading model for digital microwave radio [33] is similar to this type of channel, where its channel scattering function is assumed to be of the form,

$$\sigma(\tau) = a_1\delta(\tau_1) + a_2\delta(\tau_2) + a_3\delta(\tau_3) \tag{2.29}$$

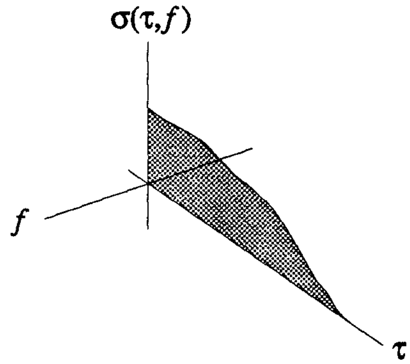

Figure 2.7: Scattering function of a purely frequency-selective fading channel.

The parameters $\{a_i\}$ and $\{\tau_i\}$ are taken to be random variables from some empirically measured distribution. Note that the Rummler model also takes $|\tau_1 - \tau_2|$ to be much less than the Nyquist period, and the first two taps are usually lumped into one. By changing the frequency delta functions to have some breadth in f, i.e. with a form $\sigma(\tau, f)$, the time dynamics of the channel (i.e. time-selective behaviour) are also modeled. Note that no physical channel will be purely frequency-selective without time variation, since any macroscopic scattering object, because of its physical extent, will have some range of delays on the scale of a carrier wavelength.

An interesting characterization of the frequency-selective channel may be made that points out the duality between time and frequency-selective fading [15]. It is well known, through the Wiener-Khintchine relation, that the time correlation function of a random process may be represented by its power spectral density, via the Fourier transform. To measure the power spectrum for the time-selective channel, a single frequency is transmitted, which is then Doppler broadened by the channel. The spectrum of the fading process is thus just the spectrum of the Doppler broadened signal i.e. the *frequency domain* power impulse response of the channel.

It is seen that $\sigma(\tau)$ for the frequency-selective channel above represents a power "spectrum" in the delay variable τ. Consider a stationary random Gaussian process defined in the frequency variable, f, rather than in time. Although a random process is usually considered to evolve sequentially in time as a filtered sequence of independent, identically distributed random variables, frequency may be used to index the process values just as well. This process would then have an autocorrelation function as a function of Δf. Moreover, a corresponding power spectrum of the process could be defined, again via a Fourier transform, that would be a function of a conjugate time variable. *Conversely*, if a power spectrum as a function of time exists, such as $\sigma(t)$, then it must correspond to a correlation function in frequency of a frequency domain Gaussian random process. Thus, a purely frequency-selective fading channel may be thought of as a channel with a frequency response that is a random Gaussian process in f. This is discussed further in Bello [34] where he explicitly breaks out the various Fourier transform relationships between the time and frequency variables and their corresponding delay variables.

In (2.8), the signal received from a time-selective fading channel was shown to be,

$$r(t) = u(t)a(t) \tag{2.30}$$

where a(t) is a stationary Gaussian random process. But from the above discussion, it is seen that the signal received from a frequency-selective fading channel can be represented in the frequency domain as,

$$\mathcal{R}(f) = \mathcal{U}(f)\mathcal{A}(f) \tag{2.31}$$

where $\mathcal{A}(f)$ is also a stationary Gaussian random process in frequency, with a power spectra $\sigma(\tau)$. An example of this, measured in an indoor radio environment [35], is shown in Figure 2.8. In (a), the impulse response, which may be taken as a measure of the delay power spectrum[2], is narrow, and is analogous to a narrow spectrum signal with a correspondingly broad correlation function in frequency. This results in a slowly varying random process in frequency, which is shown in (b), a single time snap shot of the channel frequency response. In Figure 2.9(a), the delay spectrum is much broader, and analogously to a broad-spectrum signal, corresponds to a much more rapidly varying frequency response process. There is a striking similarity of (b) to the simulated time selective process of Figure 2.4.

2.4 Time Dynamics of the Channel Frequency Response

From the above, if a purely frequency-selective channel had its spectra broadened to some finite width, then the time dynamics of the channel frequency response could be modeled. This is simply the time and frequency fading channel again. For this channel, the frequency response will now be a random process in both time *and* frequency. At a particular time

[2] The true delay power spectrum would be an ensemble average of impulse responses.

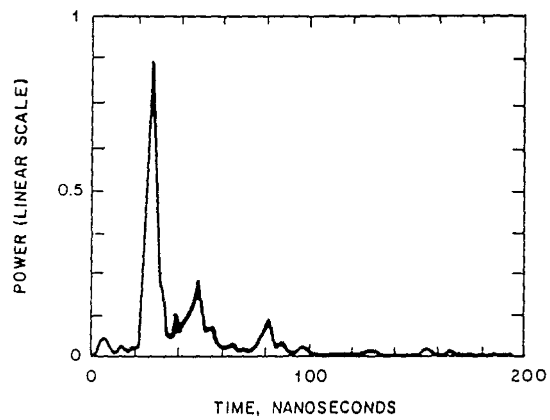

(a)

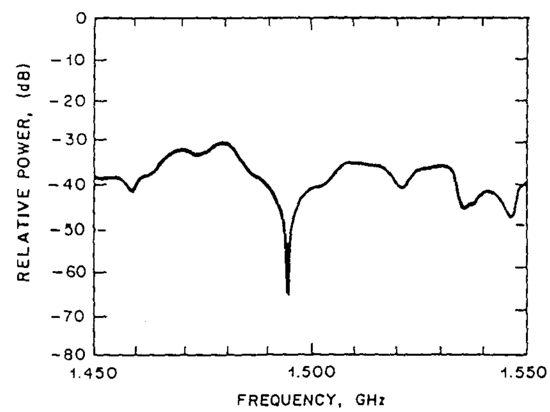

(b)

Figure 2.8: Slow frequency-selective fading channel measurements. (a) Impulse power response, (b) Measured instantaneous channel frequency response.

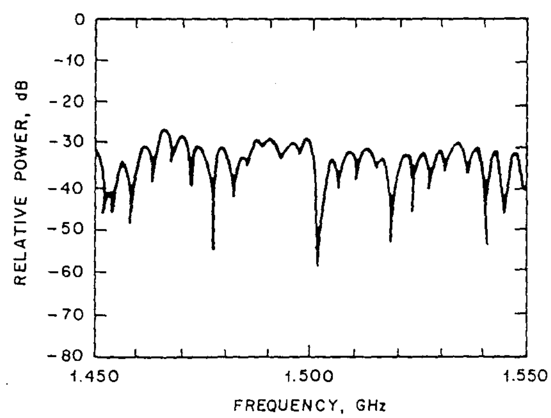

(a)

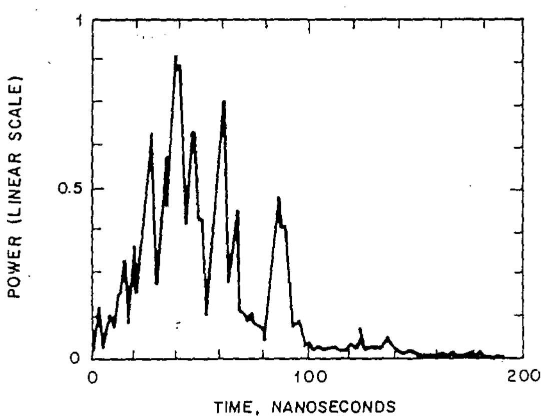

(b)

Figure 2.9: Fast frequency-selective fading channel measurements. (a) Impulse power response, (b) Measured instantaneous channel frequency response.

instant, t_o, where t_o is treated as a parameter, the frequency response of the channel is the Fourier transform of its impulse response, or tap weights, in the delay variable τ. That is,

$$\mathcal{A}(f, t_o) = \mathcal{F}_\tau\{a(\tau, t_o)\} \tag{2.32}$$

where $\mathcal{A}(f, t_o)$ is a random process in f, as discussed in the previous section. It becomes reasonable to ask what is the correlation of the channel response at a particular frequency, between two time instants. Defining this correlation as $R_{\mathcal{A}}(f, \Delta t)$, and assuming uncorrelated scatterers, we find,

$$\begin{aligned}
R_{\mathcal{A}}(f, \Delta t) &= \overline{\mathcal{A}(f,t)\mathcal{A}^*(f, t+\Delta t)} && (2.33)\\
&= \overline{\int_{\tau_1} a(\tau_1, t) e^{-2\pi i f \tau_1}\, d\tau_1 \int_{\tau_2} a(\tau_2, t+\Delta t) e^{2\pi i f \tau_2}\, d\tau_2} && (2.34)\\
&= \int_{\tau_1}\int_{\tau_2} \overline{a(\tau_1, t) a(\tau_2, t+\Delta t)} e^{-2\pi i f(\tau_1 - \tau_2)}\, d\tau_2\, d\tau_1 && (2.35)\\
&= \int_{\tau_1}\int_{\tau_2} R_a(\Delta t, \tau_1)\delta(\tau_1 - \tau_2) e^{-2\pi i f(\tau_1 - \tau_2)}\, d\tau_2\, d\tau_1 && (2.36)\\
&= \int_{\tau} R_a(\Delta t, \tau)\, d\tau && (2.37)
\end{aligned}$$

which is independent of the particular frequency one is interested in. That is, $R_{\mathcal{A}}(f, \Delta t) = R_{\mathcal{A}}(\Delta t)$. The above shows that the frequency response of the channel, at a particular constant frequency, is a random process in time, with the autocorrelation function given in (2.37). However, the previous section also showed that the frequency response is a random process in frequency as well. Extending the analysis to include the correlation of the frequency response between two frequencies, gives the straightforward result,

$$R_{\mathcal{A}}(\Delta f, \Delta t) = \mathcal{F}_\tau\{R_a(\Delta t, \tau)\} \tag{2.38}$$

Hence, the frequency response of a time and frequency-selective channel is a random process in both time and frequency, i.e. a *two-dimensional* Gaussian random process. Although the correlation properties of general fading channels tend to be exclusively thought of in terms of time or frequency, its two-dimensional correlation function means that the two characteristic correlation variables (time and frequency) are coupled intimately. Figure 2.10 [3] shows an example of this, where in 2.10–(a) the channel scattering function, $\sigma(\tau, f)$, is

[3] The sample random processes in this figure and the next were generated by masking a 128×128 two-dimensional field of independent complex Gaussian random variables. The masks were 2×10 and 10×10 samples in size respectively. The two-dimensional Fourier transform was taken of the masked spectra to give a sample realization of the channel transfer process in time and frequency.

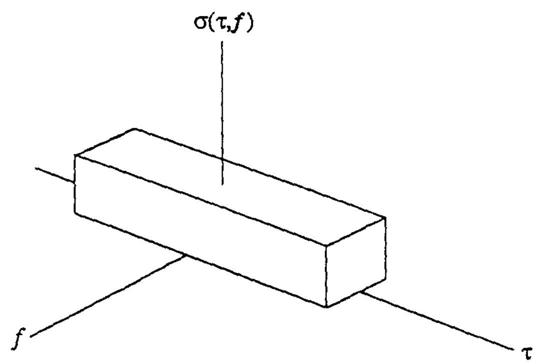

(a)

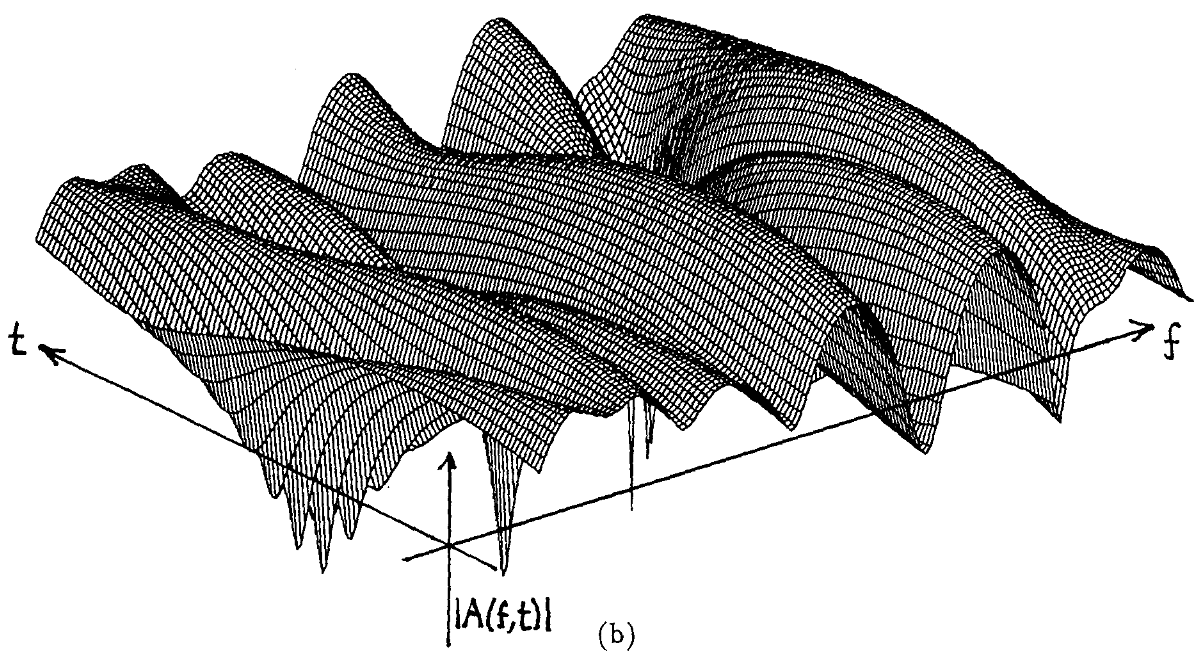

(b)

Figure 2.10: An example of an asymmetric two-dimensional channel fading process. (a) its rectangular scattering function, (b) a sample realization of the magnitude of the complex process. Note that (b) has a log vertical scale.

assumed to be a rectangular box. Here, the channel delay is several times the extent of the Doppler bandwidth. Figure 2.10–(b) shows a sample realization of this process, where it is seen that the channel's frequency response varies several times faster in the frequency direction than along the time direction. This example also shows how the frequency nulls in a random channel evolve in time, experiencing significant variations in position and depth. The rate and magnitude of these variations are determined by the statistical description of the channel — its scattering function. In Figure 2.11 the scattering function is now a square box, with its width in Doppler spread comparable to the channel delay in Figure 2.10. It is seen in 2.11–(b) that the time variations in the channel frequency response are much more severe. The units in these examples are arbitrary and are not intended to represent any particular channel. They should be used only to help to visualize the dynamics of a fading channel, and are useful to keep in mind when analyzing channel measurements and characterizations.

Note that although these channels vary in time, they are still *stationary* random processes. Where channels are truly dual fading, any optimal signal processing would have to include joint, two-dimensional, processing of the signals [31].

2.5 Coherence Measures of the Channel

In the previous sections it was discussed how a fading channel will distort a signal, and how this may be statistically characterized. However, the importance of the fading and its effect on a receiver's performance depend primarily on the period and bandwidth of the signal in relation to the channel process' statistics. This is seen in Figure 2.3 (b) for a time-selective, frequency flat channel, where symbol periods are superimposed on the single tap's fading process. Clearly, for an extremely short symbol period the channel would closely approximate the slow fading channel. Moreover, if the symbol period were considerably lengthened to include several "loops" of the process, the multiplicative fading process would completely scramble the signal and appear as "fast fading". There would be enough time between the symbols (or samples) for the process to be considered uncorrelated.

This may be quantified by defining the coherence time of the channel process, T_c, as the delay for the covariance function of a time-selective channel, $R_a(\Delta t)$, to equal 0.0. As the mobile channel produces a strictly bandlimited fading spectra for vertical dipole antenna [4], the oscillating correlation function is guaranteed to have zeros. For non- oscillatory

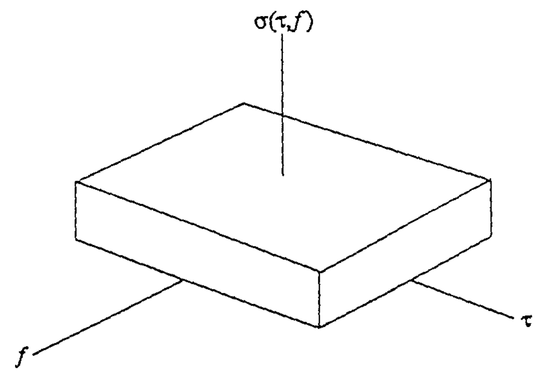

(a)

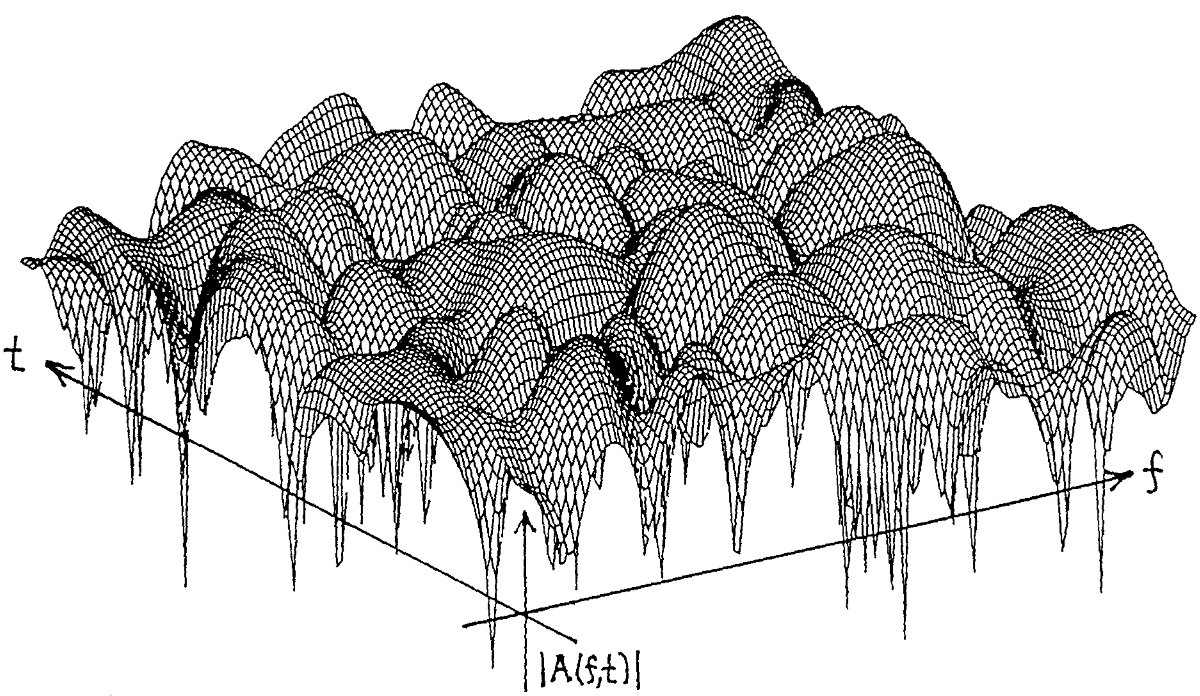

(b)

Figure 2.11: An example of a symmetric two-dimensional channel fading process. (a) its cubic scattering function, (b) a sample realization of the magnitude of the process. Note that (b) has a log vertical scale.

decaying covariance functions, a suitable measure of the support (i.e. non-zero extent) of the covariance function would be acceptable.

A relative measure, then, between the rate of envelope fading and symbol transmission rate, is given by T/T_c, where T is the symbol period. As the coherence time, T_c, is inversely related to the bandwidth of the fading process, B, this is usually expressed as the fading time bandwidth product, BT. For typical mobile communications symbol and fading rates, this value ranges from about 0.01 to 0.10. As the frequency bandwidth occupied by the signalling waveforms is typically much less than the corresponding frequency coherence bandwidth, the channel also appears to have flat frequency fading. However, these typical channel characteristics are very data rate dependent. See Proakis [10] for a more complete discussion.

2.6 Diversity Representation of a Time-Selective Fading Channel

For a Rayleigh fading channel, the continuous-time received channel process, $r(t)$, may be represented as a set of independent waveforms, as given by the Karhunen-Loéve expansion and described in Appendix A. That is,

$$r(t) = \sum_{i=1}^{\infty} r_i \phi_i(t) \quad ; \ 0 \leq t \leq T \tag{2.39}$$

where T is the observation interval, usually of one symbol. The orthogonal eigenfunctions, $\phi_i(t)$, are solutions of the eigenvalue equation,

$$\lambda_i \phi_i(t) = \int_0^T R_r(t,\tau)\phi_i(\tau)\, d\tau \tag{2.40}$$

where $R_r(t,\tau)$ is the correlation function of the received channel process, which was given previously as,

$$R_r(t,\tau) = u(t)u^*(\tau)R_a(t-\tau) \tag{2.41}$$

and $R_a(t-\tau)$ is the fading channel correlation function. The coefficients of the K-L expansion of the received process are given by,

$$r_i \equiv \int_0^T r(t)\phi_i^*(t) \tag{2.42}$$

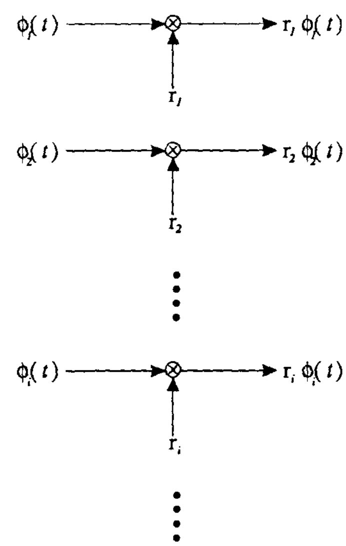

Figure 2.12: Diversity representation of a time-selective fading channel.

Any receiver with knowledge of the transmitted waveforms and channel fading statistics may decompose the received signal into its component orthogonal eigenfunctions, each weighted according to (2.42). The weights, or coefficients, will be independent complex Gaussian random variables with variances equal to their corresponding eigenvalues. That is,

$$\overline{r_i r_j^*} = \lambda_i \delta_{ij} \tag{2.43}$$

Although the received signal is the sum of these weighted eigenfunctions, their independence and the ability of the receiver to decompose the signal in terms of them allows the channel to be visualized as a set of independent parallel paths. Each path corresponds to a particular eigenfunction, and is weighted by a complex Gaussian random variable with a variance equal to its corresponding eigenvalue. When there is an AWGN source in the channel as well, the variance is then equal to the sum of the noise variance and the eigenvalue. This is shown in Figure 2.12. Note that this representation is identical to a diversity system[3, 1], and that a receiver operating with knowledge of the channel statistics may form decisions using optimal diversity combining techniques [3, 21]. The implications of this for the performance curves of the optimal receiver will be demonstrated in the following chapters.

Chapter 3

Optimal Demodulation of Fading Signals

This chapter will review optimal receiver structures for random Gaussian processes buried in additive Gaussian noise, giving developments for both continuous and discrete time representations of signals. Each appears to lead to a different approach to solving the problem. The continuous time problem requires manipulating involved integral equations, while the discrete time approach uses more common matrix operations and decompositions. However, it should be realized that both approaches are equivalent, in the exact same way discretizing the K-L expansion leads to the standard eigen-decomposition of matrices. Each may be converted into the other.

3.1 Continuous Time Optimal Demodulation

Given the strictly analogue nature of radio communications in the first half of this century, it is not surprising that the continuous time approach was the first to be developed [36]. However, it uses the less familiar techniques of integral equations, and results in rather formidable looking equations, few of which may be analytically solved. The discrete time approach, discussed in the next section, was developed shortly after and offers an alternate view of channel effects and the demodulation of signals [18, 21].

To start, we assume the channel is the general random, time variant, linear filter discussed in the previous chapter, and shown in Figure 2.5. For a transmitted signal, $s(t)$, the received signal is given by,

$$r(t) = \int_{\tau} a(t,\tau)s(t-\tau)\,d\tau + n(t) \tag{3.1}$$

where $a(t,\tau)$ and $n(t)$ are assumed to be Gaussian zero mean, and stationary in t. The covariance function of the received signal is given by,

$$\begin{aligned}
K_r(u,v) &= \overline{r(u)r^*(v)} && (3.2)\\
&= \int_{\tau_1}\int_{\tau_2} \overline{a(u,\tau_1)s(u-\tau_1)a^*(v,\tau_2)s^*(v-\tau_2)\,d\tau_1\,d\tau_2} + \overline{n(u)n^*(v)} && (3.3)\\
&= \int_{\tau_1}\int_{\tau_2} \overline{a(u,\tau_1)a(v,\tau_2)}s(u-\tau_1)s^*(v-\tau_2)\,d\tau_1\,d\tau_2 + K_n(u-v) && (3.4)\\
&= \int_{\tau_1}\int_{\tau_2} K_a(\tau_1,u-v)\delta(\tau_1-\tau_2)s(u-\tau_1)s^*(v-\tau_2)\,d\tau_1\,d\tau_2 + K_n(u-v) && (3.5)\\
&= \int_{\tau} K_a(\tau,u-v)s(u-\tau)s^*(v-\tau)\,d\tau + K_n(u-v) && (3.6)
\end{aligned}$$

where τ is the channel delay variable. Here, $K_a(\tau,\Delta t)$ is the time and frequency-selective, channel covariance function discussed in the previous section. It is relabeled from $R_a(\cdot)$ to emphasize its role as an integral kernel, in keeping with the literature. For a purely time-selective channel, with only a single modulating tap, $K_a(\tau,\Delta t) = K_a(\Delta t)\delta(\tau)$ and the received signal covariance function is,

$$K_r(u,v) = K_a(u-v)s(u)s^*(v) + K_n(u-v) \tag{3.7}$$

Note that although the channel covariance function, $K_a(u-v)$, and additive noise, $K_n(u-v)$, are stationary, the covariance function of the received signal will not be in general. However, it is Hermitian in u and v.

Formally writing the K - L expansion of the channel correlation kernel (see Appendix A), $K_a(u-v)s(u)s^*(v)$, we obtain the set of orthonormal functions $\{\phi_i(t)\}$ and eigenvalues $\{\lambda_i\}$. Because the additive noise is white and independent of the channel's tap process, the eigenfunctions of the total received process will also be $\{\phi_i(t)\}$, and the eigenvalues $\{\lambda_i + \mathcal{N}_o\}$. This method of breaking up the received signal's covariance kernels and eigenvalues serves only to make the role of the additive noise explicit. The received signal, $r(t)$, may be expanded in terms of the eigenfunctions,

$$r(t) = \sum_{i=1}^{\infty} r_i\phi_i(t) \tag{3.8}$$

with the coefficients, r_i, given by,

$$r_i = \int_0^T r(t)\phi_i^*(t)\,dt \tag{3.9}$$

As discussed in the previous chapter, only the first M "significant" eigenvalues of the channel, λ_i, will be used, in practice, giving a finite expansion. This corresponds to the usual orthogonal expansion of deterministic signals in a finite number of dimensions. Although the additive white noise is effectively infinite dimensional, only the finite number of relevant orthogonal functions containing components of the signal need be considered. The infinite energy white noise is always bandlimited to the signal bandwidth at some point, forcing the truncation of its otherwise arbitrary orthogonal expansion [17].

With the assumption of complex Gaussian processes, the coefficients will be independent complex Gaussian random variables, with zero mean and variance $\lambda_i + \mathcal{N}_o$. Thus, the two dimensional probability density function of each r_i, over the complex plane, will be,

$$p(r_i) = \frac{1}{\pi(\lambda_i + \mathcal{N}_o)} e^{-\frac{|r_i|^2}{\lambda_i + \mathcal{N}_o}} \tag{3.10}$$

Because of the independence of the random variables r_i, the pdf of the complex vector $\mathbf{r}$, for the first M terms, may be written as,

$$p(\mathbf{r}) = \prod_{i=1}^{M} \frac{1}{\pi(\lambda_i + \mathcal{N}_o)} e^{-\frac{|r_i|^2}{\lambda_i + \mathcal{N}_o}} \tag{3.11}$$

The above analysis assumes a known covariance kernel, $K_r(u,v)$, which depends on the specific message signal, $s(t)$, transmitted. Making the assumption of multiple messages, the covariance kernel is now indexed by the particular signal, $s^k(t)$, that was transmitted. That is, each message signal produces a random process with the unique second order statistic $K_r^{(k)}(u,v)$. Substituting the eigenvalues of the indexed covariance kernel into (3.11), gives the pdf of the received signal vector conditioned on the particular signal transmitted, namely $p(\mathbf{r}|s^k(t)) \equiv p(\mathbf{r}|k)$. Taking the logarithm of the conditional form of (3.11), gives the k'th decision variable to be maximized over all messages in the signaling alphabet,

$$\ell_k(\mathbf{r}) = \frac{-1}{\pi^M} \sum_{i=1}^{M} \left\{ \ln(\lambda_i^k + \mathcal{N}_o) + \frac{|r_i|^2}{\lambda_i^k + \mathcal{N}_o} \right\} \tag{3.12}$$

where the eigenvalues have been explicitly indexed to their corresponding covariance kernel. Note that the sum of the log terms in the bracket above may be also expressed as a logarithm of a product of eigenvalues. The product of eigenvalues is recognized as a determinant of a matrix, known as the Fredholm determinant [36, 17], and is a commonly occurring quantity. It is defined as,

$$D_{\mathcal{F}}(z) = \prod_{i=1}^{\infty}(1 + z\lambda_i) \tag{3.13}$$

for all values of z, where the $\{\lambda_i\}$ are the eigenvalues of the given kernel function. This term will act as a bias value in (3.12), independent of the received signal, but may vary between the decision branches. In the next section, the discrete form of this analysis will show that signal sets may be chosen to make this bias invariant to the decision branch. This term will then have no bearing in comparing the various decision variables, and will be ignored here, as can the constant $1/\pi^M$ scaling. Substituting the K-L expansion of (3.9) into (3.12), where (3.9) gives the random coefficients in terms of the original continuous time signal, results in,

$$\ell_k = \int_{u=0}^{T}\int_{v=0}^{T} r(u)\left\{\sum_{i=1}^{M}\frac{1}{\lambda_i^k + \mathcal{N}_o}\phi_i(u)\phi_i^*(v)\right\} r^*(v)\,du\,dv \tag{3.14}$$

Defining the bracketed term above as $Q^{(k)}(u,v)$, one obtains the k'th decision variable as,

$$\ell_k = -\int_{u=0}^{T}\int_{v=0}^{T} r(u)Q^{(k)}(u,v)r^*(v)\,du\,dv \tag{3.15}$$

which is an integral quadratic form of the received signal waveform. This expression defines the operations of a maximum likelihood receiver for the general, fading random channel. However, it involves a defined quantity, and the role and interpretation of the kernel-like function, $Q^{(k)}(u,v)$, still needs to be examined.

Recalling that the eigenvalues of the kernel $K_r^{(k)}(u,v)$ are $\lambda_i^k + \mathcal{N}_o$, and from the properties of the K-L expansion, the kernel may be represented by,

$$K_r^{(k)}(u,v) = \sum_{i=1}^{M}(\lambda_i^k + \mathcal{N}_o)\phi_i(u)\phi_i^*(v) \tag{3.16}$$

It is seen from the definition of $Q(u,v)$ in (3.14) that $Q^{(k)}(u,v)$ is fundamentally related to the original received signal's correlation kernel. This is shown explicitly by considering the expression,

$$\int_0^T K_r(u,t)Q(t,v)\,dt \tag{3.17}$$

where the k indexing has been dropped for convenience. Substituting the eigenfunction expansion of the two kernels into the above and simplifying, one finds,

$$\int_0^T K_r(u,t)Q(t,v)\,dt = \int_0^T \sum_{i=1}^{M}(\lambda_i + \mathcal{N}_o)\phi_i(u)\phi_i^*(t)\sum_{j=1}^{M}\frac{\phi_j(t)\phi_j^*(v)}{\lambda_i + \mathcal{N}_o}\,dt \tag{3.18}$$

$$= \sum_{i,j}\frac{\lambda_i + \mathcal{N}_o}{\lambda_j + \mathcal{N}_o}\phi_i(u)\phi_j^*(v)\int_0^T \phi_i^*(t)\phi_j(t)\,dt \tag{3.19}$$

$$= \sum_{i,j}\frac{\lambda_i + \mathcal{N}_o}{\lambda_j + \mathcal{N}_o}\phi_i(u)\phi_j^*(v)\delta_{i,j} \tag{3.20}$$

$$= \sum_i \phi_i(u)\phi_i^*(v) \tag{3.21}$$

$$= \delta(u-v) \tag{3.22}$$

It is seen that $Q(u,v)$ can be interpreted as a form of *inverse kernel* of $K_r(u,v)$. When the original integral of (3.17) is discretized, the matrix form of the relationship is,

$$\mathbf{K}_r\mathbf{Q} = \mathbf{I} \tag{3.23}$$

where $\mathbf{I}$ is the identity matrix. So, $\mathbf{Q}$ is the inverse of the discrete time covariance matrix of the received signal, $\mathbf{K}_r$, and the continuous time kernel $Q(u,v)$ is, in a valid sense, the inverse of $K_r(u,v)$.

Although this is a simple and elegant relationship, there is still the question of the physical significance of the integral quadratic operation performed by the optimal receiver. This is best answered by considering the optimal receiver as if we knew exactly the channel's impulse response, $a(t,\tau)$, for all time, i.e. it is deterministic. This is a simple generalization of the additive coloured noise receiver, and similarly involves a whitening type of filter, which is now time-variant. Figure 3.1 shows that the k'th decision branch of the receiver will *predistort* the k'th known message signal, to give $z_k(t)$, before correlating it with the received signal. This correlation is then used as the k'th decision variable.

In Figure 3.1, it is seen that the received signal, $r(t)$, is simply $z_k(t)+n(t)$, assuming that the k'th message was transmitted. For the case of a true random channel, we don't know what $z_k(t)$ is in particular, except that it is a zero mean random process with a correlation kernel $K_r^k(u,v) - K_n(u,v)$. However, assuming signal $s_k(t)$ has been transmitted, and with its known correlation kernel, we may *estimate* from $r(t)$ what $z_k(t)$ *would* have been, before the additive noise.

This is made clearer in the simplified example, shown in Figure 3.2. Here, we have a zero mean random process, $z(t)$, with a known correlation kernel, $K_z(u,v)$, which is

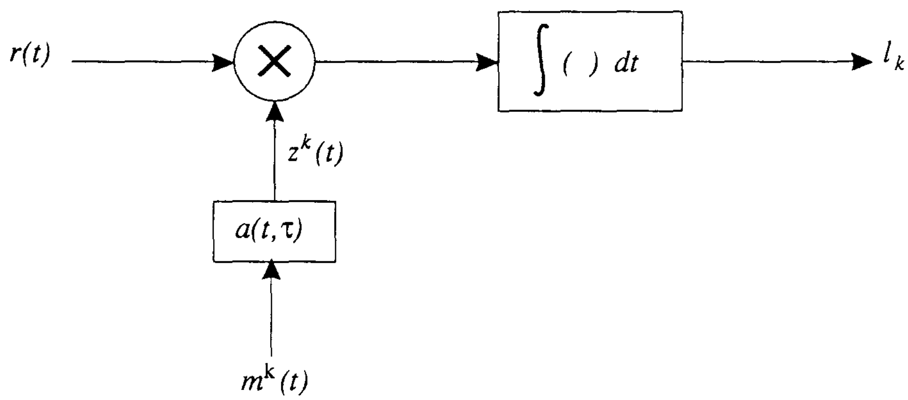

Figure 3.1: Optimum receiver for k'th message signal for a known deterministic linear channel.

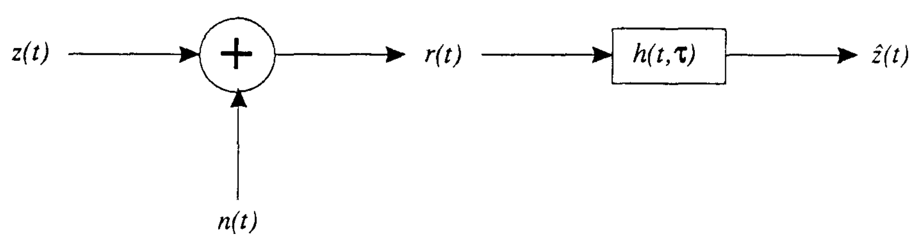

Figure 3.2: Estimation of a random process with known statistics, corrupted by additive noise.

corrupted by additive noise, again with a known correlation kernel, $K_n(u, v)$. The problem is to derive a time-variant linear filter, $h(t, u)$, that will estimate $z(t)$ from the received signal with minimum mean squared error. That is, from

$$r(t) = z(t) + n(t) \tag{3.24}$$

form the estimate,

$$\hat{z}(t) = \int_0^T h(t, u) r(u)\, du \tag{3.25}$$

This is a standard linear estimation problem whose solution is given in [2]. The solution for $h(t, u)$ is given implicitly by the integral equation,

$$K_z(t, u) = \int_{v=0}^{T} h(t, v) K_r(v, u)\, dv \tag{3.26}$$

where,

$$K_r(u, v) = K_z(u, v) + \mathcal{N}_o \delta(u - v) \tag{3.27}$$

assuming the additive noise is white and independent of the process $z(t)$. Multiplying (3.26) by the inverse kernel of $K_r(u, v)$ and integrating gives,

$$\begin{aligned}
K_z(t, u) Q_r(u, w) &= \int_{v=0}^{T} h(t, v) K_r(v, u) Q_r(u, w)\, dv && (3.28)\\
\int_{u=0}^{T} K_z(t, u) Q_r(u, w)\, du &= \int_{v=0}^{T} h(t, v) \int_{u=0}^{T} K_r(v, u) Q_r(u, w)\, du\, dv && (3.29)\\
&= \int_{v=0}^{T} h(t, v) \delta(v - w)\, dv && (3.30)
\end{aligned}$$

Thus, the optimum time-variant filter is given by,

$$h(t, w) = \int_{u=0}^{T} K_z(t, u) Q_r(u, w)\, du \tag{3.31}$$

However, from (3.27), this is simply,

$$\begin{aligned}
h(t, w) &= \int_{u=0}^{T} (K_r(t, u) - \mathcal{N}_o \delta(t - u)) Q_r(u, w)\, du && (3.32)\\
&= \delta(t - w) - \mathcal{N}_o Q_r(t, w) && (3.33)
\end{aligned}$$

since $Q_r(u, v)$ is the inverse kernel of $K_r(u, v)$. Thus, the inverse kernel of a received signal process is directly related to the optimal estimator of the process prior to the addition of noise. That is,

$$Q_r(t, w) = \frac{1}{\mathcal{N}_o} \delta(t - w) - \frac{1}{\mathcal{N}_o} h(t, w) \tag{3.34}$$

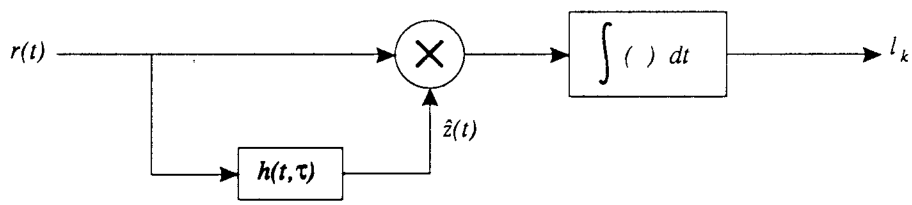

Figure 3.3: Optimal continuous receiver for a random linear channel with known statistics.

However, this $Q_r(u,v)$ has the same formulation as the inverse kernel for the original optimal receiver of a faded signal, given in Equation (3.15). Substituting (3.34) into (3.15), one finds,

$$\ell_k = \int_{u=0}^{T}\int_{v=0}^{T} r(u)h_k(u,v)r^*(v)\,du\,dv \tag{3.35}$$

where the first term of (3.34) is dropped since it is independent of the particular symbol transmitted. It is straightforward to show that $h_k(u,v)$ may be written in terms of the channel kernel's eigenvalues,

$$h_k(u,v) = \sum_{i=1}^{M} \frac{\lambda_i^k}{\lambda_i^k + \mathcal{N}_o}\phi_i(u)\phi_i^*(v) \tag{3.36}$$

The k'th branch of the optimal receiver is shown in Figure 3.3. The lower branch may be interpreted as forming the estimate of $z_k(t)$, assuming that the k'th message was transmitted. This estimate is then correlated with the actual received signal to form the decision variable. This intuitively corresponds to the optimal receiver of a known deterministic linear channel.

Some important points should be noted here:

1. The derivation of the optimum receiver's general structure made extensive use of eigenvalues and integral equations. However, these were applied only formally, and at intermediate steps. At no point did the eigenvalues or equations need to be explicitly solved for. This is not the case when the *performance* of the receiver is to be evaluated [17].

2. Although the interpretation of the optimum receiver as an estimator-correlator is intuitively satisfying, in practice there is no need to really calculate $h_k(u,v)$ for a receiver; the inverse kernel of the channel correlation function, $Q_k(u,v)$, will suffice.

3. The above analysis assumed *known* statistics of the channel and additive noise. In practice they must be estimated somehow from the received signals, and the K-L expansion performed within the receiver

3.2 Discrete Time Optimal Demodulation

In this section we assume that all signals are time sampled, and the model of the channel fading is taken as the M tap, delay line shown in Figure 2.5. The N-sample snapshot at time i of the input signal is written in the matrix form,

$$\mathbf{s} = \begin{bmatrix} s(i-N+1) \\ s(i-N+2) \\ \vdots \\ s(i) \end{bmatrix} \tag{3.37}$$

with the corresponding channel output vector, $\mathbf{z}$, similarly defined. The tap vectors are defined as,

$$\mathbf{a}_j = \begin{bmatrix} a_j(i-N+1) \\ a_j(i-N+2) \\ \vdots \\ a_j(i) \end{bmatrix} ; \; j = 0 \ldots M-1 \tag{3.38}$$

The relationship between the input vector, the channel tap vectors, and the output vector may be expressed in matrix form. However, the time dependence of the channel filter coefficients (regardless of their being random processes), results in a formulation that is slightly different from the more familiar definitions used in spectrum estimation and adaptive filtering [37, 31]. This is seen best by first considering a channel with a single time-variant tap. Setting $i = N$ for simplicity, the *channel matrix* is then defined as,

$$\mathbf{A} = [\mathbf{a}_0] = \begin{bmatrix} a_0(1) \\ a_0(2) \\ \vdots \\ a_0(N) \end{bmatrix} \tag{3.39}$$

and the signal input matrix as,

$$\mathbf{S} = \mathrm{diag}(\mathbf{s}) = \begin{bmatrix} s(1) & 0 & & \\ 0 & s(2) & & \\ & & \ddots & 0 \\ & & 0 & s(N) \end{bmatrix} \tag{3.40}$$

The channel output vector may then be written,

$$\begin{aligned} \mathbf{z} &= \mathbf{SA} && (3.41) \\ &= \begin{bmatrix} s(1) & 0 & & \\ 0 & s(2) & & \\ & & \ddots & 0 \\ & & 0 & s(N) \end{bmatrix} \begin{bmatrix} a_0(1) \\ a_0(2) \\ \vdots \\ a_0(N) \end{bmatrix} && (3.42) \\ &= \begin{bmatrix} a_0(1)s(1) \\ a_0(2)s(2) \\ \vdots \\ a_0(N)s(N) \end{bmatrix} && (3.43) \end{aligned}$$

The channel correlation matrix, $\mathbf{K_A}$, may be expressed as,

$$\begin{aligned} \mathbf{K_A} &= \overline{\mathbf{AA}^H} && (3.44) \\ &= \overline{\begin{bmatrix} a_0(1) \\ a_0(2) \\ \vdots \\ a_0(N) \end{bmatrix} \begin{bmatrix} a_0(1) & a_0(2) & \cdots & a_0(N) \end{bmatrix}^*} && (3.45) \\ &= \mathbf{K_{a_0}} && (3.46) \end{aligned}$$

The correlation matrix of the channel output is seen to be,

$$\begin{aligned} \mathbf{K_z} &= \overline{\mathbf{zz}^H} && (3.47) \\ &= \mathbf{S}\overline{\mathbf{AA}^H}\mathbf{S}^H && (3.48) \\ &= \mathbf{SK_{a_0}S}^H && (3.49) \end{aligned}$$

Noting that the $\mathbf{S}$ matrices are diagonal, it is easy to see that the element (u, v) of the channel output correlation matrix is simply $s(u)\mathbf{K_{a_0}}(u, v)s^*(v)$, which corresponds to the continuous time covariance function of (3.7). Generalizing to an M tap channel, we now have for the signal matrix, $\mathbf{S}_M$, the $(N+M-1)\times(MN)$ matrix,

$$\mathbf{S}_M = \begin{bmatrix} \mathbf{S} & \mathbf{0} & \mathbf{0} & \cdots & \mathbf{0} \\ \mathbf{0} & \mathbf{S} & \mathbf{0} & \cdots & \mathbf{0} \\ \mathbf{0} & \mathbf{0} & \mathbf{S} & \cdots & \mathbf{0} \\ \vdots & \vdots & \vdots & \ddots & \vdots \\ \mathbf{0} & \mathbf{0} & \mathbf{0} & \cdots & \mathbf{S} \end{bmatrix} \tag{3.50}$$

where $\mathbf{0}$ is an N element null row vector, and $\mathbf{S}$ is the $N\times N$ signal matrix defined for the case of a single channel tap. In each successive column, the $\mathbf{S}$ matrices are staggered (down) by one row. The channel matrix, $\mathbf{A}$, is defined in turn as,

$$\mathbf{A} = \begin{bmatrix} \mathbf{a}_0 \\ \mathbf{a}_1 \\ \vdots \\ \mathbf{a}_M \end{bmatrix} = \begin{bmatrix} a_0(1) \\ a_0(2) \\ \vdots \\ a_0(N) \\ a_1(1) \\ a_1(2) \\ \vdots \\ a_1(N) \\ \vdots \\ a_M(1) \\ a_M(2) \\ \vdots \\ a_M(N) \end{bmatrix} \tag{3.51}$$

An example where we have $M=2$ channel taps, and $N=3$ input signal samples, giving $N+M-1=4$ channel output samples, is shown below.

$$\mathbf{S}_2 = \begin{bmatrix} s(1) & 0 & 0 & 0 & 0 & 0 \\ 0 & s(2) & 0 & s(1) & 0 & 0 \\ 0 & 0 & s(3) & 0 & s(2) & 0 \\ 0 & 0 & 0 & 0 & 0 & s(3) \end{bmatrix} \tag{3.52}$$

$$\mathbf{A} = \begin{bmatrix} a_0(1) \\ a_0(2) \\ a_0(3) \\ a_1(1) \\ a_1(2) \\ a_1(3) \end{bmatrix} \tag{3.53}$$

From these, we have the output vector as,

$$\mathbf{z} = \mathbf{S}_2\mathbf{A} \tag{3.54}$$

$$= \begin{bmatrix} s(1)a_0(1) \\ s(2)a_0(2) + s(1)a_1(1) \\ s(3)a_0(3) + s(2)a_1(2) \\ s(3)a_1(3) \end{bmatrix} \tag{3.55}$$

The channel correlation matrix, $\mathbf{K_A}$, is similarly expressed as before in the form,

$$\mathbf{K_A} = \overline{\mathbf{A}\mathbf{A}^H} \tag{3.56}$$

$$= \overline{\begin{bmatrix} \mathbf{a}_0 \\ \mathbf{a}_1 \\ \vdots \\ \mathbf{a}_{M-1} \end{bmatrix} \begin{bmatrix} \mathbf{a}_0{}^H & \mathbf{a}_1{}^H & \cdots & \mathbf{a}_{M-1}{}^H \end{bmatrix}} \tag{3.57}$$

$$= \begin{bmatrix} \mathbf{K}_{\mathbf{a}_0} & \mathbf{0} & \cdots & \mathbf{0} \\ \mathbf{0} & \mathbf{K}_{\mathbf{a}_1} & \cdots & \mathbf{0} \\ \vdots & \vdots & \ddots & \mathbf{0} \\ \mathbf{0} & \mathbf{0} & \cdots & \mathbf{K}_{\mathbf{a}_{M-1}} \end{bmatrix} \tag{3.58}$$

The diagonal structure of the matrix occurs because the channel tap processes are assumed to be mutually uncorrelated. Again, the correlation matrix of the channel output is given by, $\mathbf{K_z} = \mathbf{S}_M\mathbf{K_A}\mathbf{S}_M^H$. It is seen that this expression also corresponds directly to the continuous time covariance function (3.6) derived in the previous section for a general time and frequency-selective channel.

If the transmitted signal is indexed on the particular message vector, $\mathbf{s}_k$ being sent, then the channel output correlation matrix is given as,

$$\mathbf{K}_\mathbf{z}^{(k)} = \mathbf{S}_k\mathbf{K_A}\mathbf{S}_k^H \tag{3.59}$$

where we have dropped the M indexing. The received signal is,

$$\begin{aligned}\mathbf{r} &= \mathbf{z}+\mathbf{n} && (3.60)\\ &= \mathbf{S}_k\mathbf{A}+\mathbf{n} && (3.61)\end{aligned}$$

The received signal correlation matrix is given by,

$$\mathbf{K_r} = \mathbf{K_z}^{(k)} + \mathbf{K_n} \tag{3.62}$$

Since the received signal vector, conditioned on $\mathbf{S}_k$, is the sum of two complex Gaussian processes, it also will be Gaussian, and its distribution is an N variate complex normal pdf [38, 39],

$$p(\mathbf{r}|\mathbf{s}_k) = \frac{1}{\pi^N|\mathbf{K_r}^{(k)}|}e^{-\mathbf{r}^H\mathbf{K_r}^{(k)^{-1}}\mathbf{r}} \tag{3.63}$$

If the probabilities of transmission for the messages are assumed to be equal, the decision variable may be derived from the a priori probability directly. Taking the logarithm of (3.63), and neglecting the scaling, the decision variable for the k'th message may be written,

$$\ell_k = -\ln|\mathbf{K_r}^{(k)}| - \mathbf{r}^H\mathbf{K_r}^{(k)^{-1}}\mathbf{r} \tag{3.64}$$

The first term plays the identical role to the Fredholm determinant in the previous section. However, it can be shown that the value of the determinant is independent of the signalling waveforms if only the phase of the waveforms is used to encode the message. This can be seen straightforwardly by expanding the received signal correlation matrix, $\mathbf{K_r}^{(k)}$,

$$\begin{aligned}\mathbf{K_r}^{(k)} &= \mathbf{K_z}^{(k)} + \mathbf{K_n} && (3.65)\\ &= \mathbf{S}_k\mathbf{K_A}\mathbf{S}_k^H + \mathbf{S}_k\mathbf{S}_k^{-1}\mathbf{K_n}\mathbf{S}_k^{H^{-1}}\mathbf{S}_k^H && (3.66)\\ &= \mathbf{S}_k\left(\mathbf{K_A} + \mathbf{S}_k^{-1}\mathbf{K_n}\mathbf{S}_k^{H^{-1}}\right)\mathbf{S}_k^H && (3.67)\\ &\equiv \mathbf{S}_k\mathbf{K}_c\mathbf{S}_k^H && (3.68)\end{aligned}$$

where $\mathbf{K}_c$ is defined as,

$$\mathbf{K}_c = \mathbf{K_A} + \mathbf{S}_k^{-1}\mathbf{K_n}\mathbf{S}_k^{H^{-1}} \tag{3.69}$$

and is a modified channel correlation matrix. The determinant of $\mathbf{K_r}^{(k)}$ is then given by,

$$\begin{aligned}|\mathbf{K_r}^{(k)}| &= |\mathbf{S}_k||\mathbf{K}_c||\mathbf{S}_k^H| && (3.70)\\ &= |\mathbf{S}_k||\mathbf{S}_k^H||\mathbf{K}_c| && (3.71)\\ &= |\mathbf{S}_k\mathbf{S}_k^H||\mathbf{K}_c| && (3.72)\end{aligned}$$

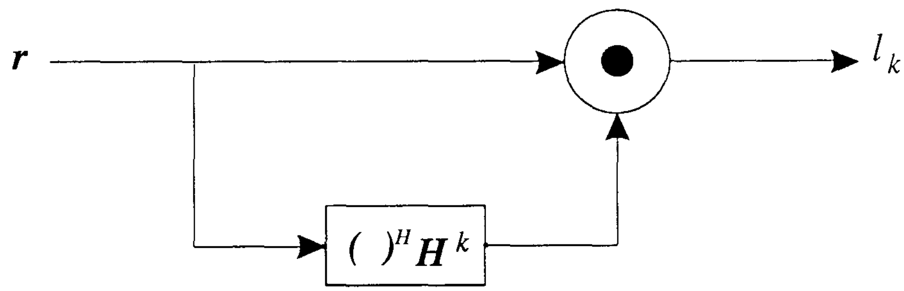

Figure 3.4: Optimal discrete receiver branch for a random linear channel with known statistics. The $\odot$ symbol represents the vector inner product.

where we note that $\mathbf{S}_k\mathbf{S}_k^H = \mathbf{I}$ for PSK signals and a single channel tap. Thus, if the k dependence of the signal matrices exists only in the phase of the signal samples, the Fredholm determinant will be independent of the signal transmitted.

The k'th decision variable may then be simplified to,

$$\ell_k = -\mathbf{r}^H \mathbf{K}_{\mathbf{r}}^{(k)^{-1}} \mathbf{r} \tag{3.73}$$

This quadratic form corresponds directly to the integral form of the continuous time optimal receiver, given in Equation (3.15). As shown by Kailath [18], when the additive noise is white, the matrix $\mathbf{K}_{\mathbf{r}}^{(k)^{-1}}$ may be written in the form,

$$\mathbf{K}_{\mathbf{r}}^{(k)^{-1}} = \frac{1}{\mathcal{N}_o}\left(\mathbf{I} - \mathbf{H}^{(k)}\right), \tag{3.74}$$

where $\mathbf{H}$, as defined above, is the least mean squares estimator of the fading channel output process, $\mathbf{z}$, in additive noise. Thus, $\mathbf{H}^{(k)}$ corresponds directly to the time-variant filter impulse response, $h_k(u,v)$, of the previous section, and we have the discrete time branch for the optimal receiver as shown in Figure 3.4. Again, the optimal receiver first *estimates* from the received signal the k'th faded signal (before the additive noise), and then correlates the estimate with the actual received signal vector.

Adding the effects of a specular (i.e. deterministic) component to the received signal is done by including a non-zero mean signal vector, $\bar{\mathbf{r}}$, in the pdf of received signal vector. Modifying (3.63) appropriately and solving again for the decision variable gives,

$$\ell_k = -(\mathbf{r} - \bar{\mathbf{r}})^H \mathbf{K}_{\mathbf{r}}^{(k)^{-1}} (\mathbf{r} - \bar{\mathbf{r}}) \tag{3.75}$$

Like the inverse signal correlation matrix, however, this receiver structure requires either knowledge of, or an estimate of the specular component. As well, the effects of non-white additive noise may be considered, with Kailath [18] and Hancock and Wintz [21] providing a thorough treatment and interpretation of the problem.

This chapter has briefly surveyed the design of optimum receivers for general time and frequency-selective fading channels. Two important points that still require analysis are:

1. Evaluation of the theoretical performance of an optimal-receiver and a conventional differential receiver in fading channels.

2. Integration of estimators of channel statistics into the overall receiver structure.

These will be examined in detail in the following chapters. Although the discussion until now has been for general time and frequency-selective fading channels, in the following we will consider the specific case of purely time-selective fading. This is done as an initial step toward analyzing the general random channel communications problem. In addition, there has been a great deal of work accomplished on receivers for frequency-selective fading channels. Although most make the assumption of an unknown but deterministic selectivity that is fixed in time, the adaptive nature of the receivers allow them to track slow temporal variations of the channel, and provide suboptimal performance that is generally adequate for practical applications. Random time selectivity, however, still carries something of a mystique, although the duality that exists between the two forms certainly suggests that the frequency selective approach may be applied to the time-selective channel.

In the conventional differential receiver, where the channel statistics are unknown and no attempt is made to estimate them, the decision variable calculated may be written in a form similar to (3.73),

$$\ell = -\mathbf{r}^H \mathbf{A} \mathbf{r} \tag{3.76}$$

where A has the form,

$$\mathbf{A} = \begin{bmatrix} \mathbf{0} & \mathbf{I} \\ \mathbf{I} & \mathbf{0} \end{bmatrix} \tag{3.77}$$

Here $\mathbf{0}$ and $\mathbf{I}$ have dimensions $(N) \times (N)$ where N is the number of signal samples taken per transmitted symbol interval. Note that the conventional receiver must still form *some* estimate of the second order statistics of the received signal, which contains the transmitted information. Although the conventional differential receiver does not use the optimal kernel, ${\mathbf{K}_{\mathbf{r}}^{(k)}}^{-1}$, in its quadratic form receiver, $\mathbf{A}$ has the advantage of being independent of the particular channel in use. As previously mentioned though, the suboptimal receiver also has an error floor as a fundamental performance limitation when used in a fading channel environment. This limitation is entirely owing to the inappropriate kernel being chosen for the receiver, and *not* to some inherent characteristic of the channel. Unfortunately, the error floor is usually attributed to the fading alone, and the receiver structure is not considered.

Chapter 4

Performance Analysis of DPSK in Fading

The previous chapter examined the form of optimal receivers for the random, fading channel. This chapter will examine the performance of DPSK forms of these receivers for two cases — one in which the channel has a special form of its correlation function, and one where a completely general channel correlation function is allowed. Although the first case is not useful for a practical system, due to its assumptions on the channel statistics, it is interesting since it provides a fully analytic solution for the case of M-ary DPSK, using complex signalling. As well, its assumptions on the correlation function are plausible as a first approximation, and provides a "toy" channel that an optimal receiver may be designed for and its operation interpreted. M-ary DPSK performance for general time-selective fading channels may also be evaluated, but requires much less satisfying Monte-Carlo methods to estimate the receiver performance. The performance of the optimal receiver will be evaluated for binary as well as general M-ary DPSK signalling, and a geometric interpretation of the operation of receivers in fading channels will be given.

4.1 Analysis of Receiver Performance for a Special Case of Correlation Function

This section will examine the performance of conventional and optimal continuous time receivers for time-selective fading with a special form of channel covariance function. Cf.

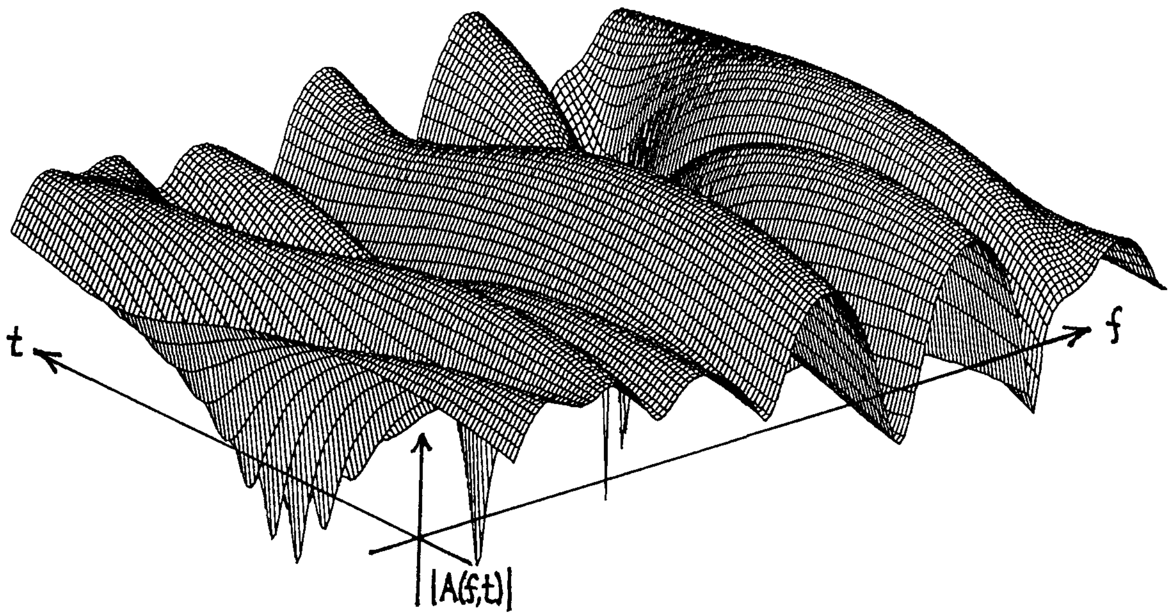

Figure 4.1: A sample realization of the magnitude of the time variation of the fading channel's frequency response. Note that a log vertical scale is used.

Chapter 2. This is based on the work by Walker [22] for a transmitted reference scheme for binary signals. He suggested using two separate frequency bands, one for the data signal and one for a reference phase tone, where each band experiences time selective fading, as well as fading between the frequency channels. That is, the random time-selective fading processes in each channel are not independent, but have some measure of correlation between them. Figure 4.1, taken from Figure 2.10, can be used to illustrate this case, where the frequency bands are imagined to be two lines on the surface, running parallel to the time axis. For two channels relatively close to each in frequency, the time variations in the two channels will follow each other closely in step. As the the two channels are further separated, there is less correlation in their time variations.

The form of frequency selective fading is assumed to be characterized by a single decorrelation parameter between the transmitted and reference slots, an approximation which is often used even in present-day analysis. This concept may be straightforwardly applied to a time-differential form of signalling, where the reference and data signals occupy two consecutive slots in time, rather than in frequency. Within each slot, the full continuous time random process will be characterized statistically through the K - L expansion. In PSK signalling, frequency-selective behaviour of the channel may be ignored due to the narrow bandwidth of the signalling band. Here, Walker's analysis is extended to complex signalling for M-ary DPSK.

From the discussion of Appendix B, the channel is assumed to have a correlation function over two symbol intervals of the form,

$$R_2(\tau) = \left\{ \begin{array}{lll} R(\tau) & ; & |\tau| < T \\ \rho R(|\tau| - T) & ; & T < |\tau| < 2T \end{array} \right\} \tag{4.1}$$

where $R(\tau)$ is the actual channel correlation function. A Karhunen-Loéve expansion [38], described in Appendix A, is performed on each of the fading signals over one symbol interval, where the eigenfunctions, $\{\phi_i(t)\}$, and eigenvalues, $\{\lambda_i\}$, satisfy the Fredholm integral equation,

$$\lambda_i \phi_i(t) = \int_0^T K(t,\tau)\phi_i(\tau)\, d\tau \tag{4.2}$$

The kernel $K(t,\tau)$ is given by,

$$K(t,\tau) = s(t)R(t-\tau)s^*(\tau), \tag{4.3}$$

where $s(t)$ is the modulating waveform. In practice, this equation would be solved numerically, and the number of eigenvalues resolved will equal the number of samples over a symbol interval used in evaluating the integral.

From the eigenvalue spectrum of the combined channel correlation function and signal waveform, the probability of correct detection of a conventional continuous time QDPSK receiver may be shown to be,

$$P_c = C_N \int_{s=-\infty}^{\infty} \sum_{j=1}^{N} \frac{1}{\left(it_j^1 + s^2\right)\left(t_j^1 - t_j^2\right)} \left[\prod_{\substack{k=1 \\ k \neq j}}^{N} \frac{1}{\left(t_j^1 - t_k^1\right)\left(t_j^1 - t_k^2\right)} \right] ds \tag{4.4}$$

where C_N and $t_j^{1,2}$ are defined as,

$$C_N = \frac{1}{\pi}\left(\frac{-4}{1-\rho^2}\right)^N \prod_{j=1}^{N} \frac{1}{{\lambda_j}^2} \tag{4.5}$$

$$t_j^{1,2} = i\,\frac{2\rho \mp \sqrt{{\lambda_j}^2 s^2 \left(1-\rho^2\right)^2 + 4}}{\lambda_j\left(1-\rho^2\right)} \tag{4.6}$$

and N is the number of "significant" eigenvalues found from (4.2). Note that the relatively slow rate of the fading process makes the covariance kernel $K(t,\tau)$ very nearly singular,

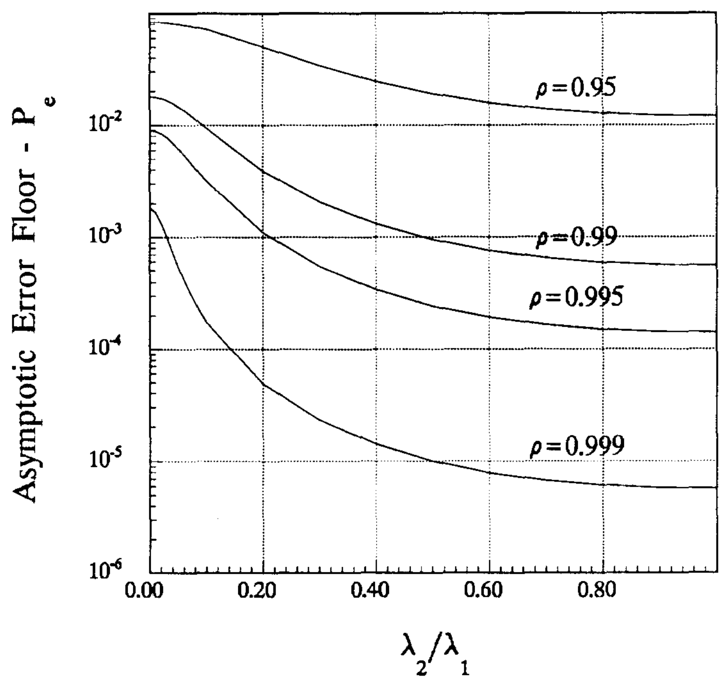

Figure 4.2: The asymptotic error floor for a conventional receiver in a fading channel with two significant eigenvalues, as a function of the eigenvalue ratio, λ_2/λ_1 and intersymbol correlation, ρ.

and the eigenvalue spectrum quickly decays to zero. The error expression above, may be numerically evaluated for an arbitrary number of eigenvalues and values of ρ.

Figure 4.2 shows the asymptotic error floor for the case of two significant eigenvalues as a function of the symbol correlation factor, ρ, and the ratio of the two eigenvalues. Setting λ_2 to zero corresponds to the single eigenvalue result given by Voelcker [11]. It is seen that for a given ρ, the error floor of a conventional receiver is dependent on the spectrum of the eigenvalues, which is determined from the fading correlation function and waveform shape through (4.2) and (4.3). This is somewhat surprising, since virtually all analyses of receivers in fading make the assumption of a single significant eigenvalue; that is, correlated staircase fading. The best performance that may be achieved for a given ρ occurs for equal eigenvalues, and can result in significant decreases in the error floor.

Extending the above to additional eigenvalues gives the same general results, where the asymptotic error experienced by the receiver is a function of both the channel's intersymbol correlation, *and* the eigenvalue spectrum of the received signal process. Again, the minimum asymptotic error occurs for the case of equal eigenvalues. This is discussed

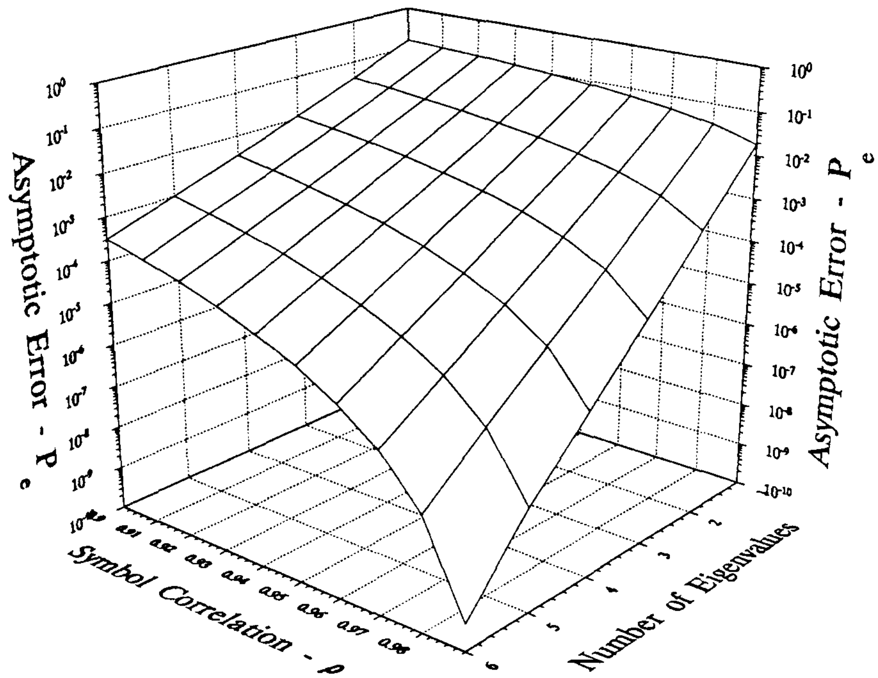

Figure 4.3: Asymptotic error performance of the optimal receiver as a function of the number of channel eigenvalues and intersymbol correlation.

further in Appendix B. It is seen that even in a conventional receiver, the asymptotic error floor is not an absolute or irreducible quantity, and, may vary over several orders of magnitude, depending on the values of ρ and $\{\lambda_i\}$ from the combined channel fading and signalling waveforms. Using fixed signal pulse shapes, performance is constrained only by the channel's ρ, number of resolvable eigenvalues, and their spectrum. The latter may still be determined in part by the chosen pulse shape, $s(t)$, as given in (4.2) and (4.3).

From Appendix B, it can then be shown that the statistics of the decision variables for an optimal, or maximum likelihood receiver are equivalent to those of the conventional receiver, operating in a channel where all of the eigenvalues equal one. This is independent of the actual channel eigenvalue spectrum. The optimal receiver is seen to perform something of a whitening of the eigenvalue spectrum.

Equation (4.4), for a conventional QDPSK receiver, was numerically evaluated in the limit as all eigenvalues approach 1. The results are shown in Figure 4.3, where the asymptotic error floor is given as a function of the number of resolved eigenvalues and the correlation parameter, ρ. It is seen that for a given channel correlation between symbols, the error floor decreases exponentially with an increasing number of resolved eigenvalues.

4.2 Form of an Optimal DPSK Receiver for General Correlation Functions

In the previous section, receivers for detecting M-ary DPSK transmitted through a specially correlated Rayleigh fading channel was examined. However, in the extension of Walker's scheme [22] to time-differential signalling, it was seen that this imposed the form given by (4.1) on the autocorrelation function of the channel fading process. This autocorrelation function is a poor approximation to the actual fading process, since it discards second order statistical information about the process available in the second symbol interval. The results suggest, however, that similar, maximum likelihood improvements in performance may be possible for DPSK in an arbitrary channel.

From Chapter 3, for the case of a single channel tap and equi-energy signalling, the optimal calculation of the m'th decision variable is given by,

$$\ell_m = \mathbf{r}^H \mathbf{K}_\mathbf{r}^{m^{-1}} \mathbf{r} \; ; \; m = 0 \ldots M-1 \tag{4.7}$$

where $\mathbf{r}$ is the received sampled signal vector, $\mathbf{K}_\mathbf{r}^m$ is the correlation matrix of the received sampled signal vector, assuming symbol m was transmitted, and M is the number of symbols in the signalling alphabet. The inverse of $\mathbf{K}_\mathbf{r}^m$ is often termed the "decision kernel" and is assumed to be precomputed or known. It may be expanded as,

$$\begin{aligned} \mathbf{K}_\mathbf{r}^m &= \mathbf{K}_\mathbf{z}^m + \mathbf{K}_\mathbf{n} && (4.8) \\ &= \mathbf{S}_m \mathbf{K}_\mathbf{a} \mathbf{S}_m{}^H + \mathbf{K}_\mathbf{n} && (4.9) \end{aligned}$$

where $\mathbf{S}_m$ is the diagonal matrix of the time samples of the m'th message envelope, $\mathbf{K}_\mathbf{a}$ is the estimated or known correlation matrix of the channel tap over two symbol intervals, and $\mathbf{K}_\mathbf{n}$ is the correlation matrix of the additive noise. Assuming the noise is white with variance σ^2, then we have $\mathbf{K}_\mathbf{n} = \sigma^2\mathbf{I}$ where $\mathbf{I}$, here, is an $(2N) \times (2N)$ identity matrix.

We now assume the signals are constant amplitude DPSK, with the form,

$$\mathbf{S}_m = \begin{bmatrix} \mathbf{I} & \mathbf{0} \\ \mathbf{0} & e^{i\theta_m}\mathbf{I} \end{bmatrix} \tag{4.10}$$

where $\mathbf{I}$, here, is an $N \times N$ identity matrix. The correlation matrix of the received signal vector, $\mathbf{K}_\mathbf{r}^m$, may then be expanded as,

$$\begin{aligned}
\mathbf{K}_\mathbf{r}^{m^{-1}} &= \left(\mathbf{S}_m \mathbf{K_a} \mathbf{S}_m^H + \sigma^2 \mathbf{I}\right)^{-1} && (4.11)\\
&= \left(\mathbf{S}_m \mathbf{K_a} \mathbf{S}_m^H + \sigma^2 \mathbf{S}_m \mathbf{S}_m^H\right)^{-1} && (4.12)\\
&= \left[\mathbf{S}_m \left(\mathbf{K_a} + \sigma^2 \mathbf{I}\right) \mathbf{S}_m^H\right]^{-1} && (4.13)\\
&= \mathbf{S}_m \left(\mathbf{K_a} + \sigma^2 \mathbf{I}\right)^{-1} \mathbf{S}_m^H && (4.14)\\
&= \mathbf{S}_m \mathbf{K}_c^{-1} \mathbf{S}_m^H && (4.15)
\end{aligned}$$

where $\mathbf{K}_c$ is defined as the channel correlation matrix, and is the correlation matrix of the received signal when $\theta_m = 0$. Note from the above that the dependence on m of the receiver's decision kernel may be conveniently factored out of the decision variable expression. The expression for $\mathbf{K}_\mathbf{r}^{m^{-1}}$ may then be written as,

$$\mathbf{K}_\mathbf{r}^{m^{-1}} = \mathbf{K}_c^{-1} \otimes \begin{bmatrix} \mathbf{1} & e^{-i\theta_m}\mathbf{1} \\ e^{i\theta_m}\mathbf{1} & \mathbf{1} \end{bmatrix} \tag{4.16}$$

where $\otimes$ is the Hadamard product, giving element by element multiplication, and $\mathbf{1}$ is an $N \times N$ square matrix with elements all of 1. The second matrix is seen to act as a multiplicative mask on the inverse channel covariance matrix. Once the inverse covariance matrix of the channel is given or estimated, the M individual decision variable kernels may be computed straightforwardly.

Comparing the above to the analysis of Appendix B for the specialized receiver, we see that we are performing an almost identical inversion of the received signal's covariance matrix in calculating the optimal decision variables. However, we previously assumed that the channel process had already been decomposed into its K-L components over one symbol interval. This leads to the simplified structure of the decision kernel given in (B.64), with the upper and lower diagonal bands arising from the single symbol decomposition, and the use of a single correlation coefficient, ρ, between symbols. Although the simple structure of the covariance matrix leads to closed form expressions for the receiver performance, the calculation of the K-L coefficients is left implicit in the analysis. Here we will work directly with the time sampled received data vector, $\mathbf{r}$, and its covariance matrix, $\mathbf{K}_\mathbf{r}^m$. As shown in Chapter 3, the conventional receiver may be placed in a similiar quadratic form.

4.3 A Theorem Useful in Evaluating Receiver Performances

In order to analyze the performance of general receivers in Rayleigh fading channels, we make use of a theorem given in [40], which allows the simultaneous diagonalization of two Hermitian matrices, one of which must be positive definite. Given an indefinite Hermitian quadratic form of the complex Gaussian vector, $\mathbf{u}$,

$$\ell = \mathbf{u}^H \mathbf{Q} \mathbf{u} \tag{4.17}$$

where $\mathbf{u}$ has the positive definite covariance matrix,

$$\overline{\mathbf{u}\mathbf{u}^H} = \mathbf{\Sigma}, \tag{4.18}$$

there exists a transformation matrix, $\mathbf{T}$, with $\mathbf{v} = \mathbf{T}\mathbf{u}$, such that,

$$\ell = \mathbf{v}^H \mathbf{\Gamma} \mathbf{v} \tag{4.19}$$

and,

$$\overline{\mathbf{v}\mathbf{v}^H} = \mathbf{I} \tag{4.20}$$

where $\mathbf{\Gamma}$ is an indefinite real diagonal matrix, which from the following, is shown to be a function of the eigenvalues of the correlation matrix, $\mathbf{\Sigma}$.

Forming the eigen-decomposition of the positive definite matrix $\mathbf{\Sigma}$, one obtains,

$$\mathbf{\Phi}^H \mathbf{\Sigma} \mathbf{\Phi} = \mathbf{\Lambda} \tag{4.21}$$

where $\mathbf{\Phi}$ is the unitary matrix of eigenvectors, and $\mathbf{\Lambda}$ is the diagonal matrix of real, positive eigenvalues. Defining $\mathbf{P} = \mathbf{\Phi}\mathbf{\Lambda}^{-1/2}$, it is seen from the eigen-decomposition above that,

$$\mathbf{P}^H \mathbf{\Sigma} \mathbf{P} = \mathbf{I} \tag{4.22}$$

Then forming the eigen-decomposition of $\mathbf{P}^H \mathbf{Q} \mathbf{P}^{H^{-1}}$, results in,

$$\mathbf{\Theta}^H \mathbf{P}^H \mathbf{Q} \mathbf{P}^{H^{-1}} \mathbf{\Theta} = \mathbf{\Gamma} \tag{4.23}$$

where $\mathbf{\Theta}$ is the matrix of eigenvectors and $\mathbf{\Gamma}$ is a diagonal matrix of positive and negative eigenvalues. Now define the transformation matrix $\mathbf{T} = \mathbf{\Theta}^H \mathbf{P}^H$, and let $\mathbf{v} = \mathbf{T}\mathbf{u}$. It is straightforward to show then that the above theorem holds with the definitions given.

It is seen that the general quadratic form decision variables may be reduced to a canonical form, given by (4.19) and (4.20), which is a weighted sum of independent Chi-Square variables, each with 2 degrees of freedom.

4.4 Performance of Binary DPSK Receivers

This case was also analyzed by Barrett [28] where he derives a convenient algebraic expression for the binary receiver error performance through the use of residues. The approach taken here will yield identical results, but requires a numerical integration for its solution. However, this approach offers a route to calculating the performance of M-ary DPSK, which does not appear to be possible with Barrett's method.

In the optimal binary receiver, we form the two decision variables,

$$\ell_0 = \mathbf{r}^H \mathbf{K}_{\mathbf{r}}^{0^{-1}} \mathbf{r} \tag{4.24}$$

$$\ell_\pi = \mathbf{r}^H \mathbf{K}_{\mathbf{r}}^{\pi^{-1}} \mathbf{r} \tag{4.25}$$

where the minimum variable is the maximum likelihood decision, and 0 corresponds to zero phase shift between symbol intervals, and π to a phase shift of 180° between symbol intervals. Thus, the receiver decision kernels are given by,

$$\mathbf{K}_{\mathbf{r}}^{0^{-1}} = \mathbf{K}_c{}^{-1} \tag{4.26}$$

$$\mathbf{K}_{\mathbf{r}}^{\pi^{-1}} = \mathbf{K}_c{}^{-1} \otimes \begin{bmatrix} 1 & -1 \\ -1 & 1 \end{bmatrix} \tag{4.27}$$

Assuming a zero phase shift was transmitted, the covariance matrix of $\mathbf{r}$ is given by $\mathbf{K}_c$, and an error occurs when the random variable $\Delta\ell \equiv (\ell_\pi - \ell_0) < 0$. The receiver may then be cast in the form,

$$\Delta\ell = \mathbf{r}^H \mathbf{K}_\Delta \mathbf{r} \tag{4.28}$$

where we define,

$$\mathbf{K}_\Delta = \mathbf{K}_{\mathbf{r}}^{\pi^{-1}} - \mathbf{K}_{\mathbf{r}}^{0^{-1}} \tag{4.29}$$

Note that although $\mathbf{K}_{\mathbf{r}}^{\pi}$ and $\mathbf{K}_{\mathbf{r}}^{0}$ are positive definite Hermitian matrices, as are their inverses, the *difference* between their inverses, $\mathbf{K}_\Delta$, will generally not be positive definite, although it will be Hermitian. Its eigenvalues will be real, but be allowed to be negative as well as positive. It is these negative eigenvalues of the decision variables kernel that correspond to errors in the receiver's decisions.

In order to evaluate the performance of the optimal receiver, the theorem of Section 4.3 is used, where we identify,

$$\boldsymbol{\Sigma} = \mathbf{K}_c \tag{4.30}$$

$$\mathbf{Q} = \mathbf{K}_\Delta \tag{4.31}$$

Then a statistically equivalent quadratic form to (4.28) is given by,

$$\Delta\ell = \mathbf{v}^H \mathbf{\Gamma} \mathbf{v} \tag{4.32}$$

where,

$$\overline{\mathbf{v}\mathbf{v}^H} = \mathbf{I} \tag{4.33}$$

$$\overline{\mathbf{v}} = \mathbf{0} \tag{4.34}$$

Since $\mathbf{\Gamma}$ is a real diagonal matrix of positive and negative values, the decision variable $\Delta\ell$ is reduced to a weighted sum of i.i.d. unit variance complex Gaussian random variables. The conventional receiver may be put into an identical form, where we now use the decision kernel,

$$\mathbf{A} = \begin{bmatrix} \mathbf{0} & \mathbf{I} \\ \mathbf{I} & \mathbf{0} \end{bmatrix} \tag{4.35}$$

rather than $\mathbf{K}_\Delta$, and an error similarly occurs when the decision variable is less than zero. Once the diagonal matrix $\mathbf{\Gamma}$ has been evaluated, the pdf of the canonical form may be numerically integrated, as described by Imhof [41], to calculate the error performance of binary receivers. Note that the binary case leads to a single, real decision variable, whose sign determines whether an error has been made or not. The general M-ary case will be examined in the next section.

4.4.1 A Geometric Interpretation of Binary Receivers in a Fading Channel

The previous section's discussion on reducing the decision variable of a binary DPSK receiver in Rayleigh fading to a canonical form may also be interperated geometrically. Note that (4.32) defines a boundry, $\Delta\ell = 0$, between an error and no error in the space of transformed random variables. This boundary has the shape of a $4N$ dimensional cone, where N is the number of samples per symbol. Although this is similar to the signal space description of a conventional receiver in AWGN, i.e. error regions are defined and the probability of error is the integral of a Gaussian distribution within that region, Equation (4.32) is based entirely on the theorem of Section 4.3 and the analogy between the two should not be examined too closely. This view of the receiver's operation, however, does make the analysis of the previous section more plain, as simple cases may be solved for analytically, and the qualitative behaviour of the receiver follows clearly as the channel parameters are varied. An example is given here for a conventional binary differential receiver. The optimal receiver may be similarly evaluated, with the matrix $\mathbf{A}$ below replaced by the optimal kernel $(\mathbf{K}_\pi - \mathbf{K}_0)$.

Assuming 1 sample per symbol, the receiver uses a quadratic kernel of the form,

$$\mathbf{A} = \begin{bmatrix} 0 & 1 \\ 1 & 0 \end{bmatrix} \tag{4.36}$$

for its decision variable, with the sign of the calculated variable determining the decision of the receiver. Assuming no phase shift between symbols, so that $\Delta\ell < 0$ corresponds to a receiver error, the received signal has a correlation matrix of the form,

$$\Sigma = \begin{bmatrix} \sigma_f^2 + \sigma_n^2 & \rho\sigma_f^2 \\ \rho\sigma_f^2 & \sigma_f^2 + \sigma_n^2 \end{bmatrix} \tag{4.37}$$

where σ_n^2 is the additive white noise variance, σ_f^2 is the fading channel variance, and ρ is the correlation between symbol intervals. In addition, we assume that the received signal has a non-zero mean, specular component of magnitude K. Performing the diagonalization of the decision variable as described in (4.17) –(4.20) results in an expression for the decision variable in terms of independent, unit variance complex Gaussian random variables,

$$\Delta\ell = \left(\sigma_n^2 + (1+\rho)\sigma_f^2\right)|v_1|^2 - \left(\sigma_n^2 + (1-\rho)\sigma_f^2\right)|v_2|^2 \tag{4.38}$$

where we have the correlation,

$$\overline{\begin{bmatrix} v_1 \\ v_2 \end{bmatrix} \begin{bmatrix} v_1^* & v_2^* \end{bmatrix}} = \begin{bmatrix} 1 & 0 \\ 0 & 1 \end{bmatrix} \tag{4.39}$$

and the corresponding mean values are given by,

$$\begin{bmatrix} \overline{v}_1 \\ \overline{v}_2 \end{bmatrix} = \begin{bmatrix} \frac{\sqrt{2}K}{\sqrt{\sigma_n^2 + (1+\rho)\sigma_f^2}} \\ 0 \end{bmatrix} \tag{4.40}$$

Note that each v may be decomposed into its real and imaginary parts, so that $|v|^2 = (\Re v)^2 + (\Im v)^2$. In order to illustrate the basic geometry, we suppress one component of each of the two v's, to give a 2 dimensional view, shown in Figure 4.4. The decision boundary of the receiver, corresponding to $\Delta\ell = 0$, forms a 2 dimensional cone centred on

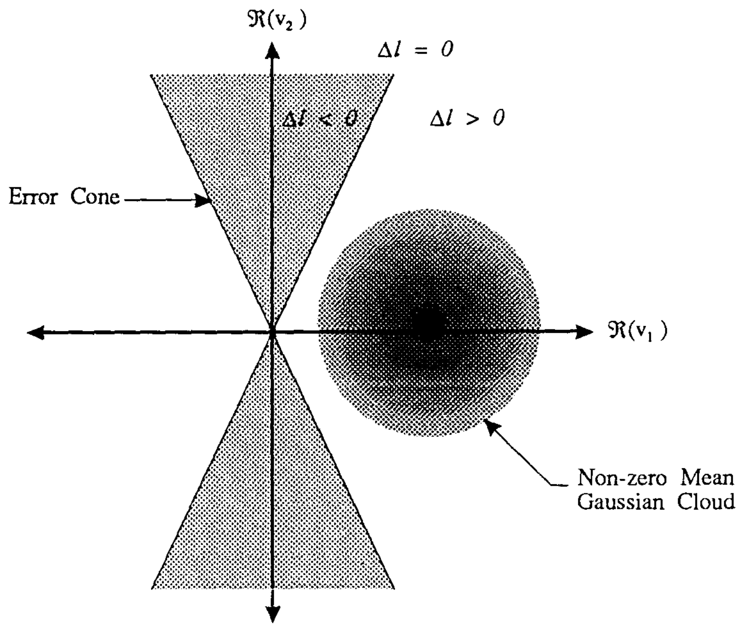

Figure 4.4: Sketch of the decision boundries of a differential binary receiver in a fading channel with a receiver sampling rate of 1 sample per symbol.

the origin, with sides of slope,

$$m_{cone} = \pm\sqrt{\frac{\sigma_n^2 + (1+\rho)\sigma_f^2}{\sigma_n^2 + (1-\rho)\sigma_f^2}} \tag{4.41}$$

The random variables v_1 and v_2 form a unit variance, non-zero mean, spherical Gaussian cloud of possible signal realizations.

This somewhat abstract view of a receiver operating in a fading channel demonstrates the essential behaviour of a conventional receiver as the channel parameters are varied. For example, setting $K = 0$ places the center of the Gaussian cloud at the origin and corresponds to a purely Rayleigh fading channel. As the noise variance, σ_n^2, is then decreased for a fixed channel variance, the slope of the cone's sides is seen to increase, decreasing the area corresponding to an incorrect decision. As $\sigma_n^2 \rightarrow 0$, we reach the asymptotic slope, $\pm\sqrt{(1+\rho)/(1-\rho)}$, leaving a finite error area. This corresponds to the error floor in a conventional receiver, and its value may be calculated by integrating the Gaussian cloud over the full 4-dimensional error cone. As well, varying ρ is seen to change both the error area and the Gaussian cloud's mean. Letting $\rho \rightarrow 1$, corresponding to a perfectly correlated channel with no time selectivity, is seen to eliminate the asymptotic slope as $\sigma_n^2 \to 0$, with $m_{cone} \to \pm\infty$. Letting $\rho \to 0$, corresponding to completely uncorrelated fading between the symbols, leads to an error cone with sides of slope ± 1 which takes up half of the signal plane. For a channel with no specular component, this gives an error rate of 1/2, as would be expected in differential signalling.

As well, setting $\sigma_f^2 = 0$ and keeping a specular component, which is just the standard AWGN channel, the error cone again occupies half of the signal plane. For a fixed K, then, the position of the unit variance Gaussian cloud is dependent on the variance of additive noise, so that the amount of overlap between the fixed size Gaussian cloud and constant error areas changes only with the position of the cloud. This is different from, but still equivalent to, the standard signal space view where the position of the Gaussian cloud is fixed and its *variance* changes with the additive noise power. Again, these examples are intended more to illustrate the principle behind the canonical reduction and how it agrees with the known operation of receivers in fading channels.

Although generalizing to N samples per symbol and including the imaginary components of the Gaussian cloud to yield a $4N$ dimensional cone, will change the particulars of this example, it should not change the overall behaviour.

As well, this figure is curiously similar to the light-cone of special relativity, where $\Re v_1$ and $\Re v_2$ correspond to the time and space coordinates, the diagonalized kernel of (4.38) corresponds to the Lorentz metric, and $\Delta\ell$ is the proper distance from the origin [42]. It is unclear if viewing a decision variable as a distance in a non-Euclidean plane offers any advantages, however, it is somewhat surprising to see it arise in the analysis of fading channels.

4.4.2 Example Calculations of Binary DPSK Receiver Performance

This section provides an example calculation and typical theoretical performance curves of conventional and optimal binary DPSK receivers. In the following examples, time-bandwidth products of $BT = \{0.16, 0.08, 0.04\}$ will be used for the fading channel process, and the number of baseband samples per symbol period will be set to values of 2, 4, or 8. Finite duration, square pulses are assumed, with no bandlimiting due to the channel considered. As well, the receiver is assumed to have perfect symbol timing.

After generating an appropriate set of L FIR filter taps, corresponding to the channel fading process, the theoretical correlation function of the sampled channel process, across two symbol intervals, is calculated using the formula,

$$r(k) = \sum_{i}^{L-k} b_i b_{i+k}; \quad k = 0, 1, \ldots \tag{4.42}$$

where k is the correlation delay, $\{b_i\}$ is the set of filter taps, and L is the number of filter taps, typically chosen here to be a few hundred in size. The symmetric, Toeplitz correlation matrix of the fading process, $\mathbf{K_a}$, is then generated from the correlation vector, with the $\pm k$'th diagonal having the value $r(k)$, where $k = 0$ corresponds to the main diagonal.

The total channel correlation matrix, $\mathbf{K_c}$, is given as described before as, $\mathrm{K_a} + \sigma_n^2\mathbf{I}$, where σ_n^2 is the variance of the additive white Gaussian noise. The correlation function of the additive noise is thus assumed to have the form,

$$\begin{aligned} R_n(\tau) &= \mathcal{N}_0\delta(\tau) &(4.43)\\ &= \sigma_n^2\delta(\tau) &(4.44)\end{aligned}$$

where $\mathcal{N}_0$ is the double sided (i.e. positive and negative frequencies included) power spectral density of the additive noise, in units of [W/Hz]. Assuming unit amplitude transmitted pulses, i.e. unit transmitted power, the average received signal energy per symbol is given by $n_{sb}\sigma_f^2$, where n_{sb} is the number of samples taken over one symbol interval, and $\sigma_f^2 = r(0)$ is the variance of the stationary fading process. The additive white noise power spectral density, in units of $(Energy/Time)/Hertz = Energy$, is $\mathcal{N}_0 = \sigma_n^2$. Thus, the average-received-signal-energy—to—noise-power-spectral-density ratio is defined as [3],

$$SNR = \frac{n_{sb}\sigma_f^2}{\sigma_n^2} \tag{4.45}$$

Assuming equiprobable binary signalling and using the conventional and optimal receiver kernels described in the previous section, the probability of symbol error may be straightforwardly calculated using the techniques described previously.

Figure 4.5[1] shows the theoretical performance curves of a conventional BDPSK receiver operating under the various time-bandwidth products and sampling rates. Qualitatively the behaviour is as expected. The larger BT products, corresponding to faster, less correlated fading processes, yield larger error floors. As well, it is observed that as the fading process becomes more correlated, the closer the initial slope in the performance curve

[1]Note that in this chapter and the next, all performance curves were evaluated at SNR intervals of 5 dB, with linear interpolation used between the data points.

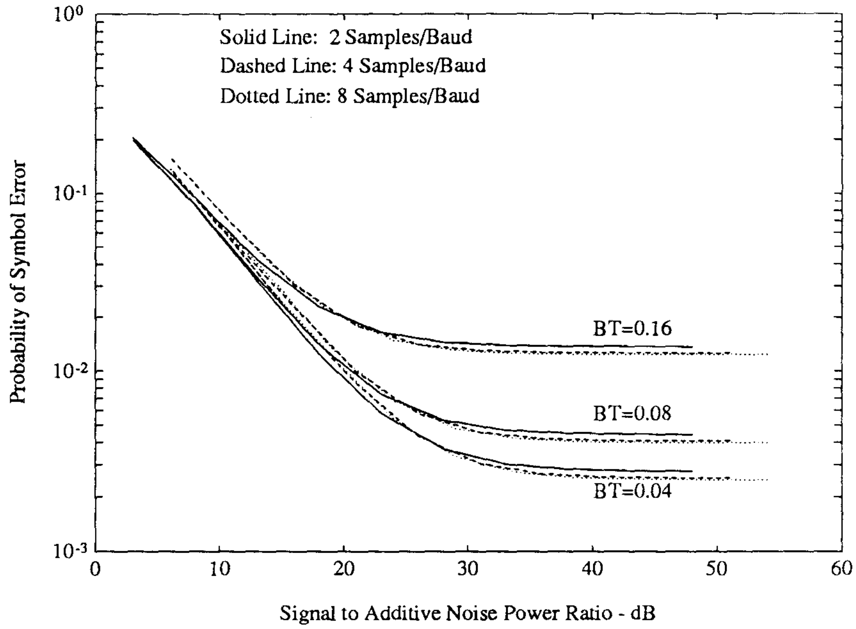

Figure 4.5: Performance of a conventional BDPSK receiver in a fading channel under various channel fading rates and receiver sampling rates.

approaches the expected of -1 decade/10 dB. A less correlated channel process decreases the magnitude of the initial slope.

The observed error floors also agree closely with the theoretical one-sample-per-symbol formula, $P_e = \frac{1-\rho}{2}$ [4]. The values of ρ for the different channels and the expected asymptotic error rates are shown in Table 4.1. There is a very close agreement with the theoretical multi-sampling results derived in this chapter, and the more approximate one-sample-per-symbol values.

BT	ρ	P_e
0.16	0.96410	1.80e-2
0.08	0.98830	5.85e-3
0.04	0.99268	3.66e-3

Table 4.1: Theoretical asymptotic error floors at 1 sample per symbol for BDPSK under various channel fading rates.

The sampling rate is also seen to play a role in the performance of the receiver, with two observable regimes. At high SNR's where we are operating in the error floor, increased sampling yields a slightly lower error floor, which appears to reach an asymptotic limit. This is consistent with the theoretical evaluation of Section 4.3, where the spectrum of the eigenvalues of the fading process was seen to determine the asymptotic performance of a continuous time receiver. The floor was seen to decrease as more of the eigenvalues were included in the evaluation, with the exponential tailing of the spectrum to zero producing a similar asymptotic limit in the error floor as a function of the number of resolved eigenvalues.

At lower SNR values the relationship between sampling and the error performance seems to be reversed, with higher sampling rates yielding slightly worse performance. This may be due to numerical precision problems. In the numerical procedures described in the previous section, the low additive noise is seen to create a large portion of eigenvalues closely equal in magnitude, but opposite in sign. In order to obtain reasonable results with the numerical precision available, a judicious number of the smallest balancing positive and negative eigenvalues are simply zeroed. The remaining set of eigenvalues provide a reasonable performance curve, but the truncation required at the higher sampling rates may distort these curves somewhat.

Figure 4.6 shows the theoretical performance of an optimal BDPSK receiver, operating with knowledge of the the statistics (i.e. correlation matrix) of the fading channel process, for a fixed fading time-bandwidth product of $BT = 0.08$ and number of samples per symbol interval equal to 2, 4, and 8. It is seen that within the SNR range shown, the error floor for a conventional receiver, exhibited in Figure 4.5, has been eliminated. Again, increasing the sampling rate is seen to slightly improve the receiver performance asymptotically. This was examined closer for the case of a channel with a fading rate of $BT = 0.16$, and sampling of $n_{sb} = \{2, 4, 8, 16, 32, 64\}$. It was found that $n_{sb} = 8$ provides virtually the full sampling gain. The gains in going from $n_{sb} = 2$ to $n_{sb} = 16$ at a symbol error rate of 10^{-4} are given in Table 4.2. The incremental gains for $n_{sb} = 32$ and $n_{sb} = 64$ are negligible.

Figure 4.7 shows the performance curves of an optimal BDPSK receiver sampling at 4 samples per symbol, at various fading channel time-bandwidth products. Although there are some differences in the curves, the receiver is seen to be fairly invariant to the channel fading characteristics. This is further seen in Figure 4.8, where all 9 of the evaluated performance curves are superimposed on the same graph.

Although the optimal receiver performance curves show the elimination of the error

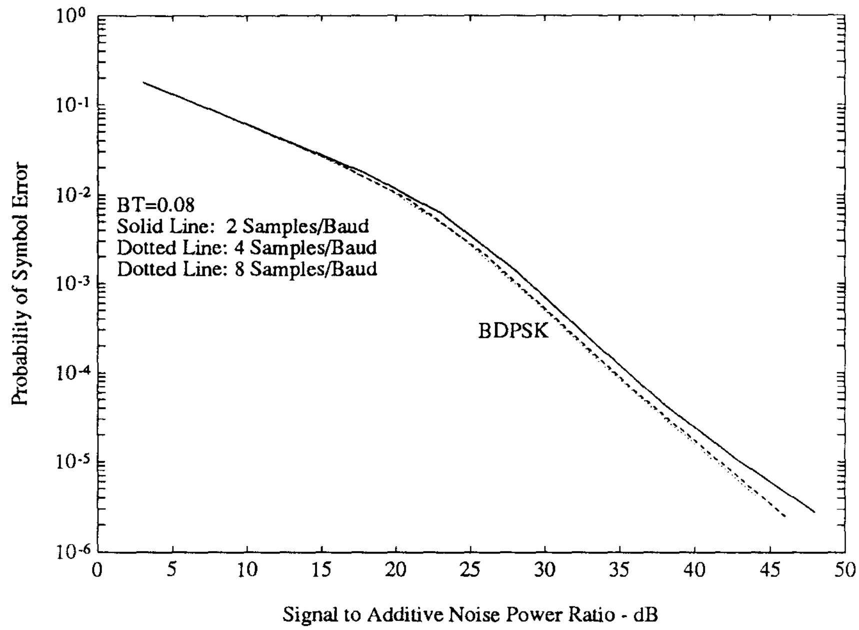

Figure 4.6: Theoretical performance of an optimal BDPSK receiver in a fading channel at various sampling rates. $BT = 0.08$, $n_{sb} = \{2, 4, 8\}$.

n_{sb}	$Gain(dB)$
$2 \rightarrow 4$	1.15
$2 \rightarrow 8$	1.38
$2 \rightarrow 16$	1.44

Table 4.2: Gains in SNR at $P_e = 10^{-4}$ for various sampling rates in a fading channel with BT=0.16

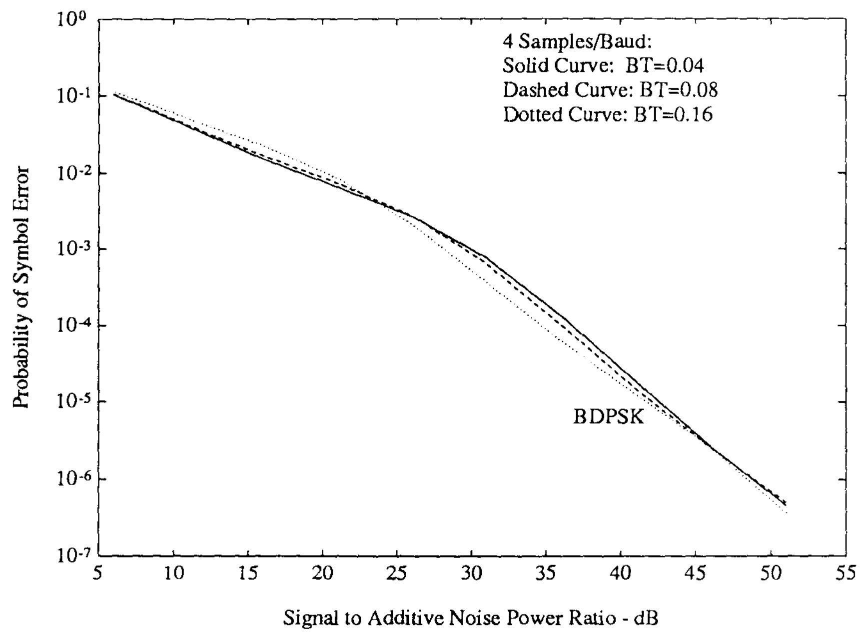

Figure 4.7: Theoretical performance of an optimal BDPSK receiver in a fading channel at various fading rates. $n_{sb} = 4$, $BT = \{0.16, 0.08, 0.04\}$

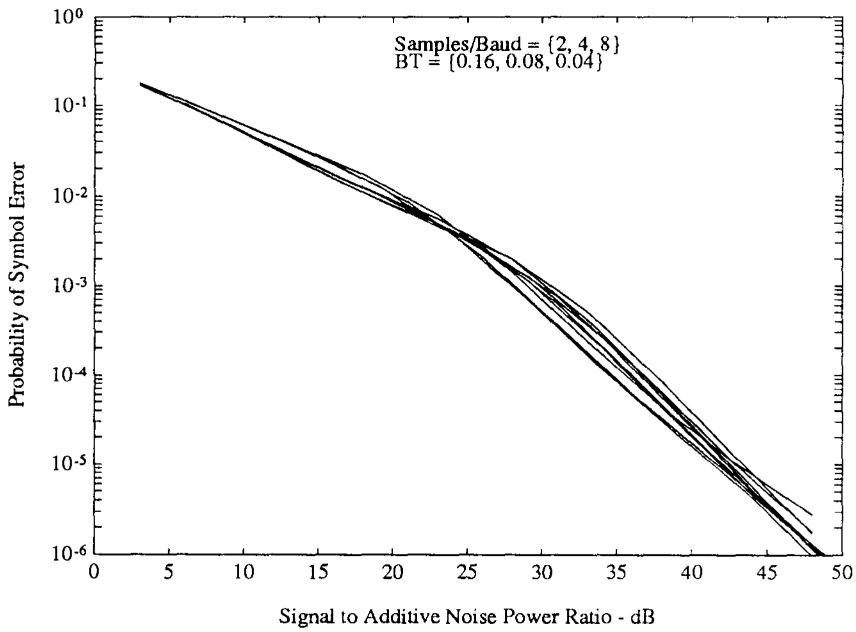

Figure 4.8: Superposition of the performance curves of an optimal BDPSK receiver at various channel fading rates and receiver sampling rates. $BT = \{0.16, 0.08, 0.04\}$, $n_{sb} = \{2, 4, 8\}$

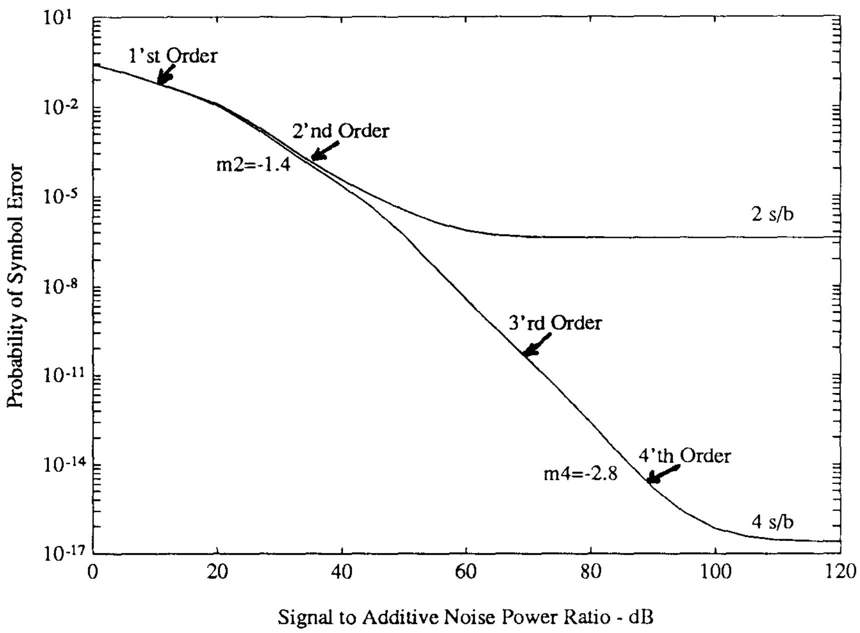

Figure 4.9: Extended performance curves of optimal BDPSK in a fading channel. $n_{sb} = \{2, 4\}$, $BT = 0.16$. Also shown are its diversity regimes and maximum slopes.

floor at reasonable SNR values, an error floor still exists for finite sampling, or equivalently a finite number of resolved eigenvalues. Figure 4.9 shows the extended performance curves of an optimal receiver, at sampling rates of 2 and 4 samples per symbol, and with a channel time-bandwidth product of $BT = 0.16$. As expected, a higher sampling rate lowers the error floor, although this is not apparent until extremely high signal-to-noise ratios. Figure 4.10 shows the relation between the asymptotic error floor and the number of samples taken per symbol interval, again for a channel with $BT = 0.16$. An asymptotic leveling off in the performance curve is seen. A comparison of this curve, normalized to the error floor at 1 sample per symbol, is made with the normalized eigenvalue spectrum of the fading process in Figure 4.11. The spectrum is evaluated from the correlation matrix of the process over two symbol periods, at 16 samples per symbol. Since each sample per symbol yields two eigenvalues, the spectrum contains 32 eigenvalues in total.

There appears to be a close relation between the asymptotic error and the eigenvalue spectrum of the fading channel. This is not unexpected, since as discussed in Chapter 2, and noted by Kennedy [3], the optimal receiver is exploiting the diversity implicit in the fading

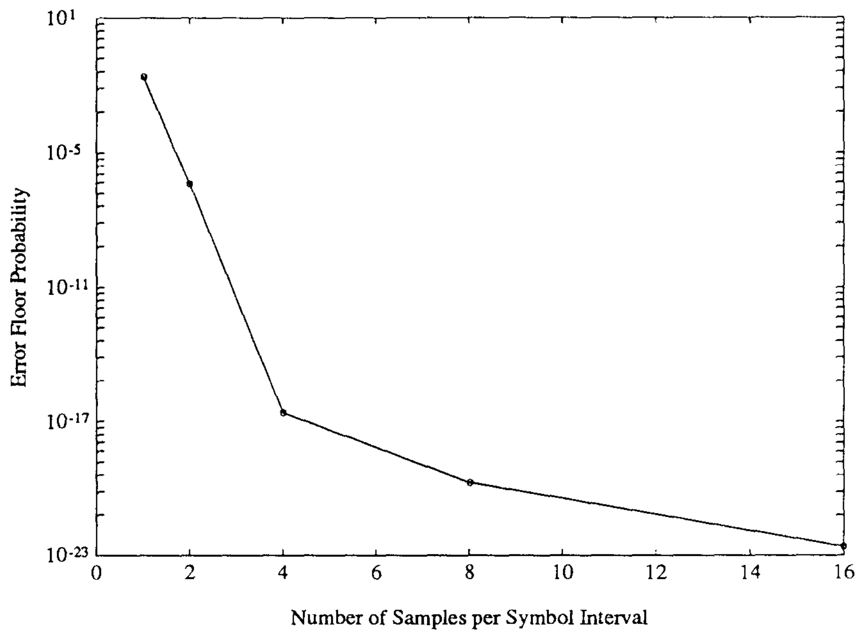

Figure 4.10: Asymptotic error floor of an optimal BDPSK receiver in a fading channel with $BT = 0.16$, as a function of the sampling rate.

channel. Although higher sampling rates provide more of the implicit diversity paths, these paths have much smaller energies — proportional to the higher order eigenvalues. It seems reasonable that if the incremental energies of additional diversity paths are progressively smaller, their incremental contributions to the receiver performance will likewise be smaller. This is the pattern shown in Figure 4.11. This behaviour is also consistent with that seen in Section 4.1 for the specialized channel.

As discussed in [4], higher order explicit diversity will also steepen the symbol-error-rate performance curves of a conventional receiver which combines the independently received signals optimally. Application of this to the implicit diversity of a fading channel is also discussed in [3]. For the logarithmic plots used here, the slope of a fully correlated channel's performance should be $-M$ decade/10 dB, where M is the order of the diversity. As an example, Figure 4.12 shows the theoretical performances of a conventional receiver with no diversity, operating in a perfectly correlated channel, and in a channel with a correlation between symbols of $\rho = 0.9555$. This corresponds to a time bandwidth product of $BT = 0.16$ in the calculations. Although the perfectly correlated performance curve is

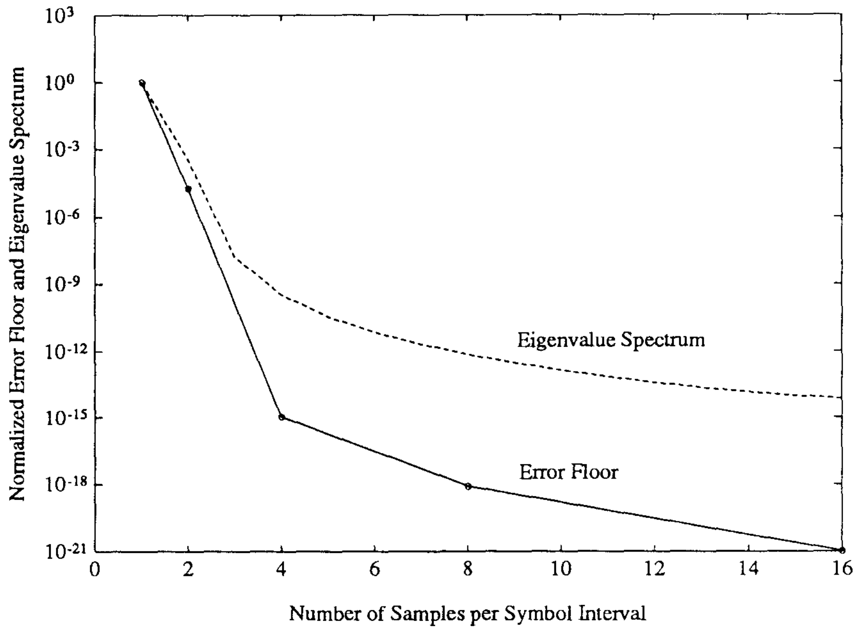

Figure 4.11: Plot of the normalized relationship between the the asymptotic error floor of the optimal BDPSK receiver and the eigenvalue spectrum of the channel fading process.

seen to achieve its expected asymptotic slope of -1 decade/10 dB, the partially correlated curve only manages to achieve a slope of -0.65 decade/10 dB before leveling out in the error floor.

Figure 4.9 shows the optimal performance curves for 2 and 4 samples per symbol in the same channel. Note that the 2 sample per symbol curve shows two distinct linearly sloped segments with increasing SNR before tailing into the error floor, while the 4 sample per symbol curve shows four. For the optimal receiver, the number of samples per symbol corresponds to the number of implicit diversity paths resolved by the receiver, with each path having a signal energy equal to an eigenvalue of the correlation function over one symbol interval. The additive white Gaussian noise is simply a second random variable, with a constant variance equal to σ_n^2, added to each path. At very low SNR's, the large additive noise energy submerges the higher order diversity paths with very low energies (i.e. small eigenvalues), and there is effectively only a single path. The other paths supply only irrelevant AWGN. As the SNR is increased, the other paths will emerge from the noise one by one as the eigenvalues increase in value relative to the noise variance. The point of

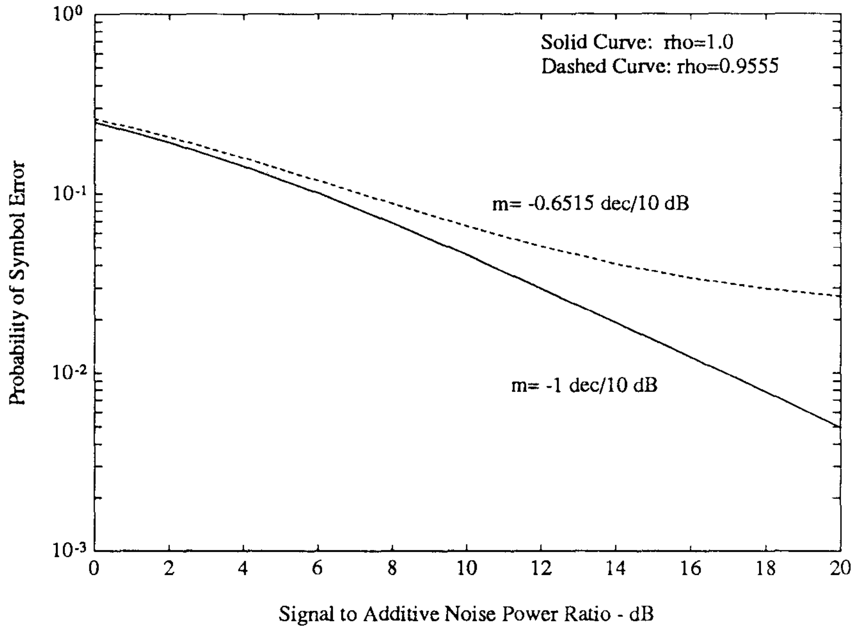

Figure 4.12: Error performance curves of a conventional, one sample per symbol, differential receiver operating in perfectly correlated and partially correlated fading channels.

emergence may be loosely defined as the point at which the energy of the noise equals the fading energy of the diversity path, i.e. $2\sigma_n^2 = \lambda_i$. The total received SNR is given by,

$$SNR_{tot} = \frac{\sum_i \lambda_i}{2\sigma_n^2} \tag{4.46}$$

$$\approx \frac{\lambda_0}{2\sigma_n^2} \tag{4.47}$$

where it is reasonably assumed that the eigenvalue spectrum rapidly falls off. This is valid for the fairly slow, narrow bandwidth correlated fading of mobile channels. The SNR of the i'th diversity path is similarly given by,

$$SNR_i = \frac{\lambda_i}{2\sigma_n^2} \tag{4.48}$$

The value of the total received SNR *at the point of emergence of the i'th path*, is then simply,

$$SNR_{tot}^i = \frac{\lambda_0}{\lambda_i} \tag{4.49}$$

As an example for the 4 sample per symbol curve, the normalized eigenvalue spectrum of the fading process over one symbol, and the corresponding path emergence SNR's,

λ_i	$SNR^i_{tot}(dB)$
1.0000e+00	0
7.3589e-3	21.3
1.5360e-5	48.1
1.1436e-8	79.4

Table 4.3: Estimated sequence of SNR's where the optimal receiver switches to a higher order of effective diversity operation.

	$BT = 0.16$	$BT = 0.08$	$BT = 0.04$
Turnover SNR	22.5 dB	27.4 dB	29.4 dB

Table 4.4: Estimated values of SNR where the optimal receiver switches from first to second order effective diversity operation.

are given in Table 4.3. These expected values of the total received SNR at which each additional diversity path should manifest itself, shows very good agreement with Figure 4.9.

As well, the eigenvalue spectra of the fading process' over one symbol period at 4 samples per symbol were calculated for each of the three channels of Figure 4.7. As discussed in the previous section, the second eigenvalues give the values of SNR where the 2'nd order diversity manifests itself, and are given in Table 4.4. These curves and their expected breakpoint SNR's are also shown in Figure 4.13 as vertical lines. It is seen that the curves for each fading rate turnover in the expected order and reasonably close to the tabulated SNR's. Note that the definition of the breakpoint signal-to-noise ratio is rather arbitrary, and really only defines a *region* of expected increase in received diversity. The exact placement of the lines is intended mainly for illustration. The thresholding effect exhibited here does not seem to have been mentioned previously in the literature [43].

The fraction of the diversity utilized by the receiver is also interesting. The maximum magnitude of the slope achieved for 2 samples per symbol is -1.39 decade/10 dB, at about 35 dB, while for 4 samples per symbol, it is -2.84 decade/10 dB, at about 90 dB. For 1, 2, and 4 samples per symbol, this corresponds to the receiver achieving 0.65, 0.70, and 0.71 of the total available diversity respectively, before tailing off into the error floor.

The ability of the optimal receiver to resolve the implicit diversity of a time selective fading channel is made apparant in the above, and results in measurable effects on the

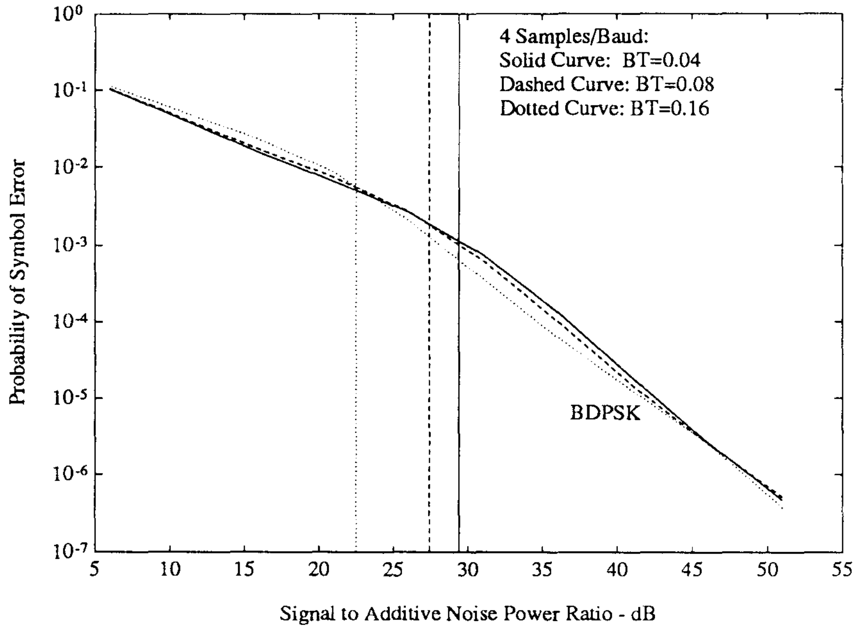

Figure 4.13: Expected breakpoint SNR's in the performance curves of an optimal BDPSK receiver at a fixed sampling rate and various channel time-bandwidth products. The vertical lines correspond to the breakpoint SNR's for each BT product.

performance curves of the receiver. However, the very high SNR's at which this occurs, at least for square pulse shapes, does not make these effects noticeable beyond the second order diversity regime for typical mobile channels. Nonetheless, we are in the position of being able to choose the pulse shapes for the signalling, and from (4.9), this is seen to affect the eigenvalue spectrum of the received signals, and thus the receiver's performance. It may be possible to select a pulse shape that will sufficiently whiten the eigenvalue spectrum of the received process for a range of channels to force the higher diversity regimes down to realistic SNR's [3, 44]. This will also affect the receiver error floor, as well as the transmitter spectrum, and needs to be examined more closely in order to balance conflicting design requirements.

4.5 Performance of M-ary DPSK Receivers

4.5.1 Conventional M-ary Receivers

The conventional M-ary DPSK receiver generates a complex decision variable from the received signal vector, which will be binned into one of the allowable signal sectors. The decision variable is given by,

$$\begin{aligned} \ell &= x_1^* y_1 + x_2^* y_2 + \cdots + x_N^* y_N && (4.50) \\ &= \mathbf{r}^H \mathbf{A} \mathbf{r} && (4.51) \end{aligned}$$

where $\mathbf{A}$ is given by,

$$\mathbf{A} = \begin{bmatrix} \mathbf{0} & \mathbf{0} \\ \mathbf{I} & \mathbf{0} \end{bmatrix} \tag{4.52}$$

and the covariance matrix of the received signal, assuming zero phase shift between symbols, is given by $\mathbf{K}_c$ as before. Unlike the binary case, the receiver kernel is not of full rank and the previous theorem cannot be directly applied. However, the kernel $\mathbf{A}$ may be broken into the sum of a symmetric and antisymmetric matrix,

$$\begin{aligned} \mathbf{A} &= \mathbf{A}_s + \mathbf{A}_a && (4.53) \\ &= \frac{1}{2}\begin{bmatrix} \mathbf{0} & \mathbf{I} \\ \mathbf{I} & \mathbf{0} \end{bmatrix} + \frac{1}{2}\begin{bmatrix} \mathbf{0} & -\mathbf{I} \\ \mathbf{I} & \mathbf{0} \end{bmatrix} && (4.54) \end{aligned}$$

and the decision variable ℓ may be written,

$$2\ell = \mathbf{r}^H \mathbf{A}_s \mathbf{r} + \mathbf{r}^H \mathbf{A}_a \mathbf{r} \tag{4.55}$$

The theorem of Section 4.3 is then used to find a transformation matrix which will simultaneously diagonalize $\mathbf{K}_c$ and $\mathbf{A}_s$. This will not diagonalize $\mathbf{A}_a$, but will be seen to still put it in a useful form. The matrix $\mathbf{P}$ is generated from the eigen-decomposition of $\mathbf{K}_c$ as before, and the eigen-decomposition,

$$\Theta_s^H \left(\mathbf{P}^{-1}\mathbf{A}_s\mathbf{P}^{H^{-1}}\right)\Theta_s = \Gamma_s \tag{4.56}$$

is performed. Forming the transformation matrix $\mathbf{T} = \Theta_s^H\mathbf{P}^H$ and defining $\mathbf{z} = \mathbf{Tr}$, then the decision variable may be expressed as,

$$2\ell = \mathbf{z}^H\Gamma_s\mathbf{z} + \mathbf{z}^H\Theta_s^H\mathbf{P}^{-1}\mathbf{A}_a\mathbf{P}^{H^{-1}}\Theta_s\mathbf{z} \tag{4.57}$$

where

$$\overline{\mathbf{z}\mathbf{z}^H} = \mathbf{I} \tag{4.58}$$

Note that the second term in the expression for ℓ is not, in general, diagonal. However, it is antisymmetric, as can be shown by expanding the sum of the second term with its Hermitian conjugate, giving a null matrix. The decision variable has been effectively split into its real and imaginary parts, corresponding to the symmetric and antisymmetric terms of (4.55) respectively.

Recall in the binary case, where the decison variable was purely real, the pdf of the random variable, ℓ, could be integrated numerically [41]. However, in the case of M-ary DPSK, where ℓ is now complex, there does not seem to be available a method of calculating the pdf of the complex random variable, except for certain special cases. The utility of the above transformation, however, is that the quadratic form of the decision variables is now in terms of an uncorrelated, unit variance signal vector, $\mathbf{z}$. Thus, the pdf of the decision variable may be efficiently *estimated* through Monte Carlo techniques by generating a suitably large ensemble of decision variable realizations. The error rate is estimated by suitably binning the simulation results. Note that the effects of the pulse shape and spectrum of the channel fading process are considered only once in the evaluation of the eigen-decompositions. After the receiver decision variable has been reduced to its canonical form, sample realizations of the receiver's decisions are straightforward to generate, and the random Gaussian variables need only be generated once and stored for future calculations. The symmetry and sparseness of the form can also be used to reduce the number of calculations required by 25% over the full evaluation of the matrix products.

4.5.2 Optimal M-ary Receivers

The procedure used in evaluating the performance of optimal receivers is very similar to that for the conventional receivers described in the previous section. For the conventional receiver, we had a singular kernel which was broken into its two symmetric and asymmetric matrix components. One of these components was then diagonalized in conjunction with the correlation matrix of the received signal vector. Here we now have a set of decision variable kernels, where, again, one kernel will be diagonalized in conjunction with the signal correlation matrix. The set of decision variables over which we choose the minimum, is given by,

$$\ell_m = \mathbf{r}^H \mathbf{K}_{\mathbf{r}}^{m^{-1}} \mathbf{r}; \;\; m = 0, \ldots, M-1 \tag{4.59}$$

If we assume zero phase change, the decision kernel corresponding to the symbol transmitted, has the form $\mathbf{K}_c^{-1}$. Using the canonical reduction of the decision variables, it is straightforward to show that the decision variables are given by,

$$\begin{aligned} \ell_m &= \mathbf{z}^H \mathbf{P}^{-1} \mathbf{K}_{\mathbf{r}}^{m^{-1}} \mathbf{P}^{H^{-1}} \mathbf{z} && (4.60) \\ &= \mathbf{z}^H \mathbf{P}^{-1} \mathbf{S}_m \mathbf{K}_c{}^{-1} \mathbf{S}_m^H \mathbf{P}^{H^{-1}} \mathbf{z} && (4.61) \\ &\equiv \mathbf{z}^H \mathbf{Q}_m \mathbf{z} && (4.62) \end{aligned}$$

where $\mathbf{Q}_m$ is defined as the m'th canonical receiver kernel. Assuming $m = 0$ corresponds to zero phase shift, then $\mathbf{Q}_0$ simplifies as,

$$\begin{aligned} \mathbf{Q}_0 &= \mathbf{P}^{-1} \mathbf{K}_c{}^{-1} \mathbf{P}^{H^{-1}} && (4.63) \\ &= \mathbf{\Gamma}^{1/2} \mathbf{\Phi}^H \mathbf{K}_c{}^{-1} \mathbf{\Phi} \mathbf{\Gamma}^{1/2} && (4.64) \\ &= \mathbf{\Gamma}^{1/2} \mathbf{\Gamma}^{-1} \mathbf{\Gamma}^{1/2} && (4.65) \\ &= \mathbf{I} && (4.66) \end{aligned}$$

Again, the correlation matrix of the transformed received signal vector, $\mathbf{z}$, is the identity matrix. As in the conventional M-ary receiver, this canonical transformation allows an efficient Monte Carlo determination of the receiver performance.

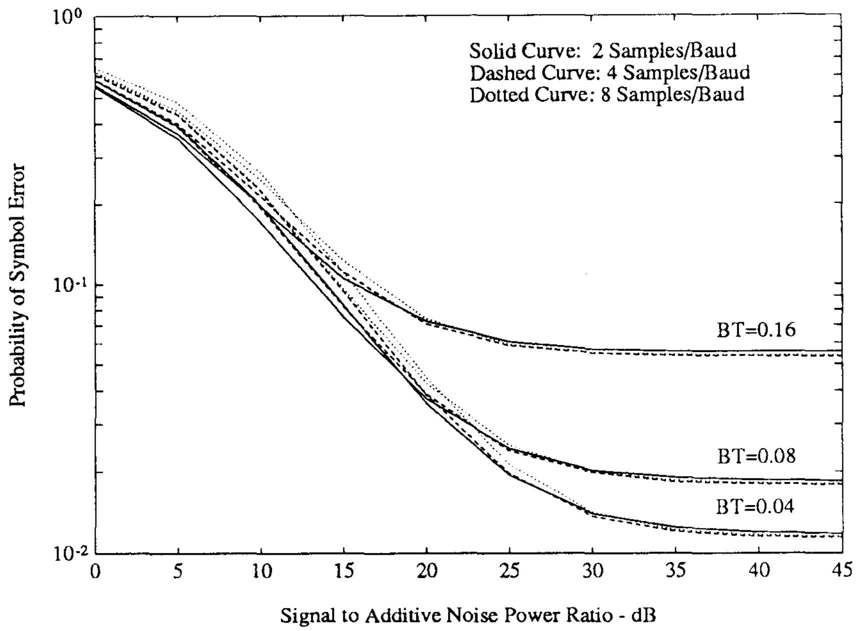

Figure 4.14: Theoretical performance curves of a conventional QDPSK receiver operating in various channel fading and receiver sampling rates.

4.5.3 Example Calculations of M-ary Receiver Performance

In this section we will show some typical theoretical performance curves for QDPSK signalling in a Rayleigh fading channel, using both conventional and optimal receiver structures. This will parallel Section 4.3 for the most part, using the same channels and concluding with the same general results. After the receiver has been reduced to canonical form, as described in the previous section, the theoretical performance is evaluated using Monte Carlo simulation to estimate the decision variables' probability distributions. Between 1,000 - 10,000 error events per data point were used to be able to accurately resolve differences between the error curves. Because of the extent to which the error floors in the optimal receiver are lowered, they were not able to be resolved within reasonable computation time here. However, the theoretical performance curves are evaluated over the range of SNR's found in realistic channels.

Figure 4.14 shows the theoretical performance curves of a conventional QDPSK receiver under various channel operating conditions. The same general performance as in BDPSK is observed, with the error rates shifted slightly higher for QDPSK due to the closer

BT	ρ	P_e
0.16	0.96410	6.16e-2
0.08	0.98830	2.09e-2
0.04	0.99268	1.32e-2

Table 4.5: Theoretical asymptotic error floors at 1 sample per symbol for QDPSK under various channel fading rates.

spacing of the signalling constellation. The observed error floors can be checked against the theoretical value calculated in Appendix B for one sample per symbol QDPSK,

$$P_e = \frac{3}{4} - \frac{\rho}{\sqrt{2-\rho^2}} + \frac{\rho}{\pi\sqrt{2-\rho^2}} \arctan \frac{\sqrt{2-\rho^2}}{\rho} \tag{4.67}$$

As shown in Table 4.5, there is good agreement between the theoretical multi-sampling results and the single sample per symbol values.

Figure 4.15 shows the performance of optimal receivers for BDPSK and QDPSK in a channel with $BT = 0.16$ and with varying number of samples per symbol. Again the error floor is greatly reduced, and the two performance curves parallel each other closely, with $\sim$ 6 dB separation between them. Asymptotic performance gains with the sampling rate are observed to be similar to those for BDPSK. The slight variations in the theoretical QDPSK curves, due to the Monte Carlo estimation technique used, prevented investigating the sampling gain as was done for the binary signalling case. However, the gains seen in the QDPSK curves seem to be roughly comparable to those of the binary curves. The gains reported earlier appear to be typical, regardless of the fading rate and order of DPSK modulation.

Figure 4.16 shows the performance curves of the optimal receivers for BSPSK and QDPSK at a fixed sampling rate of 4 samples per symbol, and under varying channel fading rates. The QDPSK curves again parallel the previously computed BDPSK curves quite closely, showing the same general perturbations of the curves with fading rate. Although it would be interesting to continue the curves to sufficiently high SNR's so as to resolve the residual error floor, as in the BDPSK analysis, the error rates involved would be far too low to be evaluated by the proposed Monte Carlo scheme. However, the close correspondence between the results of the two signalling schemes at the SNR's considered here lead one to expect similar behaviours for the asymptotic error floors.

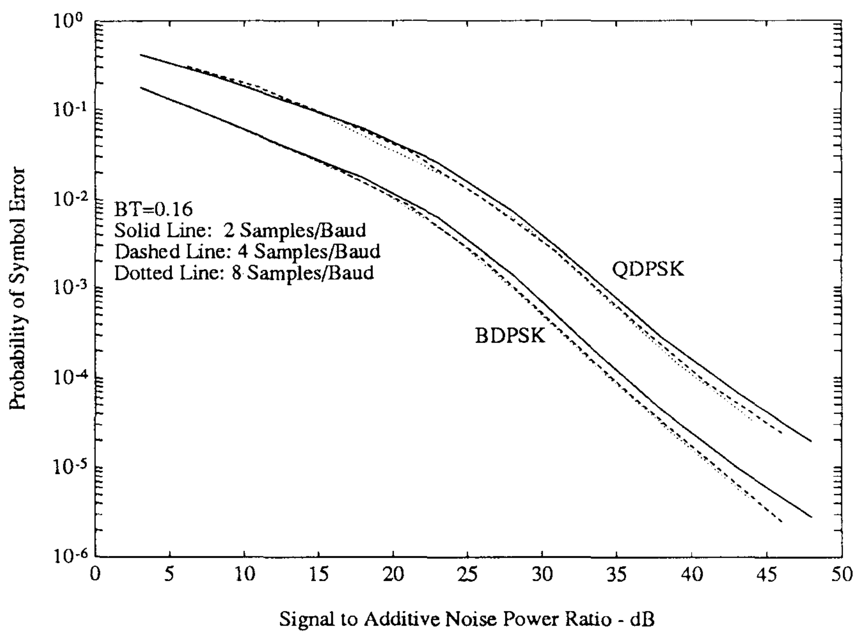

Figure 4.15: Theoretical performance of optimal BDPSK and QDPSK receivers in a fading channel at various sampling rates. $BT = 0.16$, $n_{sb} = \{2, 4, 8\}$

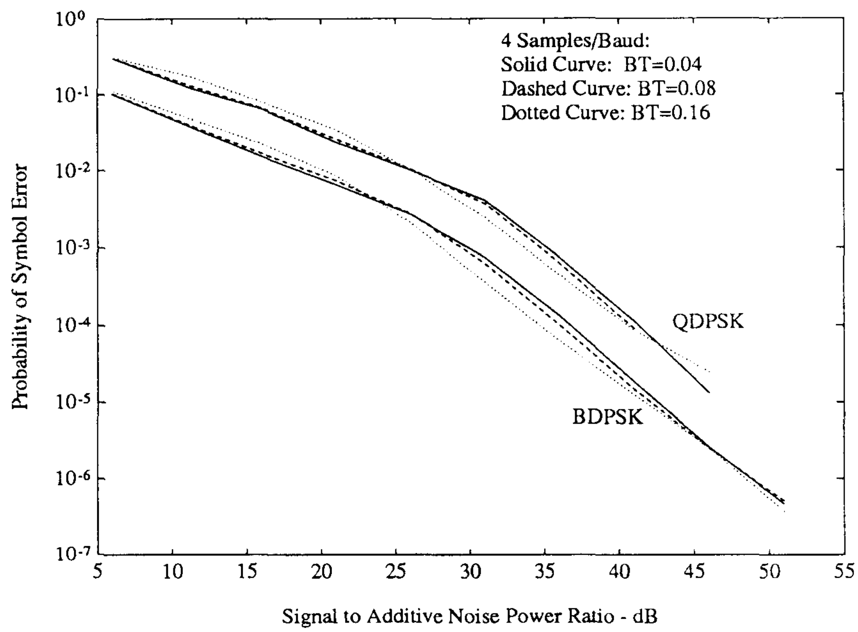

Figure 4.16: Theoretical performance of optimal BDPSK and QDPSK receivers in various fading channels, at a fixed sampling rate. $BT = \{0.16, 0.08, 0.04\}$, $n_{sb} = 4$.

4.6 Interpretation of the Operation of Optimal Receivers

4.6.1 Analytic Development

The previous sections examined the performance of conventional and optimal DPSK receivers in a fading channel, where Kaila th's estimator-correlator interpretation of the optimal receiver's operation follows directly from the discussion of Chapter 3. In brief, the optimal receiver generates from the received signal a set of minimum mean squared error estimates of the possible faded transmitted signals. These are based on the (assumed known) statistics of the fading process. The optimal decision is then the estimated message signal that is closest to, or most correlated with, the actual received signal process. Lodge [30, 29], in his discussion of optimal CPM receivers in Rayleigh fading channels, has made a similar interpretation where the optimal receiver minimizes the process prediction error of the various possible received signals based on the channel statistics.

However, the previous section's analysis of the optimal receiver's performance shows basically an inverse power relation of the error rate with SNR. This is curiously similar to the inverse relation shown by a conventional diversity receiver operating in a perfectly correlated fading channel. It is, therefore, interesting to transform the optimal receiver kernel and received signal correlation matrix into the form of an equivalent conventional receiver operating with a transformed signal correlation matrix such that the error rate is the same. This transformation would give us the *effective* statistics of the received signal using a conventional receiver, but with the performance of an optimal receiver. It may show the connection between the performance curves of the optimal receiver in partially correlated fading, and the conventional receiver in perfectly correlated fading. The effective correlation properties of the optimal receiver are separate from its ability to resolve and exploit the diversity implicit in the fading channel, as demonstrated in the previous section.

Here, we will examine only the binary case since it is tractable for analysis, and should still give the same general results as for higher order DPSK. From Section 4.4, the decision kernel is given by,

$$\mathbf{K}_{\Delta} = \mathbf{K}_{\mathbf{r}}^{\pi-1} - \mathbf{K}_{\mathbf{r}}^{0-1} \tag{4.68}$$

We then partition the correlation matrices,

$$\mathbf{K}_{\mathbf{r}}^{0} = \begin{bmatrix} \mathbf{R} & \mathbf{U} \\ \mathbf{U}^{H} & \mathbf{R} \end{bmatrix} \tag{4.69}$$

$$\mathbf{K}_{\mathbf{r}}^{\pi} = \begin{bmatrix} \mathbf{R} & -\mathbf{U} \\ -\mathbf{U}^{H} & \mathbf{R} \end{bmatrix} \tag{4.70}$$

where $\mathbf{R}$ is the $(N) \times (N)$ correlation matrix of the channel over one symbol period, and $\mathbf{U}$ is the $(N) \times (N)$ cross-correlation matrix of the channel between adjacent symbol intervals. Using the partitioned matrix inversion lemma [31], the inverses of the kernels may be written,

$$\mathbf{K}_{\mathbf{r}}^{0^{-1}} = \begin{bmatrix} \mathbf{R}^{-1} + \mathbf{R}^{-1}\mathbf{U}\boldsymbol{\Delta}^{-1}\mathbf{U}^{H}\mathbf{R}^{-1} & -\mathbf{R}^{-1}\mathbf{U}\boldsymbol{\Delta}^{-1} \\ -\boldsymbol{\Delta}^{-1}\mathbf{U}\mathbf{R}^{-1} & \boldsymbol{\Delta}^{-1} \end{bmatrix} \tag{4.71}$$

$$\mathbf{K}_{\mathbf{r}}^{\pi^{-1}} = \begin{bmatrix} \mathbf{R}^{-1} + \mathbf{R}^{-1}\mathbf{U}\boldsymbol{\Delta}^{-1}\mathbf{U}^{H}\mathbf{R}^{-1} & \mathbf{R}^{-1}\mathbf{U}\boldsymbol{\Delta}^{-1} \\ \boldsymbol{\Delta}^{-1}\mathbf{U}\mathbf{R}^{-1} & \boldsymbol{\Delta}^{-1} \end{bmatrix} \tag{4.72}$$

where,

$$\boldsymbol{\Delta} \equiv \mathbf{R} - \mathbf{U}^{H}\mathbf{R}^{-1}\mathbf{U} \tag{4.73}$$

Thus, the receiver decision kernel may be written,

$$\mathbf{K}_{\Delta} = \begin{bmatrix} \mathbf{0} & 2\mathbf{R}^{-1}\mathbf{U}\boldsymbol{\Delta}^{-1} \\ 2\boldsymbol{\Delta}^{-1}\mathbf{U}^{H}\mathbf{R}^{-1} & \mathbf{0} \end{bmatrix} \tag{4.74}$$

where the two non-zero anti-diagonal partitions are the Hermitian conjugate of each other.

Now, writing the kernel in terms of the eigen-decomposition of the upper right partition, we have formally,

$$\begin{aligned}
\mathbf{K}_{\Delta} &= \begin{bmatrix} \mathbf{0} & \boldsymbol{\Theta}\boldsymbol{\Lambda}\boldsymbol{\Theta}^{-1} \\ \boldsymbol{\Theta}^{-1^{H}}\boldsymbol{\Lambda}^{H}\boldsymbol{\Theta}^{H} & \mathbf{0} \end{bmatrix} && (4.75) \\
&= \begin{bmatrix} \boldsymbol{\Theta} & \\ & \boldsymbol{\Theta}^{-1^{H}} \end{bmatrix} \begin{bmatrix} \boldsymbol{\Gamma}^{1/2} & \\ & \boldsymbol{\Gamma}^{H^{1/2}} \end{bmatrix} \begin{bmatrix} \mathbf{0} & \mathbf{I} \\ \mathbf{I} & \mathbf{0} \end{bmatrix} \begin{bmatrix} \boldsymbol{\Gamma}^{H^{1/2}} & \\ & \boldsymbol{\Gamma}^{1/2} \end{bmatrix} \begin{bmatrix} \boldsymbol{\Theta}^{H} & \\ & \boldsymbol{\Theta}^{-1} \end{bmatrix} && (4.76) \\
&\equiv \boldsymbol{\Phi}^{H}\tilde{\boldsymbol{\Gamma}}^{H} \begin{bmatrix} \mathbf{0} & \mathbf{I} \\ \mathbf{I} & \mathbf{0} \end{bmatrix} \tilde{\boldsymbol{\Gamma}}\boldsymbol{\Phi} && (4.77)
\end{aligned}$$

Defining the transformation $\mathbf{z} = \tilde{\boldsymbol{\Gamma}}\boldsymbol{\Phi}\mathbf{r}$, then the optimal receiver decision variable may be written,

$$\begin{aligned}
\ell &= \mathbf{r}^{H}\mathbf{K}_{\Delta}\mathbf{r} && (4.78) \\
&= \mathbf{z}^{H}\mathbf{A}_{s}\mathbf{z} && (4.79)
\end{aligned}$$

where $\mathbf{A}_s$ is the symmetric conventional binary receiver kernel previously defined. The correlation matrix of the transformed received signal vector, $\mathbf{z}$, is given by,

$$\overline{\mathbf{z}\mathbf{z}^H} = \tilde{\mathbf{\Gamma}}\mathbf{\Phi}\mathbf{K_r}\mathbf{\Phi}^H\tilde{\mathbf{\Gamma}}^H \tag{4.80}$$

where it is assumed that no phase shift was transmitted.

It is seen that the optimal receiver has been cast into the form of a conventional receiver, with the received signal vector similarly transformed such that the performance is equivalent. The statistics of the equivalent received signal vector are given by (4.80). Note that the above derivation is simply a recipe for transforming the receiver into a desired equivalent form. In the following, the matrix inversions and eigen-decompositions will be evaluated numerically for specific channel correlation matrices.

4.6.2 Examples

We will first examine the case of extremely fast fading with no additive noise, with a time-bandwidth product of $BT = 1.5$, and $n_{sb} = 2$ samples per symbol interval. An appropriate set of FIR filter taps corresponding to the low pass fading process is generated, and gives the correlation vector over 2 symbols as,

1.0000e+00	3.0415e-01	-2.1295e-01	9.7453e-02

The eigenvalues of the corresponding normalized correlation matrix of the process are given by,

1.0000e+00
9.9096e-01
7.9407e-01
2.0310e-01

Note that over the period of a symbol interval, the channel fading process has a very low correlation, reflecting the very fast rate of the fading. This is also indicated in the eigenvalue spectrum, where the four eigenfunctions are excited with almost equal energies by the process. This is similar to white noise, where all of the eigenfunctions are equally excited.

Performing the transformation of the optimal receiver for this channel to the equivalent conventional differential receiver, the correlation matrix of the corresponding received signal vector is given by,

5.8789e-02	9.1598e-02	-1.0515e-03	5.6525e-02
9.1598e-02	1.9031e+00	-5.6525e-02	1.2097e+00
-1.0515e-03	-5.6525e-02	6.3114e-02	-9.8337e-02
5.6525e-02	1.2097e+00	-9.8337e-02	2.0432e+00

and the eigenvalues of the correlation matrix by,

1.0000e+00
2.3919e-01
1.8412e-02
1.6821e-02

Note that the correlation matrix of the equivalent process is no longer Toeplitz, and corresponds to a non-stationary Gaussian process. The eigen-decomposition of the equivalent transformed process shows a significant change from the original channel process in its implicit diversity; the normalized eigenvalue spectrum of the equivalent process is considerably sharpened or peaked around the first eigenvalue. This corresponds to a much more correlated process, as fewer modes of the process are excited, and to a lesser degree.

If the above is repeated for the same channel except that 8 samples per symbol are now taken, the eigenvalue spectrum of the original channel process is,

1.0000e+00
9.6542e-01
6.9889e-01
2.1835e-01
2.2835e-02
1.0071e-03
2.1775e-05
2.8092e-07

while the spectrum of the equivalent transformed process is,

1.0000e+00
1.6471e-03
1.3092e-05
5.4093e-07
3.3247e-07
2.7431e-07
1.0369e-07
2.2878e-08

It is seen that the sharpening of the eigenvalue spectrum for the equivalent conventional receiver is greatly enhanced over the 2 sample per symbol case. Although this could be continued for higher sampling rates, the filter used to model the channel fading process does not support enough significant eigenvalues in its output process to prevent the matrices involved in the calculations from approaching singularity. At sampling rates higher than 4 samples per symbol, numerical precision begins to be a problem in evaluating the matrix operations. However, the previous results suggests that the optimal receiver acts as though it were a conventional receiver operating in a fading channel which is much more correlated than the original channel. As more samples of the process are taken in infinite precision, the effective eigenvalue spectrum sharpens to a delta function, and corresponds to a perfectly correlated channel process. This needs to be shown rigorously, however.

A second example is shown here for a more realistic, much slower fading case of $BT = 0.08$ at 2 samples per symbol. The normalized correlation function of the process is now,

1.0000e+00	9.9093e-01	9.6410e-01	9.2056e-01

The process is seen to be much more correlated across a symbol interval than in the previous example. The corresponding eigenvalue spectrum of the process is,

1.0000e+00
2.2629e-02
1.0286e-04
1.4906e-07

As expected, this slower, more correlated fading process has a much narrower eigenvalue spectrum than the fast process examined previously. Solving for the equivalent conventional receiver fading process, we find an eigenvalue spectrum of,

1.0000e+00
3.2137e-05
5.2937e-07
5.9025e-07

Again, the spectrum is narrower and the fading process for the equivalent conventional receiver is seen to be much more correlated than the original channel fading process.

The above provides a useful interpretation of the optimal receiver's actions on the received signal process. In performing the maximum likelihood detection of the transmitted symbol, the receiver is effectively making the multiplicative random fading process much more correlated, or deterministic. As shown in formulae derived by Voelcker [11] and in the previous chapter, the more correlated the fading, i.e. as $\rho \to 1$ in the previous chapter, the lower the error floor becomes in a conventional receiver.

This doesn't mean that in the limit of a single effective eigenvalue the fading trajectory is straightened out to a constant line in time; only that is it now a constant function — the first eigenfunction of the channel — scaled by a complex random variable, with a variance equal to single eigenvalue of the fading process. However, the receiver has knowledge of this function, and the multiplication by the constant (non-zero) function is reversible. This is in contrast to usual narrow band random processes, where, as they become perfectly correlated in the limit, their eigen-spectrum narrows to a delta function. The first eigenfunction of these low pass processes is always the DC offset, i.e. a constant value in time. In general, it may be any arbitrary function.

Chapter 5

Simulation Results

5.1 General Form of a Practical System

The maximum likelihood receiver discussed in the previous chapter utilizes the decision variables,

$$\ell_m = \mathbf{r}^H \mathbf{K}_m^{-1} \mathbf{r} \tag{5.1}$$

$$\ell_m = \mathbf{r}^H \mathbf{S}_m \mathbf{K}_c^{-1} \mathbf{S}_m^H \mathbf{r} \tag{5.2}$$

where $m = 0, \ldots, M-1$, and the channel correlation matrix, $\mathbf{K}_c$, is given by,

$$\mathbf{K}_c = \mathbf{K_a} + \mathbf{K_n} \tag{5.3}$$

This defines the optimal receiver structure, shown in the dotted box of Figure 5.1, where the correlation matrix of the channel, $\mathbf{K}_c$, is assumed to be known a priori. Although the optimal DPSK receiver has significant theoretical performance advantages over conventional DPSK, as discussed in the previous chapter, it requires knowledge of the (Gaussian) statistics of the fading channel process. The conventional receiver, on the other hand, utilizes no knowledge of the channel, and correspondingly has a much simpler structure.

Knowledge of the channel statistics is not an uncommon requirement in optimal systems, however. A receiver operating even in a simple additive Gaussian noise channel requires similar knowledge to make optimal decisions. If the additive noise is coloured, the correlation function is no longer a delta function and the optimal receiver structure, formulated in terms of the eigenvalues of the correlation function of the noise, is seen to

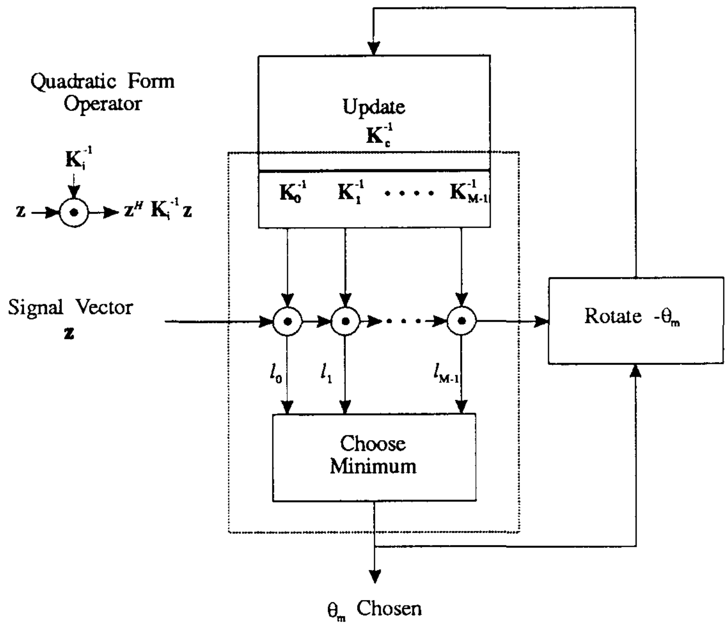

Figure 5.1: Structure of the adaptive maximum likelihood receiver. The dotted box denotes the non-adaptive, a-priori maximum likelihood portion of the receiver.

perform a simple whitening of the spectrum [2]. Thus, optimal decisions require knowledge of the noise spectrum, or equivalently the correlation function of the noise, or channel.

A similar problem occurs in linear minimum mean squared error (MSE) or Weiner filtering, which has application in channel equalization [45, 37]. In brief, an adaptive equalizer recursively solves the equation,

$$\mathbf{R}\mathbf{w} = \mathbf{p} \tag{5.4}$$

for the unknown tap weight vector $\mathbf{w}$, where $\mathbf{R}$ is the covariance matrix of the received signal, and $\mathbf{p}$ is the cross correlation vector between the desired signal and the received signal vector. That is, $\mathbf{w} = \mathbf{R}^{-1}\mathbf{p}$. The solution requires the channel correlation matrix, $\mathbf{R}$, which is generally unknown to the receiver in advance.

By defining a dummy variable $\mathbf{y}$ for the Rayleigh receiver, such that $\mathbf{K}_m\mathbf{y} = \mathbf{r}$, and then solving for $\mathbf{y}$, the decision variable ℓ may be placed in the form $\ell = \mathbf{r}^H\mathbf{y}$, where the inverse of $\mathbf{K}_m$ is used implicitly in the solution for $\mathbf{y}$. Note the similarity of the equation defining $\mathbf{y}$ and Equation (5.4) defining the optimal tap weights of an adaptive equalizer.

Both the equalizer and the Rayleigh receiver use the inverse of an estimated channel covariance matrix to calculate a quantity that may may interpreted as a tap weight vector. Lodge[30, 29] has carried this approach further to show that the $\mathbf{y}$ above is essentially acting as a set of predictor filter taps, and ℓ_m is the predictor error, assuming symbol m was transmitted. Although this work is specific to continuous phase modulation (CPM), the resulting optimal receiver has many similarities to the optimal DPSK case.

The previous discussion assumes the receiver has prior knowledge of the channel correlation matrix. However, a practical system must be able to *estimate* this matrix from the received signals, perhaps with an initial training sequence. In order to provide the adaptivity of the system necessary in non-stationary, but slowly varying channels, the symbol decisions may be used in a feed-back loop to undo the transmitted signal's phase shifts on the received signal vector. These unshifted vectors of $2N$ sample snapshots may then be used to update the estimate of the channel correlation matrix. The general structure of the receiver is shown in Figure 5.1.

In practice, the required inverse of the correlation matrix may be updated directly by recursion, as in a recursive least squares (RLS) algorithm [37]. Although the conventional $\mathcal{O}(N^2)$ version based on the matrix inversion lemma [45] may be used, it is susceptible to numerical stability problems when the correlation matrix is nearly singular [46, 47] as it is in slow fading channels. This holds as well for certain "fast" $\mathcal{O}(N)$ forms of the algorithm. However, algorithms based on Givens-QR decompositions and singular value decompositions have been shown to have improved stability in these situations [47]. The condition number (i.e. ratio of the largest and smallest eigenvalues) of the matrix involved in these algorithms is the square root of that used in the conventional algorithm. In addition, a fast, $\mathcal{O}(N)$ version of the numerically stable Givens algorithm has recently been developed [48].

Note that at the expected mobile channel data rates of less than 10 kilo-baud and sampling rates of 8 samples/symbol, the receiver should be able to be implemented using commercially available DSP technology. The initial convergence time of the RLS algorithm at moderate SNR's is approximately twice the snap shot size [37], or 4 symbol periods, allowing very short initialization and retraining sequences. In addition, a conventional differential receiver may have a sufficiently low error rate to initially allow a decision fed-back estimate of $\mathbf{K}_c$ to be made. If a conventional receiver experiences an asymptotic error of 10^{-2}, for example, then the probability of having 5 consecutive symbols demodulated correctly is 0.95. After the estimate has been generated, the maximum likelihood algorithm could be engaged. A single error event in the sequence of 5 may still provide an estimate of the correlation matrix inverse close enough to true matrix to allow convergence. This would be a useful fall back or restart mode of operation in the case of a temporary loss of signal, or when training sequences are not available.

The least squares implementation of the receiver adaptivity also suggests the use of slower converging, but simpler to implement gradient descent algorithms[37]. However, their sensitivity to the eigenvalue spread of the correlation matrix, and in particular, their very slow convergence rates for nearly singular channels [37], may make them unsuitable for the mobile channel.

The detailed description of the ML receiver is deliberately left somewhat open here since there are several possible algorithmic approaches to implementing it, depending on the specific design constraints. The situation is quite similar in the design of adaptive equalizer structures. The important point is that in order to perform maximum likelihood reception the optimal receiver requires only the channel correlation matrix, which may be estimated from the received signals, and then must use this matrix in the solution of a linear set of equations. This chapter is intended to demonstrate the feasability of a practical, adaptive, real-time system using this approach. The next sections describe the particular form of receiver used in the simulations and its performance compared to theoretical expectations.

5.2 Description of the Simulation

This section briefly describes the simulation used to check the theoretical calculations of performance for conventional and optimal receivers derived in the previous chapter. Only binary and 4-phase DPSK are simulated, which should be sufficient to suggest the system's general behaviour for higher order DPSK. All simulations were performed in single precision floating point arithmetic on a NUMERIX 432 array processor, rated at 30 MFLOPs. For the range of error rates evaluated, run times of typically a few minutes to a day were required to generate a performance curve, depending on the sampling rate and form of receiver simulated.

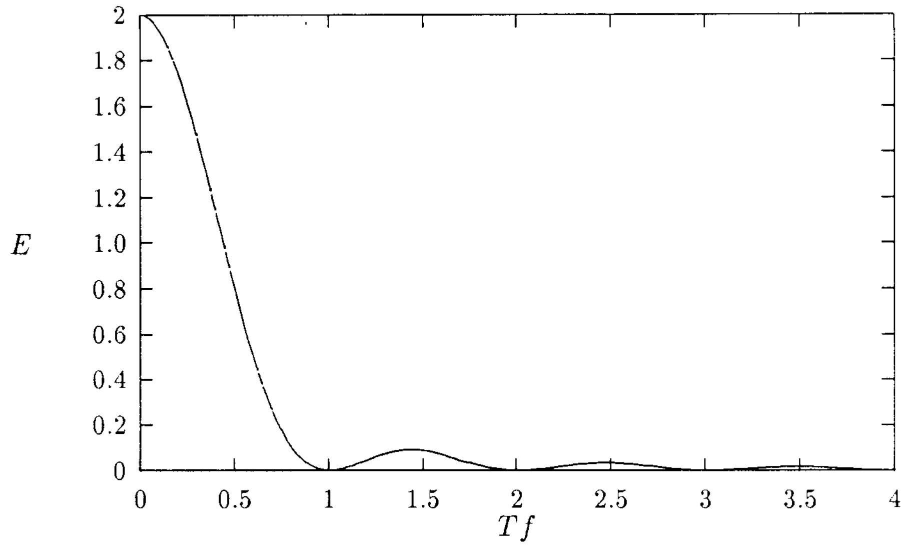

Figure 5.2: Power spectral density of phase shift keying modulation.

5.2.1 Description of the Transmitter

The baseband pulse shapes, $u(t)$, used in the DPSK signalling are assumed to be square pulses,

$$\begin{aligned} |u(t)| &= \sqrt{\frac{E}{T}} \; ; \; 0 \leq t \leq T \\ &= 0 \; ; \; \text{otherwise} \end{aligned} \tag{5.5}$$

where E is the symbol energy, and T is the symbol period. The power spectral density of equi-probable symbol, general M-ary PSK, is given by [49],

$$S(f) = \frac{2E\sin^2(\pi Tf)}{(\pi Tf)^2} \tag{5.6}$$

$$= 2E\text{sinc}^2(Tf) \tag{5.7}$$

and shown in Figure 5.2. The transmitted signals were sampled at a fixed rate of 8 samples per symbol. By the Nyquist theorem, the spectrum of the sampled signals are folded over at twice the sampling rate. Examining Figure 5.2 shows that this should lead to an acceptable overlap of the duplicated spectra, which is supported by the simulation results. The actual baseband pulses transmitted are thus of the form $u(t) = \sqrt{E/T}e^{i\theta_m}$, where $\theta_m \in \{0, \pi\}$ or $\theta_m \in \{0, \pi/2, \pi, 3\pi/2\}$ for binary and QDPSK respectively.

5.2.2 Description of the Channel

The channel was simulated as a single multiplicative tap followed by an additive white Gaussian noise source as discussed as in Chapter 2. The multiplicative random process was generated by low pass filtering a sequence of i.i.d. random Gaussian variables, with the characteristic bandwidth of the filter chosen according to the fading time-bandwidth parameter being investigated. This was done by convolving the random sequence with a set of 257 FIR filter taps. The filter size was chosen to balance the need for acceptable computation time and a reasonably sharp 3 dB low pass cutoff at the Doppler frequency. The original transmitted signal pulses were chosen to have unity amplitude, with the variance of the additive Gaussian noise set according to the level of SNR being simulated. Dynamic changes in the fading rate were not considered.

5.2.3 Description of the Receiver

In the previous analyses it was assumed that the receiver has perfect symbol timing. This is continued into the simulations and although it is less than realistic, it should still demonstrate the basic feasibility of the receiver structure. When the 8 sample-per-symbol signal is received from the channel portion of the simulation, it is sub-sampled at a receiver rate of 2, 4, or 8 samples per symbol. Using a fixed channel sampling rate, rather than adjusting it to match the receiver rate allows a single channel fading filter to be used for all of the receiver's sampling rates. This provides a fair comparison of the effects of the receiver sampling rate on performance for the same fading channel.

The general form of the receiver is shown in Figure 5.1, where it is assumed that the receiver has some form of estimate of the inverse of the channel correlation matrix, $\mathbf{K}_c^{-1}$. This estimate is initially formed from a cold start of the receiver through the use of a known training sequence. Once a channel estimate has been made, a set of M quadratic form kernels corresponding to the set of M possible received message signals is generated, as per Equation 5.1. The received signal vector, i.e. the set of samples of the received process over two symbol intervals, is then folded into each of the M quadratic operators simultaneously. The minimum of the M decision scalars is then used to select the corresponding symbol as the message that was received. Based on this decision the assumed phase shift between the two symbol intervals is then reversed on the actual received signal vector, and the unshifted version of the vector is used to update the channel correlation matrix.

The inverse of the channel correlation matrix is updated recursively, on a sample by sample basis using the conventional RLS algorithm — an update algorithm based on the matrix inversion lemma [45]. This was chosen since it is well known and can provide a standard bench-mark against other algorithms. It's known instability for nearly singular correlation matrices also provides a worst-case comparison against other more robust algorithms, as discussed previously. These more desirable algorithms were not tested in this thesis, however, due to time constraints.

Designating the unshifted version of the received signal vector as $\bar{\mathbf{r}} = \mathbf{S}_n^H \mathbf{r}$, where n is the maximum likelihood symbol decision, the direct recursive update of the correlation matrix itself may be written as,

$$\hat{\mathbf{K}}_c(i) = \lambda \hat{\mathbf{K}}_c(i-1) + \bar{\mathbf{r}}(i)\bar{\mathbf{r}}(i)^H \tag{5.8}$$

where λ is an exponential "forgetting factor" useful in non-stationary environments, and set to 1 for these simulations. Here, the variable i stands for the sample instant, and the length of the vector $\bar{\mathbf{r}}(i)$ is $2N$. Defining the inverse of the correlation matrix as $\mathbf{P}(i) = \hat{\mathbf{K}}_c^{-1}(i)$, the update of the *inverse* of the correlation matrix may be written [45],

$$\mathbf{k}(i) = \frac{\lambda^{-1}\mathbf{P}(i-1)\bar{\mathbf{r}}(i)}{1 + \lambda^{-1}\bar{\mathbf{r}}(i)^H \mathbf{P}(i-1)\bar{\mathbf{r}}(i)} \tag{5.9}$$

$$\mathbf{P}(i) = \lambda^{-1}\mathbf{P}(i-1) - \lambda^{-1}\mathbf{k}(i)\bar{\mathbf{r}}(i)^H \mathbf{P}(i-1) \tag{5.10}$$

where $\mathbf{k}(i)$ is an intermediate vector, often termed the Kalman gain vector. The initial state of the inverse correlation matrix, $\mathbf{P}(0)$, is set to,

$$\mathbf{P}(0) = \delta^{-1}\mathbf{I};\ \delta \ll 1 \tag{5.11}$$

In the simulations, δ was set to 10^{-10}. Each update in the conventional algorithm takes $16N^2 + 4N$ multiply and divides, and $12N^2 - 2N + 1$ additions and subtractions.

Note that the update of the correlation matrix inverse is about one symbol behind the current received symbol since a full symbol must be received, and a decision on the received message made, before the required phase shifting is performed on the received signal. Only then can the correlation matrix inverse be updated. Although the recursion was performed on a sample by sample basis in the simulations, such a fast rate should not be necessary in practice once reasonable convergence has been achieved. Only one update per symbol may be required, for example.

A training sequence of 5 symbols was used at the start of each of the following simulations to allow the estimate of the inverse correlation matrix to converge before switching to the decision feedback mode of the matrix update. The steady state error performance of the receiver was then estimated by comparing the transmitted messages and the receiver's decisions. Periodic initialization and retraining of the receiver's inverse correlation matrix estimate was not performed since the receiver seemed to maintain an accurate estimate of the kernel throughout the simulation. This only becames a consideration at high SNR's and low sampling rates, and is discussed further in the following results.

5.3 Simulation Performance Curves

Figure 5.3 shows the theoretical and simulated results for a conventional QDPSK receiver under fading time-bandwidth products of $BT = 0.04$ and $BT = 0.08$ for 2 and 4 samples per symbol. The simulated data points are in reasonably good agreement with the theoretical curves. The theoretical QDPSK curves used 10^4 error events in their evaluation, while the simulated points used 10^3 events. Similar results are observed for the binary case and are not shown here.

Figure 5.4 shows the results of the simulations for adaptive, maximum likelihood reception of BDPSK and QDPSK at a fixed channel time-bandwidth product of $BT = 0.08$, and sampling rates of 2 and 4 for QDPSK, and 2, 4, and 8 for BDPSK. The number of error events counted for each point ranged from 100 at low SNR's, to 10 at the higher SNR's [1]. This figure corresponds to the theoretical curves in Figure 4.15 of the previous chapter, and while the simulated curves show the expected statistical variation, they generally follow the theoretical curves. Higher sampling rates lead to modest improvement in SNR's at a fixed symbol error rate, agreeing with the previous analysis. Figure 5.5 shows the simulated performance curves of optimal BDPSK and QDPSK under a fixed number of samples per symbol, set to 4, and varying channel time-bandwidth products. Again, the simulated results are reasonably close to the theoretical results of Figure 4.16.

[1] Results for this section are shown only for steady state (i.e. converged) receiver error rates, which were observed for all channels and sampling rates up to SNR's of $\approx 45 - 50$ dB. Beyond this, some simulations exhibited a non-stationary error rate that appeared to increase in time. This instability is due to the adaptive algorithm implemented in the simulation, and suggestions for improved performance are discussed in the next section.

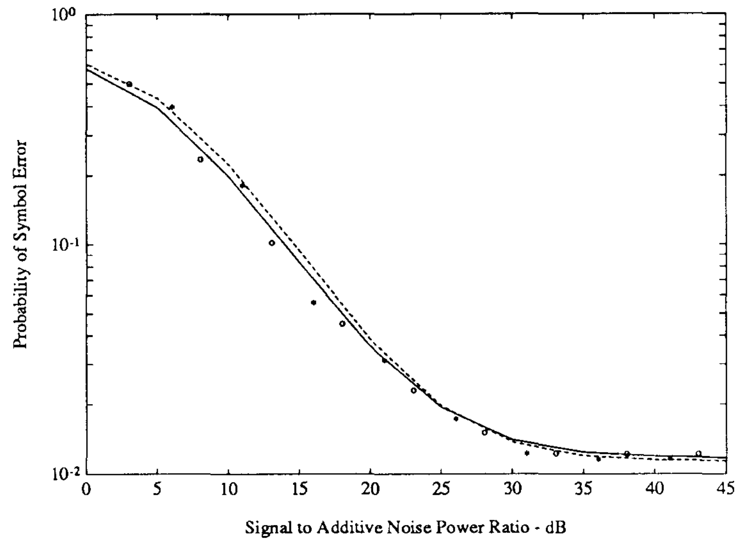

(a)

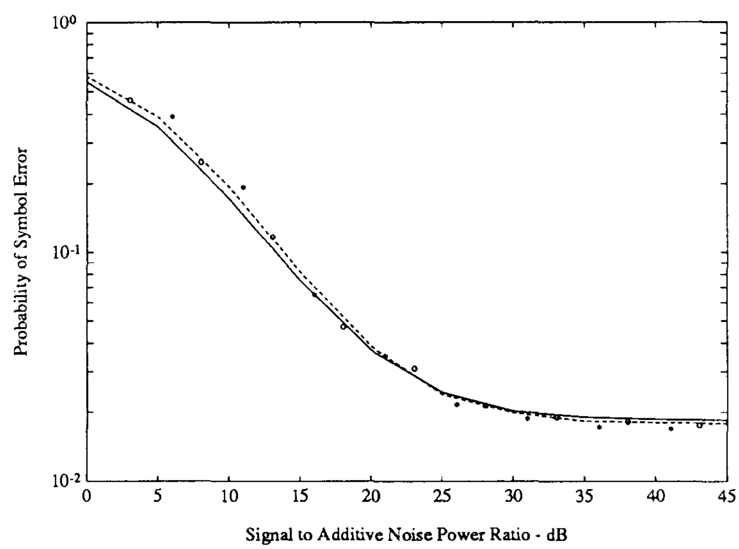

(b)

Figure 5.3: Theoretical (curves) and simulated (points) performance of a QDPSK conventional receiver in a fading channel with a fixed BT and varying samples per symbol – $n_{sb} = 2$: Solid curve, open points; $n_{sb} = 4$: Dashed curve, starred points. (a) $BT = 0.04$ (b) $BT = 0.08$

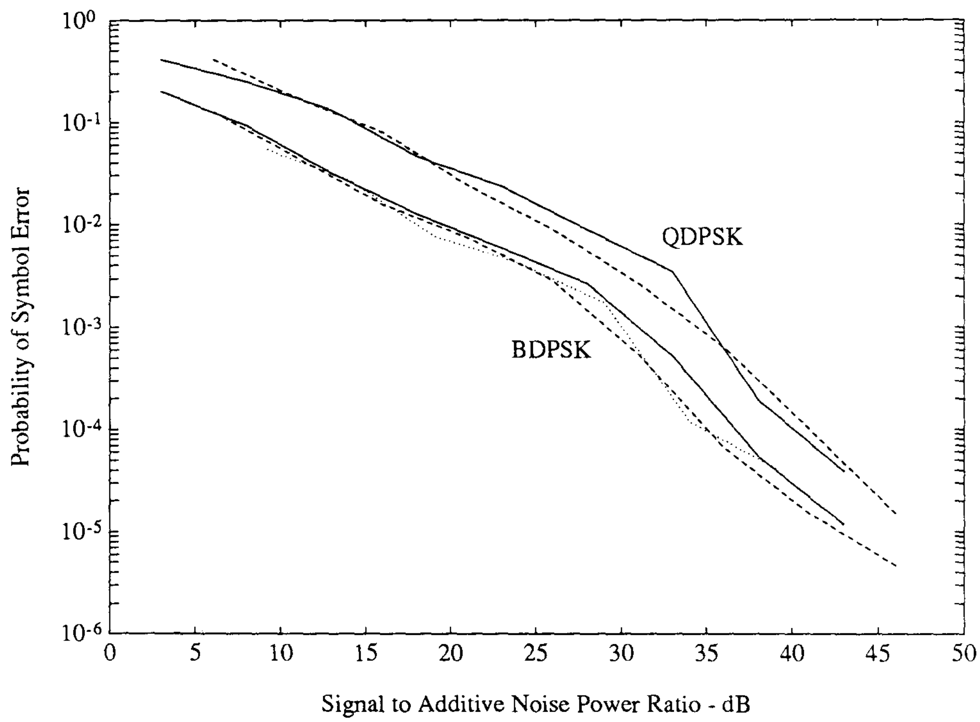

Figure 5.4: Error performance curves of the simulations for optimal BSPSK and QDPSK at a fixed fading rate and varying sampling rates. Channel fading rate is fixed at $BT = 0.08$. $n_{sb} = 2$: Solid curve; $n_{sb} = 4$: Dashed curve; $n_{sb} = 8$: Dotted curve.

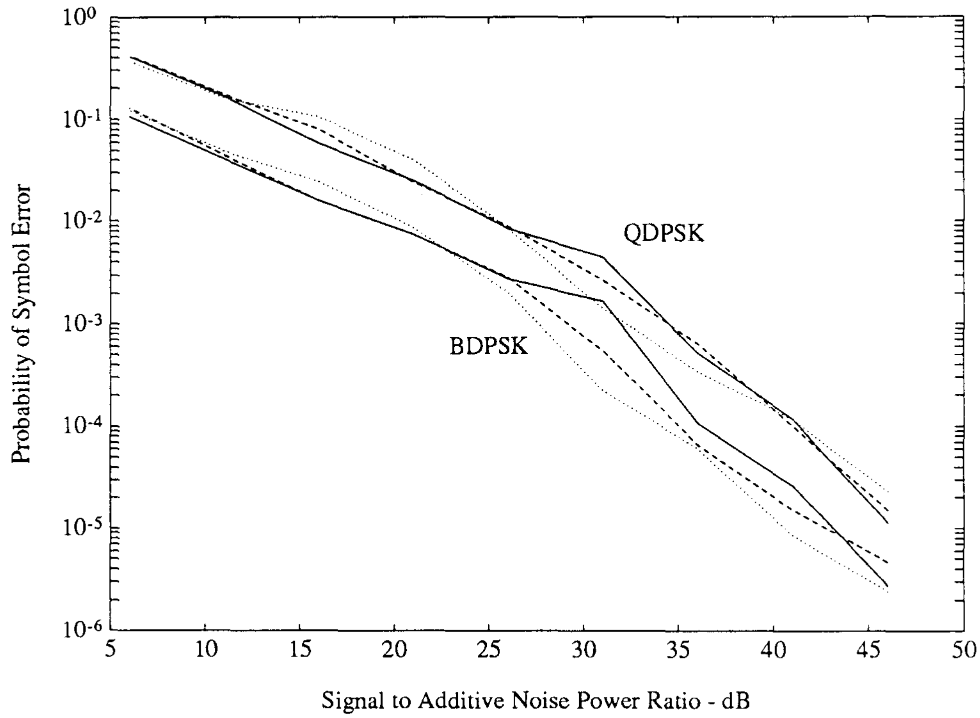

Figure 5.5: Error performance curves of the simulations for optimal BSPSK and QDPSK at a fixed sampling rate and varying channel time-bandwidth products. Sampling rate is fixed at $n_{sb} = 4$. $BT = 0.04$: Solid curve; $BT = 0.08$: Dashed curve; $BT = 0.16$: Dotted curve.

Figures 5.6 and 5.7 show plots of the theoretical and simulated performance curves for optimal BDPSK and QDPSK under varying fading and sampling rates. The simulated data points fall reasonably close to the theoretical curves, except for the circled, low SNR data in Figure 5.6 (a)–(c). These points will also be discussed in the next subsection, and may be eliminated by allowing a longer initial training sequence than the 5 symbols used here. The turnover SNR points at which the receiver switches from first order to second order diversity operation are also clearly seen in the simulated results.

These curves demonstrate the validity of the theoretical analysis of the previous section and show that an adaptive M-L receiver is feasible. The next section discusses briefly some of the performance limitations due to the training sequence length and update algorithm used in the simulated receiver.

5.4 Discussion of the Operation of the Simulated Receiver

5.4.1 Performance at Low SNR's

The simulated adaptive, maximum likelihood receiver generally shows good agreement with the theoretical analysis, except for a few anomalous points at low SNR's, which were exhibited intermittently in the simulations. It was noted that the receiver seemed to fail to converge within the 5 symbol training sequence at these times, and when it was allowed to begin the decision feedback mode of operation, it lost all ability to estimate the channel statistics and make proper symbol decisions. This behaviour is known for RLS-type algorithms, where the initial convergence is less rapid when the additive noise power becomes comparable to the signal power [50]. Unfortunately, there seems to be almost no analysis on this point in the literature, perhaps since most of the practical operations involving these algorithms occur at much higher SNR's. However, the requirement of low SNR operation could be expected for the mobile or indoor channel for environments where line-of-sight is not available.

The reason for this convergence failure may be intuitively understood by imagining the case of an extremely small signal level in strong additive white noise. The theoretical correlation matrix of the received process is just the correlation matrix of the signal plus a large diagonal constant, equal to the white noise variance. A long term estimate of the matrix from the received signal vectors, based on (5.8), can be expected to converge to the theoretical value. However, during the initial estimates of the matrix, little more than white

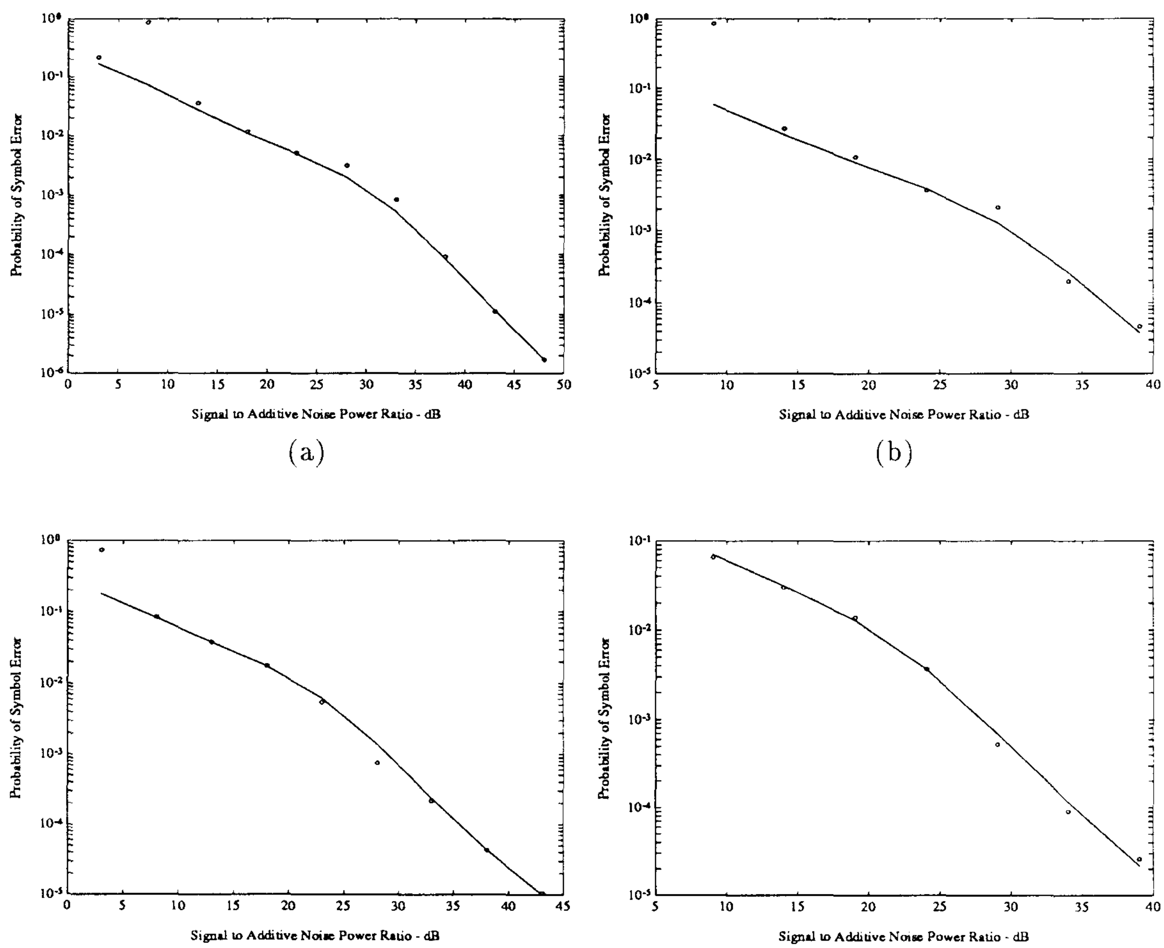

Figure 5.6: Theoretical (lines) and simulated (points) performance curves of an optimal BDPSK receiver at various channel fading rates and receiver sampling rates. (a) $BT = 0.04$, $n_{sb} = 2$ (b) $BT = 0.04$, $n_{sb} = 8$ (c) $BT = 0.16$, $n_{sb} = 2$ (d) $BT = 0.16$, $n_{sb} = 8$

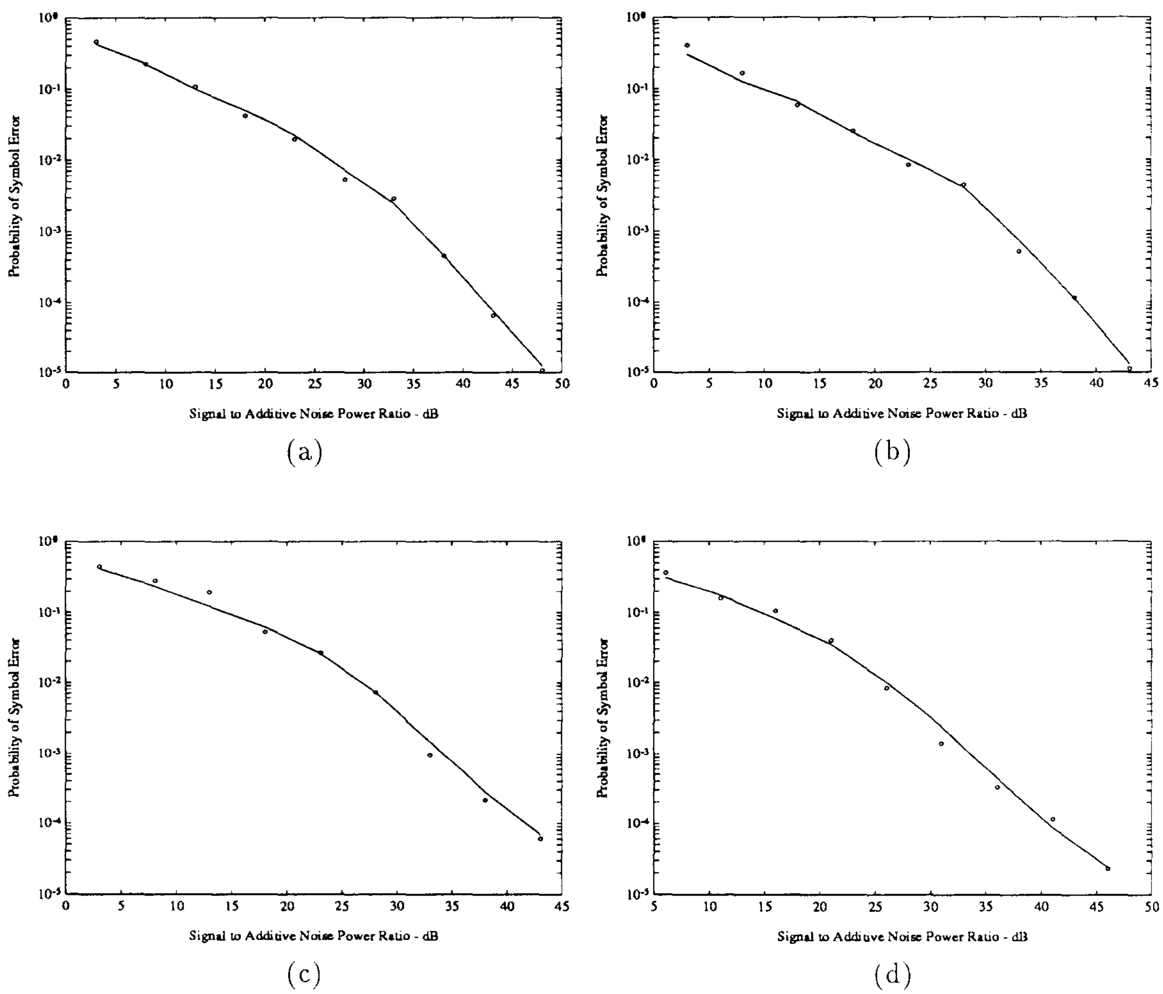

Figure 5.7: Theoretical (line) and simulated (points) performance curves of an optimal QDPSK receiver at various channel fading and receiver sampling rates. (a) $BT = 0.04$, $n_{sb} = 2$ (b) $BT = 0.04$, $n_{sb} = 4$ (c) $BT = 0.16$, $n_{sb} = 2$ (d) $BT = 0.16$, $n_{sb} = 4$

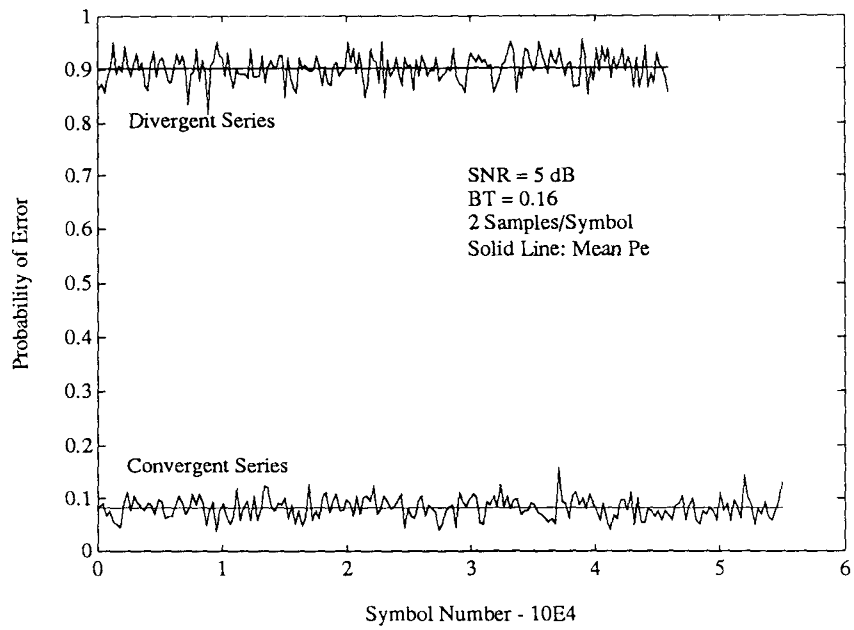

Figure 5.8: Plots of the dynamic error rates of a successfully and unsuccessfully converged optimal receiver.

noise is being used to form the correlation matrix. From the first few additive noise vectors, being entirely uncorrelated random variables, the estimated correlation matrix may have almost any form. It seems reasonable that for very low signal powers, it would take longer for the statistics of the signal to emerge from the additive noise and impose its structure on the correlation matrix estimate. If the training sequence used in the receiver is too short, then the decision feed-back mode will be engaged before any useful estimate of the true channel correlation matrix has been made, which is seen to lead to catastrophic failure of the receiver. Note that this problem should be expected to occur in a receiver using any form of a recursive update algorithm, and is not due to finite precision effects in the receiver or ill-conditioning of the signal correlation matrix.

Examples of a successful convergence and a failure event are shown in Figure 5.8, which shows the time variation of a BDPSK receiver's P_e in a Rayleigh channel. The fading time-bandwidth product is $BT = 0.16$, at a received SNR of 5 dB, and the receiver is sampling at 2 samples/symbol. An initial training sequence of 5 symbols is used for both series. For the successful series, the number of incorrect symbols in consecutive slots of

Event	No. Symbols	Symbols in Error	Symbols Correct	Mean P_e
Success	55125	4513	50612	8.187e-2
Failure	46000	41487	4513	0.9019

Table 5.1: Statistics of an adaptive receiver's symbol decisions for a successful convergence and a failure event for a Rayleigh fading channel.

approximately 250 symbols were counted and converted into a probability of error. For the failed curve, the number of correct symbols in similarly sized consecutive slots were counted and a probability of error evaluated. The statistics are given in Table 5.1. This method allowed comparable sized symbol slots and number of events per slot for comparison between the curves.

It is seen that both series converge rapidly to their steady state values and exhibit similar variations about their mean. Included in the figure is the measured mean of each of the curves. The theoretical probability of error for this channel is 8.28e-2, and cannot be distinguished from the mean of the convergent series with the graph's scale. The receiver kernel of the failed sequence seems to have converged to some stable form which is near to the "true" decision kernel form, in a space of inverse correlation matrices. The dynamics of the receiver's adaptive operation is interesting, and should be investigated further.

In order to more fully characterize this behaviour for practical implementation, simulations were run in order to estimate the failure rate as a function of various system parameters. For a given SNR, sampling rate, channel fading rate, and training sequence length, a simulation trial was run and allowed to accumulate 100 errors. If the error rate for this particular trial was above the arbitrarily chosen threshold of 0.4, then a failure-to-converge event was declared. This was repeated for 100 independent trials and the number of failure events accumulated. SNR values of 0-9 dB, training sequence lengths of 5-60 symbol periods, and sampling rates of 2, 4, and 8 samples per symbol were examined. Two channels with fading time-bandwidth products of $BT = 0.16$ and $BT = 0.04$ were examined, with the results are shown in Tables 5.2 to 5.5. Note that the results are based on a fixed number of trials, rather than failure events, so that comparisons are not strictly valid due to the statistical variation. These results are intended more for general comparison and to motivate the explanation of the convergence failures at low SNR's.

For the binary case, it is seen that the receiver generally requires longer training

	Training Length	SNR (dB)									
		0	1	2	3	4	5	6	7	8	9
$n_{sb} = 2$	5	55	54	42	28	30	21	17	13	12	11
	10	41	27	23	16	11	4	12	7	1	1
	15	16	16	8	3	4	1	0	0	2	0
	20	10	4	4	1	0	1	0	0	0	0
	30	5	1	1	0	0	0	0	0	0	0
$n_{sb} = 4$	5	77	77	64	43	40	33	34	18	22	17
	10	68	57	48	30	20	29	15	8	6	3
	15	32	23	15	3	8	0	0	0	1	0
	20	9	6	2	4	0	0	0	0	0	0
	30	2	0	0	0	0	0	0	0	0	0
$n_{sb} = 8$	5	92	95	88	82	65	64	49	45	34	26
	10	85	71	71	76	58	49	31	28	24	20
	15	43	54	24	20	14	7	3	5	4	0
	20	33	15	7	5	1	0	1	0	0	0
	30	2	0	0	0	0	0	0	0	0	0

Table 5.2: Table of the number of convergence failures in 100 trials for BDPSK, in a Rayleigh fading channel with $BT = 0.16$, under varying sampling rates and received SNR.

	Training Length	SNR (dB)									
		0	1	2	3	4	5	6	7	8	9
$n_{sb} = 2$	5	50	47	35	18	20	12	11	12	11	5
	10	35	26	25	16	8	10	3	5	2	1
	15	18	13	8	4	3	2	0	1	3	1
	20	10	3	1	1	2	0	1	0	0	0
	30	1	3	3	0	0	0	0	0	0	0
$n_{sb} = 4$	5	81	74	61	52	36	31	22	19	20	11
	10	66	56	42	37	18	13	5	6	5	5
	15	25	14	5	6	2	6	3	4	1	0
	20	16	11	5	0	6	0	0	0	0	0
	30	3	3	1	1	0	1	0	0	0	0
$n_{sb} = 8$	5	95	89	84	81	72	57	49	42	32	21
	10	88	78	75	66	59	47	33	23	13	10
	15	48	38	25	15	6	4	3	3	1	0
	20	31	18	7	3	4	1	1	1	1	0
	30	10	4	4	3	0	0	1	1	0	0

Table 5.3: Table of the number of convergence failures in 100 trials for BDPSK, in a Rayleigh fading channel with $BT = 0.04$, under varying sampling rates and received SNR.

	Training Length	SNR (dB)									
		0	1	2	3	4	5	6	7	8	9
$n_{sb} = 2$	5	100	100	99	100	100	97	83	62	65	55
	10	100	100	100	99	87	78	63	38	30	23
	15	100	100	100	91	67	44	21	5	1	4
	20	100	100	93	76	52	21	7	2	0	0
	40	100	95	73	35	6	1	0	0	0	0
	60	91	66	37	14	0	0	0	0	0	0
$n_{sb} = 4$	5	100	100	100	100	100	100	96	98	91	90
	10	100	100	100	100	100	100	94	85	67	62
	15	100	100	100	98	92	69	49	32	9	7
	20	100	99	97	95	79	52	18	12	2	0
	40	99	98	87	46	19	2	0	0	0	0
	60	95	83	47	17	0	0	0	0	0	0

Table 5.4: Table of the number of convergence failures in 100 trials for QDPSK, in a Rayleigh fading channel with $BT = 0.16$, under varying sampling rates and received SNR.

	Training Length	SNR (dB)									
		0	1	2	3	4	5	6	7	8	9
$n_{sb} = 2$	5	100	100	100	100	95	86	79	66	57	30
	10	100	100	100	92	83	60	49	22	16	14
	15	100	99	95	78	65	30	16	7	2	3
	20	100	99	84	62	41	20	4	2	2	1
	40	96	90	62	25	10	3	1	0	0	0
	60	80	64	37	11	0	0	0	0	0	0
$n_{sb} = 4$	5	100	100	100	100	100	99	95	92	83	71
	10	100	100	100	98	98	88	81	65	41	33
	15	100	100	100	95	76	52	23	19	5	1
	20	100	99	97	82	61	30	19	6	2	1
	40	99	93	78	42	19	3	1	1	0	0
	60	95	78	44	19	3	0	1	0	0	0

Table 5.5: Table of the number of convergence failures in 100 trials for QDPSK, in a Rayleigh fading channel with $BT = 0.04$, under varying sampling rates and received SNR.

sequences at low SNR's than the 5 symbols used in the general simulations. For a given training sequence length, however, the convergence failure rate tends to drop off rather rapidly with SNR, up to the 9 dB SNR evaluated. In addition, increasing the training sequence to 30 symbols virtually eliminates the convergence failures, although only a few dB decrease in the received SNR can result in a significant increase in the failure rate. Holding all of the other parameters constant, increasing the sampling rate tends to moderately increase the failure rate. The failure rate also seems to be slightly sensitive to the channel's fading time-bandwidth product. For short training sequences, a slower fading channel ($BT = 0.04$) seems to perform slightly better than a fast fading channel ($BT = 0.16$). However, for the longer training sequences, the fast fading channel is seen to have a slightly lower failure rate than the slow fading case. This is exhibited for all of the sampling rates examined.

Similar observations are seen for QDPSK signalling, except that the failure rates are larger overall, and can be expected to extend to higher values of SNR. As well, the transition across SNR's from high to low convergence failure rates seems to be relatively sharper than in the binary case. The convergence failures can again be alleviated by using longer training sequences, although they appear to require several times the length of that used in the binary signalling case. These general trends should be expected to extend to 8-DPSK and higher phase modulations. Note that at a typical transmission rate of 4.8 kilo-bits/sec, 30 symbols corresponds to a delay of 6.25 ms for BDPSK and 12.5 ms for QDPSK, representing reasonable delays for digital voice communications.

5.4.2 Performance at High SNR's

When the simulations were run at SNR's greater than 45–50 dB, the symbol error rate for 2 sample/baud receivers would occasionally be approximately an order of magnitude greater than expected from theory. After following the steady decline of the theoretical steady state performance curve, an increase of 5 dB in SNR would show an increase in the simulated error rate by approximately an order of magnitude. When the error events were followed dynamically in the simulation, it was found that the receiver operated with virtually a zero error rate up to approximately 250,000 symbols. After this, it appeared to fail catastrophically, similarly to the low SNR events described previously. This initially lead to misleading error rates as the simulations only counted the first 10 or so error events and then exited, calculating what was assumed to be a steady state rate.

The exhibited divergence is not unexpected, however, since the channel process correlation matrix, $\mathbf{K_a}$, is generally very ill conditioned at the fading rates of a mobile channel. This can be observed from the typical channel eigenvalue spectra of the previous chapter. Although the additive noise simply adds a constant equal to the noise variance to the spectra, at sufficiently large SNR's the eigenvalues of the overall channel correlation matrix, $\mathbf{K_c}$, approach those of $\mathbf{K_a}$, and the channel correlation matrix becomes ill conditioned. This creates well known, although still not clearly understood, numerical stability problems in the conventional RLS algorithm implemented in these simulations [47]. Use of the more numerically stable versions of these algorithms, described earlier, should approximately double the SNR range in dB's before stability problems are encountered. This follows from the matrix conditioning of the improved algorithms being the square root of the conventional algorithm's.

Sampling at 4, and presumably higher, samples per symbol appeared to solve the divergence problem, with simulations carried out to 4.5 million symbols at SNR's ranging from 56 to 80 dB. In all cases except one, no symbol errors were detected, the exception being a single symbol error. The increased sampling appears to average out the numerical rounding noise, and to increase the stability of the conventional RLS algorithm. It is not known if this actually solves the divergence problem, or if the point of divergence has simply been pushed past the number of symbols used in the simulation.

Note the simulations were mainly intended to validate the theory of the previous chapter and investigate the feasibility of implementing such a maximum likelihood receiver for real time communications. Any practical implementation would need to carefully examine the detailed form of the recursive algorithm used.

Chapter 6

Summary

In this thesis, we have examined a model of a general time and frequency-selective fading channel. It was seen that this form of channel may be described as a two dimensional, complex Gaussian random process, in both time and frequency. The statistical description of this this process is given by the channel scattering function. From this, the channel was specialized to a purely time-selective fading channel, which, in addition to the AWGN, acts as a random multiplicative modulation of the transmitted signal. This modulation is completely characterized by its mean, which is zero for Rayleigh channels and non-zero for Rician channels, and its correlation matrix, or function. The form of optimal receivers for this channel were then examined for the cases of continuous and sampled waveforms.

A Rayleigh channel was then examined with a special form of correlation function. It may be treated as a plausible, simplified model of a general channel which still exhibits the essential behaviour of a real channel. The advantage of this model is that it allows an analytical expression to be derived for the performance of conventional and optimal receivers for M-ary DPSK. It was found that the asymptotic error rate of a conventional receiver for this channel depends on an eigenvalue spectrum derived from the combined signalling waveforms and channel correlation matrix. Moreover, the optimal receiver performs as though it were operating in a channel with a constant eigenvalue spectrum i.e. as if the fading where white. It was seen that the optimal receiver effectively breaks the fading signal into its independent eigenfunction components, and combines them as an optimal diversity receiver would. In effect, it utilizes the diversity implicit in a random process to make its decisions. The optimal receiver was found to lower the error floor by orders of magnitude, depending on the number of eigenvalues resolved by the receiver.

The performance of sampled DPSK receivers was then evaluated for general fading channels, leading to an analytical expression for the case of binary signalling. General M-ary DPSK was found to require Monte Carlo methods to evaluate and integrate the probability distiribution functions of the decision variables. However, the performance of both conventional and optimal receivers was again found to depend on the eigenvalue spectrum of the combined signalling and channel correlation matrix. Again, the error floor was significantly lowered in the optimal receiver. The analysis used in evaluating the receiver performance was interpreted geometrically, and the effective operation of the optimal receiver on the correlation of the received process examined. It was found that the optimal receiver effectively makes the channel process more correlated, reducing the rate of magnitude nulls and phase swings in the channel process.

Finally, an adaptive receiver was developed which uses a short training sequence to estimate the channel correlation matrix. From this initial estimate, it performs optimal demodulation of the received signals and uses its decisions in updating the channel matrix estimate. This allows it to track slow changes in the statistics of the channel. The receiver was simulated and found to perform close to theoretical expectations at typical channel SNR's. However, longer training sequences were required at very low SNR's (typically 0-15 dB). At high SNR's, when sampling at 2 samples per symbol, the receiver becomes unstable after approximately 250,000 symbols. Higher sampling rates appeared to eliminate this problem. This behaviour can be explained as an averaging out of the round-off errors in the update algorithm by the larger number of samples.

6.1 Future Research

During the course of this work a number of points were raised that were not within the original scope of the thesis, or could not be completed in a reasonable amount of time.

One item is the inablitiy to put the performance of M-ary DPSK for Rayleigh fading channels in a closed analytic form, as was done for the channel with the special correlation function of Equation (1.1). The correspondence between the two channels strongly suggests that it is possible, using techniques similar to those used for the special channel. There seems to be very little literature on general quadratic forms of complex Gaussian random vectors, however, which would be very useful here.

The analysis should also be extended for conventional and optimal receivers to the case of general time and frequency-selective fading, where the channel is modelled as a *series* of random multiplicative taps. As well, the nature of the coupling within the optimal receiver between the time and frequency selective portions of the process should be examined. This may justify splitting the receiver into independent time and frequency-selective portions while still providing an acceptable, though sub-optimal, performance level.

The adaptive version of the optimal receiver described in Chapter 5 should also be evaluated more closely. In particular, the use of more numerically stable update algorithms should be examined, as well as a more realistic simulation, using shaped envelopes and/or phase modulation, and symbol timing derived from the received signals. The use of an initial estimate of the inverse channel correlation matrix which is "close" to a typical fading channel, rather than the scaled identity matrix used in the simulations, should also be examined. This may help reduce the required training sequence lengths.

For the expected symbol rates of approximately 10 kilo-baud, it is expected that this receiver may be implemented using commercially available DSP technology. A hardware prototype of receiver design, using a fading channel simulator or recorded channel data, would be a valuable next step in proving the algorithm for more realistic situations.

The use of codes was also not examined in this thesis, and provides a very broad range of possibilities to further improve performance. For example, see [32].

It also seems that the model of a Rayleigh fading channel as a multiplicative tap may be refined further, into a picture similar to that of the signal space representation of the AWGN channel. The interpretation of a conventional receiver in a fading channel, given in Section 4.4.1, is similar to this, but a much more satisfying description should be possible. One possible approach is the recent application of differential geometry to statistical inference[51, 52]. Distance measures between different distributions of Gaussian vectors may be defined, which for the case of different means and constant correlation matrices, yields the same results as in classical detection problems [2]. For the case of equal means, but different correlation matrices, which is the case for Rayleigh fading channels, then the analysis yields distances which correspond to geodesics on a manifold, or a generalized surface with curvature. The ability to define meaningful distance measures between signal points is required if signal-space, or Ungerboeck codes [53] are to be used in an insightful way in this channel. Here, the "signal-space" may become a generalized manifold, rather than the conventional Euclidean space of AWGN. To date, these signal-space codes seem only to have been applied with the transmited signals in mind [32], with no consideration given to the action of the channel on the signals.

Although the analysis of a fading channel uses techniques which have existed for decades, there still appears to be much effort required in fundamentally understanding the channel. Most of the work to the present seems to treat it as a modified AWGN channel, with the practical techniques used in overcoming the channel interference reflecting this viewpoint. This thesis demonstrates that there may be advantages in treating the fading channel in its own right, providing a different perspective on the AWGN channel, perhaps, in return.

Appendix A

The Karhunen-Loéve Expansion

The notion of expanding a deterministic waveform in a series of orthogonal functions is very common in applied mathematics, and has been used to develop the signal space description of communications in additive Gaussian noise [9]. In this appendix we describe the extention of this approach to stochastic processes for both continuous and discrete time representations.

A.1 Continuous Time Representation of Random Processes

Assume that we are given a zero-mean, generally non-stationary, complex stochastic process, $x(t)$, with a covariance function $K_x(t,\tau)$, Hermitian in t and τ, and that we have a set of N orthonormal functions, $\{\phi_1(t), \phi_2(t), \ldots \phi_N(t)\}$ over the interval $[0,T]$. In a mean square sense, we may expand $x(t)$ such that,

$$x(t) = N \overset{\text{l.i.m}}{\longrightarrow} \infty \sum_{i=1}^{N} x_i \phi_i(t) \quad ; \; 0 \leq t \leq T \tag{A.1}$$

for some particular realization of the process $x(t)$, and where we have defined,

$$x_i \equiv \int_0^T x(t)\phi_i^*(t)\, dt \quad ; i = 1, \ldots, N \tag{A.2}$$

The symbol l.i.m. stands for *limit in the mean.* It is seen from (A.2) that the coefficients x_i will be zero mean random variables, with their values depending on the particular realization of the random process $x(t)$.

We have not as yet specified or constrained the orthogonal expansion function functions, and and the higher order statistics of the expansion coefficients will depend on the particular set of waveforms chosen. However, it is generally convenient to have the complex random variables x_i statistically uncorrelated. That is, we require,

$$\overline{x_i x_j^*} = \lambda_i \delta_{ij} \quad (A.3)$$

$$\overline{x_i x_j} = 0 \quad (A.4)$$

for some unknown set of constants $\{\lambda_i\}$. The functions, $\{\phi_i(t)\}$, and corresponding constants, $\{\lambda_i\}$, that produce this condition are given by the Karhunen-Loéve theorem [54]. It states that the $\{\phi_i(t)\}$ and the $\{\lambda_i\}$ are solutions of the homogeneous Fredholm integral equation,

$$\lambda_i \phi_i(t) = \int_0^T R_x(t,\tau)\phi_i(\tau)\,d\tau \quad (A.5)$$

This is an integral form of an eigen-equation, with a kernel $R_x(t,\tau)$, where the $\{\phi_i(t)\}$ are the normalized eigenfunctions, and the $\{\lambda_i\}$ are the corresponding eigenvalues. From the theory of integral equations it can be shown that if the kernal is Hermitian in its arguments, i.e.

$$R_x(t,\tau) = R_x^*(\tau,t) \quad (A.6)$$

then we have the following properties:

1. The eigenvalues are real.

2. The eigenfunctions corresponding to distinct eigenvalues, with $\lambda_i \neq \lambda_j$, are orthogonal.

3. If the kernal is square integrable, that is,

$$\int_{t=0}^T \int_{\tau=0}^T |R_x^2(t,\tau)|^2\,d\tau\,dt < \infty \quad (A.7)$$

   then each eigenvalue $\lambda_i \neq 0$ has a finite number of corresponding eigenfunctions.

4. If $R_x(t,\tau)$ is positive definite, its eigenfunctions form a complete orthonormal set.

5. If the kernal is non-negative definite, it may be expanded in the form,

$$R_x(t,\tau) = \sum_{i=1}^{\infty} \lambda_i \phi_i(t)\phi_i^*(\tau) \quad (A.8)$$

   This is also known as Mercer's Theorem.

A wide sense stationary process, with $R_x(t,\tau) = R_x(|t-\tau|)$, will have the above properties when it is expanded in terms of its eigenfunctions. The eigenvalues, $\overline{|x_i|^2} = \lambda_i$, will correspond to the energy of the process contained in the i'th eigenfunction. If the random process is Gaussian as well, then the expansion coefficients will also be statistically independent random Gaussian variables.

A trivial, but interesting example of applying the K - L expansion to the AWGN channel can be used to suggest how this technique may be applied to more general cases. Although communication through the AWGN channel is usually thought of in terms of deterministic signals, it should still be recognized that the receiver is actually detecting a Gaussian process. In this case the mean of the process is the original transmitted signal, and the covariance function of the process is just a delta function with magnitude $\mathcal{N}_o/2$.

$$R_r(t,\tau) = \mathcal{N}_o/2\,\delta(t-\tau) \tag{A.9}$$

Solving the Fredholm integral equation for the received process gives,

$$\begin{aligned} \lambda\phi(t) &= \mathcal{N}_o/2 \int_T \delta(t-\tau)\phi(\tau)\,d\tau && \text{(A.10)} \\ &= \mathcal{N}_o/2\,\phi(t) && \text{(A.11)} \end{aligned}$$

where the integral is performed over one symbol period. It is seen that *any* complete orthonormal set of functions will satisfy the integral equation, with all eigenvalues equal to $\mathcal{N}_o/2$. If the deterministic portion of the signal is expanded in some finite set of orthonormal waveforms, the the relevent additive Gaussian noise may also be represented in the same set, with each independent component of the noise represented as a random Gaussian variable of variance of $\mathcal{N}_o/2$. This is just the usual signal space approach to analyzing the AWGN channel.

When the additive Gaussian noise is no longer white, it will have a covariance function with a non-zero width. This will result in a "preferred set" of eigenfunctions when solving the Fredholm equation. A set of orthonormal functions originally used to specify the deterministic, unfaded transmitted signals may no longer be appropriate when forming the independent Gaussian random variables used in the maximum likelihood receiver. It can be shown [2] that employing the channel eigenfunctions in a M-L receiver is equivalant to the heuristic whitening filter approach to receivers in this channel. It can be seen that this more fundamental approach to analyzing channels and receivers is extremely powerful in the fading channel case, where the received information is encoded in the second order statistics of the received process, rather than the mean as in the additive noise channel.

A.2 Discrete Time Representation of Random Processes

The previous section described a representation of continuous time second order random processes, which involved the solution of an integral equation using the assumed known covariance function of the process. Unfortuantely, in real channels, the covariance function is generally unknown. Moreover, exact analytical solutions of the integral equation exist for only a very few known correlation kernals, notably the sinc function for boxcar bandlimited processes, which results in the prolate spheriodal set of orthogonal wavefunctions, and rational spectra [2]. These are in any case extremely tedious to calculate. Although much of the early work concentrated on continuous time analysis and implementation of these systems, most signal processing today is based on discrete time sampling and digital processing of signals.

When the covariance kernel is a known continuous function, the Fredholm integral may be solved numerically for its eigenvalues and eigenfunctions (evaluated at discrete time intervals). Although there are several methods available, the most straightforward is to evaluate the integral of (A.5) numerically by converting it into an appropriately weighted discrete summation (depending on the integration rule being used, e.g. trapezoidal or Simpson's)[55] in τ. In addition, the variable t is discretized, and without loss of generality, we assume unit time sampling. By taking the weights to be unity, i.e. a staircase approximation to the kernel, we have,

$$\lambda\phi(t_i) = \sum_j R(t_i, \tau_j)\phi(\tau_j) \tag{A.12}$$

Indexing the discrete function evaluations with subscripts then gives

$$\lambda\phi_i = \sum_j R_{ij}\phi_j \tag{A.13}$$

This may then be placed in matrix form,

$$\lambda\boldsymbol{\phi} = \mathbf{R}\boldsymbol{\phi} \tag{A.14}$$

where

$$\boldsymbol{\phi} = \begin{bmatrix} \phi(t_1) \\ \phi(t_2) \\ \vdots \end{bmatrix} \equiv \begin{bmatrix} \phi_1 \\ \phi_2 \\ \vdots \end{bmatrix} \tag{A.15}$$

This may also be written in an expanded matrix form,

$$\mathbf{\Phi\Lambda} = \mathbf{R\Phi} \tag{A.16}$$

where

$$\mathbf{\Phi} = [\phi_1\phi_2\cdots] \tag{A.17}$$

$$= \begin{bmatrix} \phi_1(t_1) & \phi_2(t_1) & \cdots \\ \phi_1(t_2) & \phi_2(t_2) & \cdots \\ \vdots & \vdots & \ddots \end{bmatrix} \tag{A.18}$$

Note that in the limit of an infinitesimal sampling period, these matrices may become seminfinite.

It is seen from (A.13) and (A.16) that numerically evaluating the K - L expansion directly corresponds to the eigendecompostion of the sampled covariance kernal. Because of the stationary assumption on the random process, this kernel will be Toeplitz. i.e. each matrix element is a function only of the difference of its indices, and the matrix appears diagonally banded and Hermitian.

Corresponding to the numerical evaluation of the K - L eigen-decomposition of the random process, we see from (A.1) that the time samples of a random process may be similarly evaluated. We have,

$$x(t_j) = \sum_{i=1}^{N} X_i\phi_i(t_j) \tag{A.19}$$

$$x_j = \sum_{i=1}^{N} X_i\phi_{ij} \tag{A.20}$$

$$\mathbf{x} = \mathbf{\Phi X} \tag{A.21}$$

where the X_i are the discrete expansion coefficients,

$$\mathbf{X} = \begin{bmatrix} X_1 \\ X_2 \\ \vdots \end{bmatrix} \tag{A.22}$$

and,

$$\mathbf{x} = \begin{bmatrix} x(t_1) \\ x(t_2) \\ \vdots \end{bmatrix} = \begin{bmatrix} x_1 \\ x_2 \\ \vdots \end{bmatrix} \tag{A.23}$$

Similarly, the coefficients of (A.2) may be numerically evaluated as,

$$\mathbf{X} = \mathbf{\Phi}^H \mathbf{x} \tag{A.24}$$

It is apparant that if a given continuous time random process is sampled, then the above matrix relations for the sampled data will correspond directly with the continuous time K - L expansion of the original process.

A physical channel with a non-degenerate kernel will theoretically require an infinite expansion of (A.8), and will have an infinite number of eigenvalues. However, the spectrum of the eigenvalues will generally remain at a constant value only for a finite number of eigenvalues, before decaying away to zero. Therefore, only a finite number need to be considered as significant, for a given machine accuracy. A practical question is the sampling rate that is required in order to capture the relevant statistical information of the process through a K - L expansion. For N samples over the time period of interest, i.e. one symbol period, one may evaluate N eigenvalues and eigenfunctions. However, it is known that a process which is band limited in frequency to between $-W$ and W, has $\gtrsim 1 + 2WT$ eigenvalues, or degrees of freedom [56], where T is the observation time. Defining N_λ to be the number of significant eigenvalues of the process, and T_s to be the sampling period, we have,

$$N_\lambda \gtrsim 2WT \tag{A.25}$$

$$\gtrsim 2WNT_s \tag{A.26}$$

$$\gtrsim 2W\frac{N}{f_s} \tag{A.27}$$

where f_s is the sampling frequency. If f_s is chosen to equal $2W$, the Nyquist sampling rate, then $N_\lambda \gtrsim N$, and we will capture most of the significant eigenvalues. If we sample faster, at say $f_s = 4W$, then we have $N_\lambda \gtrsim N/2$ and the N eigenvalues we evaluate should almost certainly contain all of the significant eigenvalues. The Nyquist sampling rate is seen to form a lower bound on the sampling rate required to resolve the significant eigenvalues of the random process.

This appears to be the best estimate of the required sampling rate that can done without explicit knowledge of the the fading process and its statistics. Note that practical mobile channels generally only exhibit a single significant eigenvalue. In practice, a prudent oversampling of the signal should be used in order to capture the transition region of the eigenvalue spectrum, down to the available measurement or machine accuracy.

Appendix B

Performance Analysis for Time Selective Fading

This appendix analyses the performance of conventional and optimal continuous time receivers for time-selective fading with a special form of covariance function. This analysis is based on the work by Walker [22] for a transmitted reference scheme for binary signals. This is extended here to complex signalling for M-ary DPSK.

B.1 Performance of Standard Differential Receivers

In the classical AWGN receiver, the decision variable is computed by cross-correlating the received signal, $x(t)$, with some reference signal, $r(t)$. The $r(t)$ is either derived from the received carrier, for coherent demodulation, or from the previous symbol, as in differential demodulation. Here we take $r(t)$ and $x(t)$ to be two consecutive symbols in the signal $y(t)$, with $x(t)$ having a relative phase shift of θ with respect to $r(t)$. See Figure B.1. The decision variable, Z, is given by,

$$Z = \int_0^T x(t)r^*(t)\,dt \tag{B.1}$$

A Karhunen-Loéve expansion is performed on each of the fading signals over one symbol interval, providing uncorrelated Gaussian random variables in the expansion coefficients. The random channel is assumed to have a correlation function $R(t-\tau)$ for its single tap process. The expansion functions, $\{\phi_i(t)\}$, will satisfy the Fredholm integral equation,

$$\lambda_i\phi_i(t) = \int_0^T K(t,\tau)\phi_i(\tau)\,d\tau \tag{B.2}$$

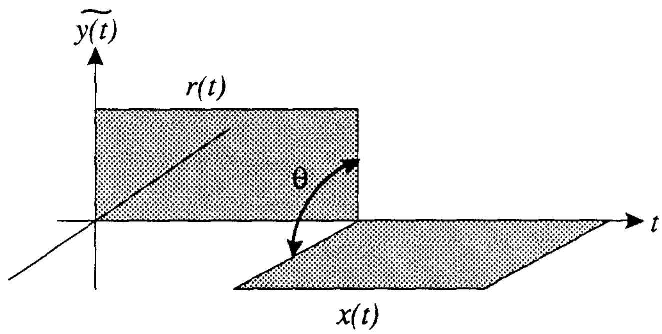

Figure B.1: Form of the DPSK signal used in the text.

where the kernel is given by,

$$K(t,\tau) = s(t)R(t-\tau)s(\tau), \tag{B.3}$$

and $s(t)$ is the purely real modulating waveform. Here we assume that within a single symbol interval, a modulating pulse's shape may be taken to have zero phase. The relative phase offset between symbolss, which carries the signalling information, will be introduced explicitly in the following. Performing the expansion on the signal waveforms, one obtains,

$$x(t) = \sum_i x_i\phi_i(t) \quad \Longleftrightarrow \quad x_i = \int_0^T x(t)\phi_i^*(t)\,dt \tag{B.4}$$

$$r(t) = \sum_i r_i\phi_i(t) \quad \Longleftrightarrow \quad r_i = \int_0^T r(t)\phi_i^*(t)\,dt \tag{B.5}$$

and,

$$Z = \sum_i x_i r_i^* \equiv \sum_i z_i, \tag{B.6}$$

which is seen by substituting the waveform expansions into (B.1) above. From Figure B.1 we have for $\tau < T$,

$$\begin{aligned}
\overline{x(t)x^*(t+\tau)} &= \overline{r(t)r^*(t+\tau)} && \text{(B.7)}\\
&= K(t,t+\tau) && \text{(B.8)}\\
\overline{x(t)r^*(t+\tau)} &= \overline{y(t)y^*(t+T+\tau)} && \text{(B.9)}\\
&= K(t,t+\tau+T)e^{i\theta} && \text{(B.10)}
\end{aligned}$$

Without loss of generality, we may assume constant amplitude modulation. That is, $|s(t)| \equiv 1$ and the kernel $K(t,\tau)$ is simply $R(t-\tau)$. If the modulating waveforms are shaped, then

$R(\cdot)$ is simply replaced by the $K(\cdot)$ of (B.3) in the following, with the eigenvalues determined by (B.2). For the constant amplitude case we have,

$$\begin{aligned}
\overline{x(t)x^*(t+\tau)} &= \overline{r(t)r^*(t+\tau)} && \text{(B.11)}\\
&= R(\tau) && \text{(B.12)}\\
\overline{x(t)r^*(t+\tau)} &= R(\tau+T)e^{i\theta} && \text{(B.13)}\\
&\approx R(T)e^{i\theta}R(\tau) && \text{(B.14)}
\end{aligned}$$

The last approximation is often used in the literature [57], where it is assumed that the fading process may be characterized by a single decorrelation parameter, $\rho \equiv R(T)$, between symbol intervals. The analysis here uses a somewhat hybrid approach, where a single parameter is used to characterize the fading between symbol intervals, but the full structure of the fading statistics is considered within the symbol interval (by way of the K - L expansion). The correlation function across two symbol intervals is thus taken to have the form:

$$R_2(\tau) = \begin{cases} R(\tau) & ; \quad \tau < T \\ \rho R(\tau - T) & ; \quad T < \tau < 2T \end{cases} \tag{B.15}$$

where $R_2(\tau)$ is the extended correlation function, and τ is the time-difference variable. Although the discontinuity implied in the correlation function across a symbol period is not accurate in the description of the channel statistics, this approach does provide an interesting analysis and interpretation of a continuous time receiver. Moreover, it is necessary here for the analysis to give results in a tractable closed form.

Using the above correlations between waveforms, we find for the K - L coefficients,

$$\begin{aligned}
\left.\begin{matrix}\overline{x_i x_j^*}\\ \overline{r_i r_j^*}\end{matrix}\right\} &= \lambda_i \delta_{ij} \\
\overline{x_i r_j^*} &= \rho e^{i\theta}\lambda_i\delta_{ij}
\end{aligned} \tag{B.16}$$

where $0 \le \rho \le 1$. It is seen then that $Z = \sum_i z_i = \sum_i x_i r_i^*$ is the sum of products of two complex Gaussian random variables, where each individual product term is independent of the others. The probability distribution function of the decision variable, Z, will be the convolution of the individual pdf's of each of the z_i. It should be noted that the pdf of the the product of two Gaussian distributed random variables is not in general Gaussian. From Miller [38] the pdf of each of the z_i may be evaluated as follows. Define the vector $\mathbf{w}$ and the correlation matrix $\mathbf{R}$ of $\mathbf{w}$ as,

$$\mathbf{w} = \begin{bmatrix} x_i \\ r_i \end{bmatrix} \tag{B.17}$$

$$\mathbf{R} = \overline{\mathbf{w}\mathbf{w}^H} \tag{B.18}$$

$$= \begin{bmatrix} \overline{|x_i|^2} & \overline{x_i r_i^*} \\ \overline{x_i^* r_i} & \overline{|r_i|^2} \end{bmatrix} \tag{B.19}$$

We now define the inverse of $\mathbf{R}$ to be $\mathbf{S} \equiv \mathbf{R}^{-1}$, and the element (1,2) of the Hermitian matrix $\mathbf{S}$ to be in the complex form,

$$S_{12} = |S_{12}|e^{i\chi_{12}} \tag{B.20}$$

In addition, a particular product, z_i, is decomposed into its real and imaginary components[1], $z_i = x_i r_i^* = u + iv$. The *joint* characteristic function of (u,v) is given by [38],

$$\psi(t,s) = \frac{4|\mathbf{S}|}{t^2 + s^2 + 4i|S_{12}|(t\cos\chi_{12} + s\sin\chi_{12}) + 4|\mathbf{S}|} \tag{B.21}$$

The corresponding joint pdf of the real and imaginary components of z_i is then given by,

$$p(u,v) = \frac{2|\mathbf{S}|}{\pi} e^{-2|S_{12}|(t\cos\chi_{12}+s\sin\chi_{12})} K_0\left(2\sqrt{S_{11}S_{22}(u^2+v^2)}\right), \tag{B.22}$$

where $K_0(\cdot)$ is the zero'th order modified Bessel function of the second kind.

From the the correlations between the x_i and r_i given in (B.16) above, the correlation matrices are,

$$\mathbf{R} = \lambda_i \begin{bmatrix} 1 & s \\ s^* & 1 \end{bmatrix}; \text{ where } s \equiv \rho e^{i\theta} \tag{B.23}$$

$$\mathbf{S} = \frac{1}{\lambda_i(1-\rho^2)} \begin{bmatrix} 1 & -s \\ -s^* & 1 \end{bmatrix} \Longrightarrow \begin{array}{rcl} |\mathbf{S}| & = & \frac{1}{\lambda_i{}^2(1-\rho^2)} \\ |S_{12}| & = & \frac{\rho}{\lambda_i(1-\rho^2)} \\ \chi_{12} & = & \theta + \pi \end{array} \tag{B.24}$$

For zero phase shift between two symbols, i.e. $\theta = 0$, the pdf for an individual z_i is given as,

$$p_{z_i}(u,v) = \frac{2}{\lambda_i{}^2(1-\rho^2)\pi} e^{\frac{2\rho}{\lambda_i(1-\rho^2)}u} K_0\left(\frac{2\sqrt{u^2+v^2}}{\lambda_i(1-\rho^2)}\right) \tag{B.25}$$

An example of this pdf is given in Figure B.2 for $\lambda_i = 1$ and $\rho = 0.8$. Note that the λ_i acts as

[1] The use of the imaginary constant i and the index i should be clear from its context.

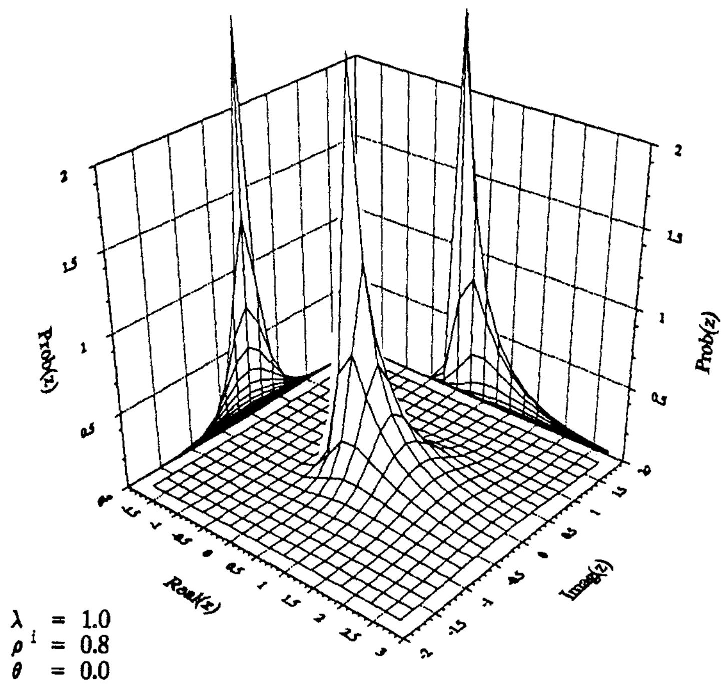

Figure B.2: Probability distribution function of the complex product $\tilde{z} = \tilde{x}\tilde{r}$, where $\tilde{x}$ and $\tilde{r}$ are correlated, zero mean complex Gaussian random variables.

an overall scaling factor in the coordinates u and v, while ρ determines the extent to which the function is stretched along the $v = 0$ plane of symmetry. The angle θ determines the angle the overall function is rotated about the z-axis. This is reasonable since the quantity $\rho e^{i\theta}$ is simply the expected value of the product, as given in (B.16), and is thus also the mean of the pdf.

From the particular correlations between the x_i and r_i given in (B.16), the joint characteristic function of one term of the sum (B.6) is found from (B.21) to be,

$$\psi_i(t, s) = \frac{1}{\frac{\lambda_i^2}{4}(1 - \rho^2)(t^2 + s^2) - \lambda_i \rho t i + 1} \tag{B.26}$$

The characteristic function of the decision variable, Z, is then the product of the individual characteristic functions of the independent z_i. That is,

$$\Psi = \prod_{i=1}^{N} \psi_i, \tag{B.27}$$

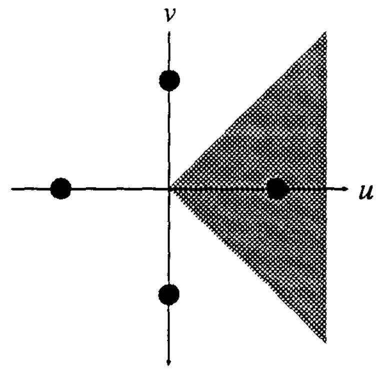

Figure B.3: Correct decision region in QDPSK for the symbol $\theta_k = 0$.

where N is the number of significant eigenvalues used to expand the original signal waveforms. Taking the inverse Fourier transform of (B.27) gives the pdf $p_Z(u,v)$ of Z.

$$p_Z(u,v) = \frac{1}{4\pi^2}\int_{-\infty}^{\infty}\int_{-\infty}^{\infty} \Psi(t,s)e^{-i(ut+vs)}\,ds\,dt \tag{B.28}$$

In a four signal DPSK scheme, the decision variable, Z, will be computed and binned into one of the four complex plane quadrants. For the $\theta = 0$ pdf given above, we have for the probability of a correct decision,

$$P_c = 2\int_{u=0}^{\infty}\int_{v=0}^{u} p_Z(u,v)\,dv\,du \tag{B.29}$$

This is shown in Figure B.3. Although the individual pdf's of the z_i, given by (B.25), may be convolved together to form the overall pdf of the decision variable, the approach does not easily yield a closed form analytical solution for the receiver perfomance. Computing this numerically is also difficult due to the infinite extent of the pdf functions. The "tails" of these two dimensional functions must be accurately considered when calculating low probabilities of error. An alternative method is to evaluate P_c in the transform domain of $\Psi(s,t)$, the characteristic function of $p_Z(u,v)$. Although this is still somewhat involved analytically, it will provide a systematized approach that allows fast and accurate calculations for computing the error performance for an arbitrary set of channel and signal eigenvalues. This is just a generalization of Walker's approach [22].

This method may be used to calculate the receiver performance at any finite SNR. However, we will only calculate the asymptotic, or infinite SNR performance limit. Although the performance behaviour at a finite SNR is also important, this thesis is primarily concerned with understanding and lowering the error floor found in receivers, and will concentrate on this fundamental limitation of performance. As well, this analysis is a useful *model* that allows relative comparisions of receivers in different channels, and suggests the design of an optimal receiver for DPSK signalling. However, the previous analysis only applies exactly for the transmitted refrence scheme, and the approximations involved in using it to model a time-differential scheme do not yield accurate predications of the performance for realistic channels. In the following chapter we will develop a much more realistic and accurate approach to predicting the error performance for conventional DPSK in time-selective fading channels.

Substituting the characteristic function expansion given by (B.28) into (B.29) gives,

$$P_c = \lim_{L\to\infty} 2\int_{u=0}^{L}\int_{v=0}^{u} \frac{1}{4\pi^2}\int_{-\infty}^{\infty}\int_{-\infty}^{\infty} \Psi(t,s)e^{-i(ut+vs)}\,ds\,dt\,dv\,du \tag{B.30}$$

By switching the order of the integral pairs and then expanding the inner integral over u and v, one obtains,

$$\begin{aligned} P_c &= \lim_{L\to\infty}\frac{1}{2\pi^2}\int_{-\infty}^{\infty}\int_{-\infty}^{\infty}\frac{\Psi(t,s)\left(1-e^{-iLt}\right)}{it\cdot is}\,dt\,ds \\ &\quad -\frac{1}{2\pi^2}\int_{-\infty}^{\infty}\int_{-\infty}^{\infty}\frac{\Psi(t,s)\left(1-e^{-iL(t+s)}\right)}{i(t+s)\cdot is}\,dt\,ds \qquad \text{(B.31)} \\ &\equiv \frac{1}{2\pi^2}\left(I_1-I_2\right) \qquad \text{(B.32)} \end{aligned}$$

where I_1 and I_2 are defined by their corresponding integrals in (B.32). This forms the basic formula for a conventional receiver's asymptotic performance. Its solution will be calculated and examined first under the assumption of a single significant channel eigenvalue, and then under a multi-eigenvalue assumption. This provides some insight into how this analysis corresponds to previous analysis of so called "slow fading" channels.

B.1.1 Single Eigenvalue Analysis

It is instructive to first evaluate P_c for a single eigenvalue, λ. This furnishes the basic approach to be used for a general number of eigenvalues, and provides an analytical expression that may be checked against previous work. Note that a single channel eigenvalue in addition to the intersymbol decorrelation, ρ, corresponds to the case of "slow fading". In brief, it can be shown that an integral equation kernel, such as the Fredholm integral equation of (B.2), may be approximated by a Taylor series expansion in two variables (see

Jerri [55]). The number of terms used in the series is equal to the number of eigenvalues that are approximately resolved by the expansion. A single significant eigenvalue would be seen to correspond to a zero'th order, or constant level approximation of the correlation function. The complex random Gaussian process corresponding to this approximation will simply be a random variable over one symbol period, with a variance, or signal power, equal to the eigenvalue λ. This approximation of the random process alone corresponds to the fast fading approximation. The additional parameter ρ, would still be used as a measure of the correlation of the random variables between symbol periods, and gives the slow or correlated fading approximation of a Rayleigh channel.

Evaluating I_1 above we have,

$$I_1 = \int_{t=-\infty}^{\infty} \frac{1 - e^{-iLt}}{it} \int_{s=-\infty}^{\infty} \frac{\psi(t,s)}{is}\, ds\, dt \tag{B.33}$$

where

$$\psi(t,s) = \frac{1}{\frac{\lambda^2}{4}(1-\rho^2)(t^2+s^2) - \lambda\rho t i + 1} \tag{B.34}$$

However, since the inner integral is seen to be odd in s, it will evaluate to zero, and $I_1 = 0$ identically. Thus, the probability of correct detection is given by I_2, which can be written,

$$\begin{aligned} P_c &= \frac{-1}{2\pi^2} \int_{s=-\infty}^{\infty} \frac{1}{is} \int_{t=-\infty}^{\infty} \frac{\psi(t,s)\left[1 - e^{-iL(t+s)}\right]}{i(t+s)}\, dt\, ds && \text{(B.35)} \\ &\equiv \frac{-1}{2\pi^2} \int_{s=-\infty}^{\infty} \frac{1}{is} I(s)\, ds && \text{(B.36)} \end{aligned}$$

where $I(s)$ is the corresponding inner integral as defined. Factoring $\psi(t,s)$ in t gives,

$$\psi(t,s) = \frac{4}{\lambda^2(1-\rho^2)} \frac{1}{(t - t_0^1)(t - t_0^2)} \tag{B.37}$$

where,

$$t_0^{1,2}(s) = i\, \frac{2\rho \mp \sqrt{\lambda^4 s^2 (1-\rho^2)^2 + 4}}{\lambda^2(1-\rho^2)} \tag{B.38}$$

Performing the inner integral of (B.35) over t by residues, in the limit $L \to \infty$ (see Figure B.4), we find that,

$$\begin{aligned} I(s) &= \frac{4}{\lambda^2(1-\rho^2)}(-2\pi i)\mathrm{Res}\left\{ \left. \frac{1}{(t-t_0^1)(t-t_0^2)\, i(t+s)} \right|_{t=t_0^1} \right\} && \text{(B.39)} \\ &= \frac{4\pi i\,(1-\rho^2)}{\sqrt{\lambda^2 s^2(1-\rho^2)^2+4}\left(-\lambda(1-\rho^2)s + i\sqrt{\lambda^2 s^2 (1-\rho^2)^2 + 4} - 2\rho i\right)} && \text{(B.40)} \end{aligned}$$

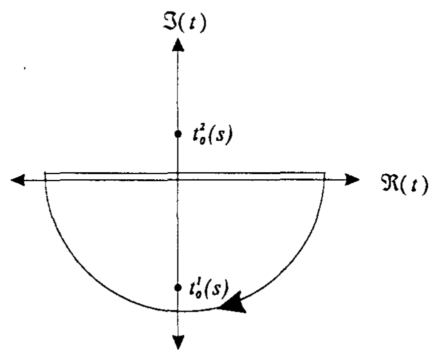

Figure B.4: Path of integration in evaluating P_c.

and

$$P_c = \frac{-1}{2\pi^2}\int_{s=-\infty}^{\infty}\frac{I(s)}{is}\,ds \tag{B.41}$$

Substituting the evaluated $I(s)$ of (B.40) into the expression for P_c above, and performing the following substitutions,

$$\left.\begin{array}{rcl} a & = & \lambda\,(1-\rho^2) \\ b & = & 2\rho \end{array}\right\} \text{ Compresses Expression Somewhat} \tag{B.42}$$

$$\left.\begin{array}{rcl} \sqrt{s^2+4/a^2} & \rightarrow & \frac{2}{a}\sec u \\ s & \rightarrow & \frac{2}{a}\tan u \end{array}\right\} \text{ Standard Trigonometric Substitutions} \tag{B.43}$$

one finds for P_c,

$$P_c = -\frac{(1-\rho^2)}{\pi}\int_{-\infty}^{\infty}\frac{\sec u}{\tan u\,(-2\tan u + 2i\sec u - bi)}\,du \tag{B.44}$$

Solving this integral[2] and writing $P_e = 1 - P_c$, one finds,

$$P_e = \frac{3}{4} - \frac{\rho}{\sqrt{2-\rho^2}} + \frac{\rho}{\pi\sqrt{2-\rho^2}}\arctan\frac{\sqrt{2-\rho^2}}{\rho} \tag{B.45}$$

This result agrees with the analysis by Voelcker and Proakis [11, 10] in their analysis of QDPSK in slow, correlated fading. Note that the single channel eigenvalue assumed here, λ, does not enter into the error expression. This should be expected since it corresponds to the received signal energy. Under the random phase modulation of the fading channel, the signal energy for DPSK will not affect the receiver performance in the asymptotic limit of infinite SNR.

[2] An algebraic manipulation package, such as Maple or Mathematica, is quite useful when evaluating or simplifying integrals and expressions like these.

B.1.2 Multi-Eigenvalue Analysis

Any signalling which uses a finite symbol period will have higher order, non-zero eigenvalues, as determined from the Fredholm equation of (B.2). The assumption of a constant fading modulation over each symbol ignores many extra degrees of freedom in the channel process. These will change the performance of the receiver compared to the slow fading (single eigenvalue and correlation parameter) approximation, and are also perhaps available to be exploited. Suitable, non-constant amplitude pulse shaping may also be used to deliberately introduce extra significant eigenvalues. This is closely related to Baggeroer's examples of the effects of pulse shape on receiver performance in additive coloured noise[44].

Note that for square, constant amplitude signalling, the eigenvalue spectrum and ρ will be strictly related through the shape of the channel correlation function, $R(\tau)$, and the signalling period, T, as given by (B.3). For example, the mobile channel, using a vertical polarized monopole antenna, has a correlation function of the form [4],

$$R(\tau) = J_0(2\pi B\tau) \tag{B.46}$$

where B is the fading process' bandwidth. The correlation factor, ρ, is given by $\rho = J_0(2\pi BT)$, and the eigenvalues are evaluated from the correlation kernel $R(t-\tau)$ over the period of a symbol. The eigenvalue spectrum and ρ are jointly determined by the fading bandwidth and the signalling period. However, for general, non-square, pulse shapes, the Fredholm kernel will not be $R(t-\tau)$, as given in (B.3). The actual pulse shape will serve to decouple ρ and the eigenvalues, and intoduce some freedom in selecting the eigenvalues and ρ independently. With this in mind, the asymptotic error performance will be evaluated for completely arbitrary ρ, number of eigenvalues, and their spectrum. In calculating the performance of a system with a particular pulse shape and a particular channel correlation function, the Fredholm equation (B.2) must first be solved for the set of eigenvalues corresponding to this system. Generalizing the characteristic function in (B.37) for the case of N eigenvalues (i.e. number of terms in the sum for Z), the characteristic function, $\Psi_N(t,s)$, is given by,

$$\Psi_N(t,s) = C_N \prod_{j=1}^{N} \frac{1}{\left(t - t_j^1\right)\left(t - t_j^2\right)} \tag{B.47}$$

where

$$C_N = \left(\frac{4}{1-\rho^2}\right)^N \prod_{j=1}^{N} \frac{1}{{\lambda_j}^2} \tag{B.48}$$

$$t_j^{1,2} = i\,\frac{2\rho \mp \sqrt{\lambda_j{}^2 s^2 \left(1-\rho^2\right)^2 + 4}}{\lambda_j \left(1-\rho^2\right)} \tag{B.49}$$

Substituting the above into the characteristic function expansion for P_c, given in (B.32), one finds as before that $I_1 = 0$. Evaluating the inner integral of (B.35) again by residues gives,

$$\begin{aligned} \int_{t=-\infty}^{\infty} \frac{\Psi(t,s)\left(1-e^{-iL(t+s)}\right)}{i(t+s)}\,dt &= -2\pi i \sum \left\{ \begin{array}{c} \text{Residues In Negative} \\ \text{Argand Plane} \end{array} \right\} && \text{(B.50)} \\ &\equiv I_N(s) && \text{(B.51)} \end{aligned}$$

which is a function of s only. Evaluating the residues results in,

$$I_N(s) = -2\pi i C_N \sum_{j=1}^{N} \frac{1}{i\left(t_j^1 + s\right)} \left[\prod_{\substack{k=1 \\ k\neq j}}^{N} \frac{1}{\left(t_j^1 - t_k^1\right)\left(t_j^1 - t_k^2\right)}\right] \frac{1}{\left(t_j^1 - t_j^2\right)} \tag{B.52}$$

Therefore, the probability of correct detection is given by,

$$\begin{aligned} P_c &= \frac{-1}{2\pi^2} \int_{s=-\infty}^{\infty} \frac{I_N(s)}{is}\,ds && \text{(B.53)} \\ &= \frac{(-1)^N C_N}{\pi} \int_{s=-\infty}^{\infty} \sum_{j=1}^{N} \frac{1}{s\left(it_j^1 + s\right)} \left[\prod_{\substack{k\neq j \\ k=1}}^{N} \frac{1}{\left(t_j^1 - t_k^1\right)\left(t_j^1 - t_k^2\right)}\right] \frac{1}{\left(t_j^1 - t_j^2\right)}\,ds && \text{(B.54)} \end{aligned}$$

where the pure imaginary t_k^j have been rewritten as explicitly imaginary, i.e. $t_k^j \rightarrow it_k^j$ in going from (B.52) to (B.54). From inspection, it is seen the above expression has its integrand's real part even in s, and its imaginary part odd in s. Thus, only the real part of the integrand will contribute to the integral. This results in the expression for the probability of correct detection,

$$P_c = \frac{(-1)^N C_N}{\pi} \int_{s=-\infty}^{\infty} \sum_{j=1}^{N} \frac{1}{\left(it_j^1 + s^2\right)\left(t_j^1 - t_j^2\right)} \left[\prod_{\substack{k=1 \\ k\neq j}}^{N} \frac{1}{\left(t_j^1 - t_k^1\right)\left(t_j^1 - t_k^2\right)}\right] ds \tag{B.55}$$

where C_N and $t_j^{1,2}$ are as defined previously, and $\rho = J_0(2\pi BT)$ for the typical mobile channel. This expression may be evaluated numerically for an arbitrary number of eigenvalues and values of ρ.

Figure B.5 shows the asymptotic error floor for the case of two eigenvalues as a

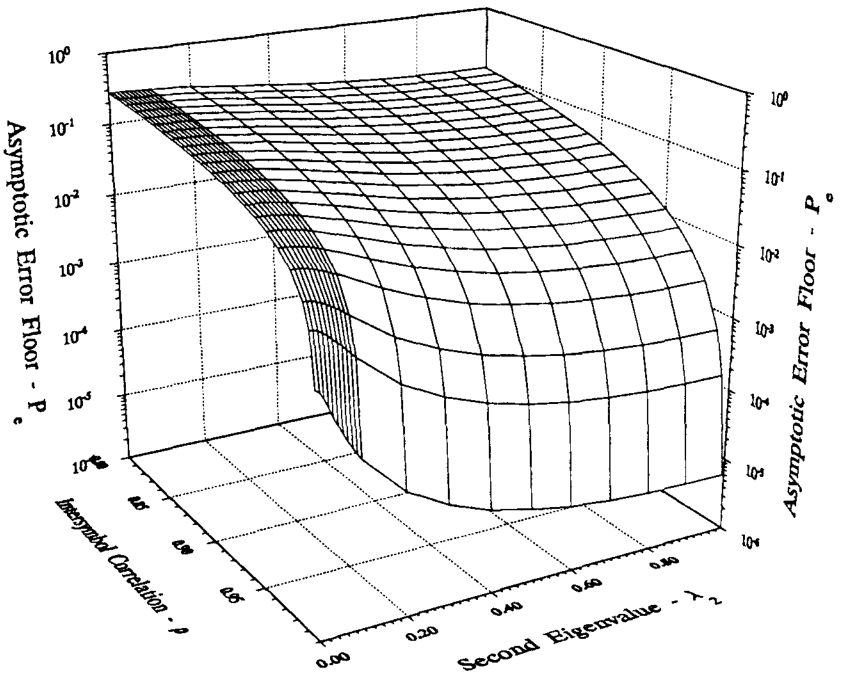

Figure B.5: Asymptotic error floor for a conventional receiver with two significant eigenvalues, as a function of the eigenvalue ratio and intersymbol correlation.

function of the symbol correlation factor, ρ, and the ratio of the two eigenvalues. Figure B.6 shows the same information, but with selected slices of the surface, parameterized by ρ, projected onto the same plane. Note that it is the *ratio* of the eigenvalues that will determine the asymptotic performance. Recalling that the error floor is independent of the signal energy, and that the sum of the eigenvalues equals the signal energy, then P_e is invariant to a constant scaling of the eigenvalues. For simplicity, we assume the normalizing constant λ_1, i.e. the first eigenvalue is set to 1, with the other eigenvalues normalized with respect to λ_1. The curves of Figure B.6 beyond $\lambda_2/\lambda 1 = 1$, are simply reflected about the abscissa of 1 and stretched in the x direction to infinity.

As seen in these figures, for a given eigenvalue ratio, the error floor drops away to zero as $\rho \to 1$. This corresponds to perfect correlation of the random variables multiplying each of the two symbols. That is, both symbol intervals are multiplyed by the same (albeit random) complex variable, which will lead to no errors in a differential scheme. Note that an eigenvalue ratio of 0, that is, λ_1 is some finite value and λ_2 is zero, corresponds to the single eigenvalue result given in (B.45).

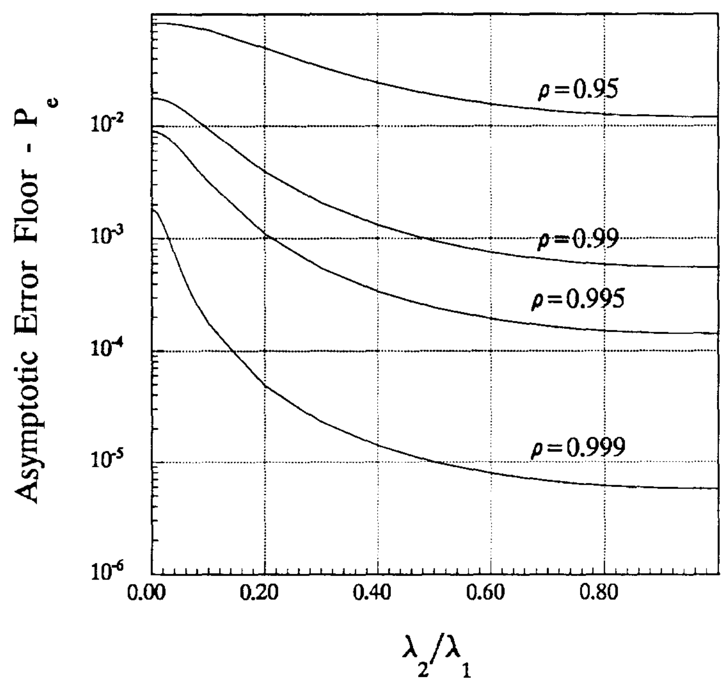

Figure B.6: Projected view of the asymptotic error floor for a conventional receiver with two significant eigenvalues, as a function of the eigenvalue ratio and intersymbol correlation.

It should also be noted that for a given ρ, which is dependent on the channel alone, the error floor of a conventional receiver may be varied by manipulating the spectrum of the eigenvalues. This is somewhat surprising, since virtually all analyses of receivers in fading channels make the assumption of a single significant eigenvalue, that is, fast fading. As was derived previously, the performance floor in this case is a function of the correlation parameter, ρ, alone. It is seen that the best performance that may be achieved for a given ρ occurs for equal eigenvalues, and can result in quite significant decreases in the error floor. For the mobile channel environment, the time bandwidth product, BT, is typically of the order 0.01—0.10, and from the correlation function given in (B.46), ρ has a typical range of approximately 0.999 — 0.905.

Figure B.7 is a continuation of the above to the case of three eigenvalues. Because of the extra parameter, the second and third normalized eigenvalues are used as coordinates for the error floor surface, and ρ is used to parameterize the different surfaces. Each surface will correspond to a particular channel's fading correlation. Setting one of the the eigenvalues to zero, and moving along the surface at an axis plane, is equivalent to the two eigenvalue

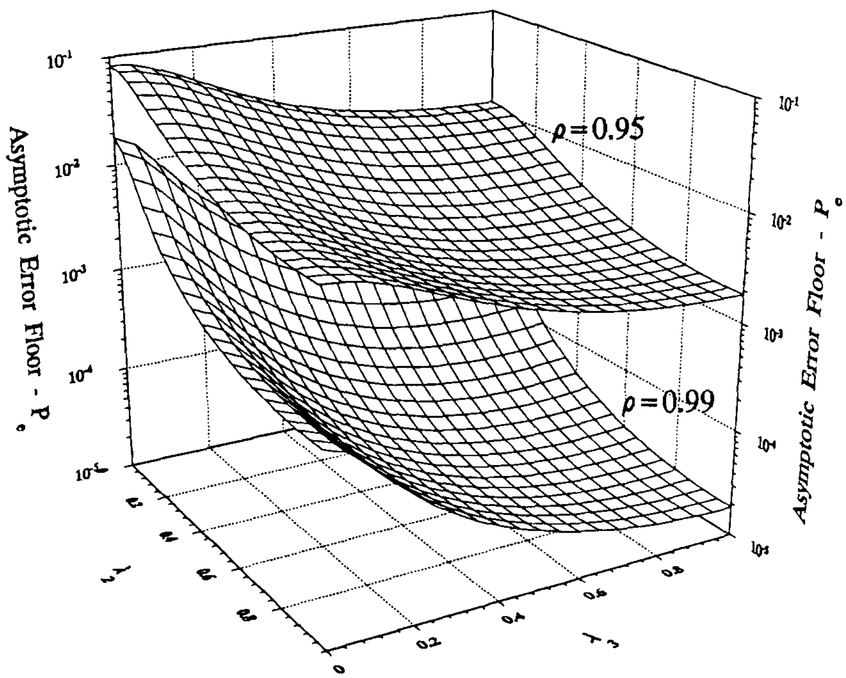

Figure B.7: Asymptotic error floor for a conventional receiver with three significant eigenvalues.

case shown in Figure B.6. The z-axis, parameterized by ρ, is simply the one eigenvalue, fast fading case. The surface corresponding to $\rho = 0.99$ is also shown in Figure B.8 with an expanded axis scale to give a greater perspective.

The general results here are similar to the two eigenvalue case, where the asymptotic error experienced by the receiver is again a function of *both* the channel's intersymbol correlation, and the eigenvalue spectrum of the received signal process. Again, the minimum asymptotic error occurs for the case of equal eigenvalues. The error floor, as a function of the number of eigenvalues considered, is seen to roughly follow a power law form, $P_e(N) \sim P_e(1)^N$. It is reasonable to expect similar results for higher order eigenvalue spectra.

It is seen that the asymptotic error floor is not such an absolute or irreducible quantity, and depending on the parameter values chosen, may vary over several orders of magnitude of P_e. Thus, a transmitter, with knowledge of the channel correlation function, $R(\tau)$, may select the appropriate pulse shapes to give virtually any desired eigenvalue spectra, and place the receiver operating point at a minimum asymptotic error rate. However, this scheme is impractical for two reasons,

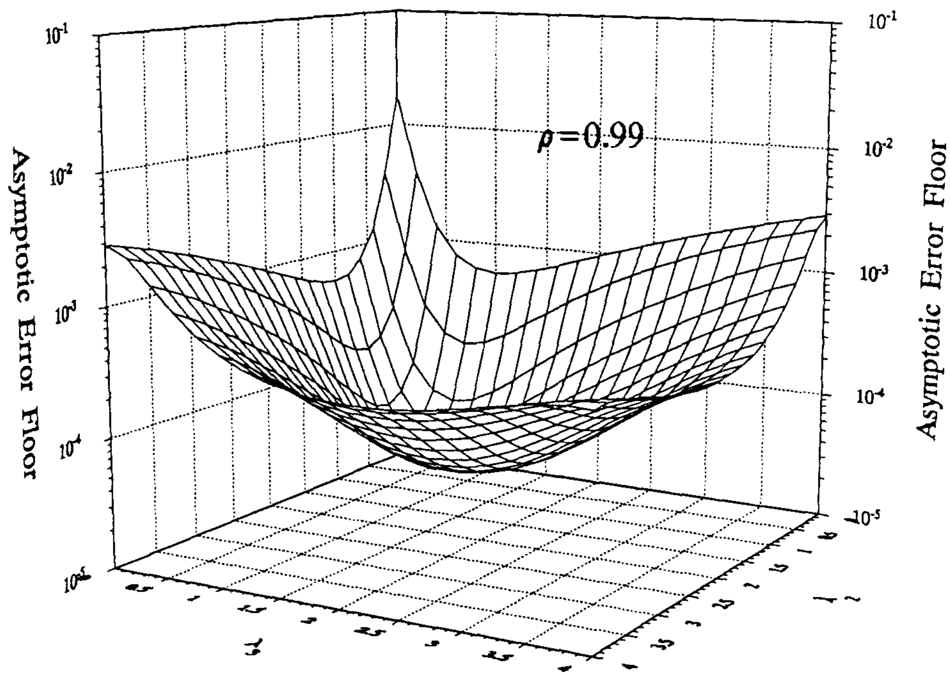

Figure B.8: Perspective view of the asymptotic error floor for a conventional receiver with three significant eigenvalues.

1. Any real channel has bandwidth restrictions, imposed by physical limitations and government regulation. As well, pulse shaping is generally used to help control intersymbol interference. This will limit the ability to arbitrarily vary the pulse shapes to control the error floor, although further concrete analysis would be necessary here.

2. Inherently, a transmitter has no way of estimating the correlation function of a channel. It would need to rely on some sort of channel probing signals, such as signals previously received at the transmitter site. This could severely limit performance if typical times between reception and transmission between sites are long enough to allow significant variation in the channel statistics.

The following section will examine a maximum likelihood receiver, whose the performance corresponds to the desirable equal eigenvalue operating point of a conventional receiver described previously. This performance will be seen to be independant of the actual eigenvalue spectrum of the the channel. Using fixed signal pulse shapes, performance is constrained only by the channel's ρ and the *number* of resolvable eigenvalues. The latter may still be determined in part by the chosen pulse shape.

B.2 Structure and Performance of an Optimal Receiver for DPSK Signals

In this section, it is assumed that the autocorrelation function of the fading process, $R(\tau)$, is known or has been estimated from the received signals. From this, the variables ρ, $\{\lambda_i\}$, and the additive white noise power spectral density, $\mathcal{N}_o$, have been calculated. The K-L coefficients, which are random complex Gaussian variables, are also assumed to have been extracted. The vector of coefficients, $\mathbf{z}$, is given by,

$$\mathbf{z} = [x_1, x_2, \dots, x_N, r_1, r_2, \dots, r_N]^T \tag{B.56}$$

From the Gaussian nature of the K - L coefficients, the pdf of $\mathbf{z}$ is given by [38],

$$p(\mathbf{z}) = \frac{1}{\pi^N |\mathbf{\Lambda}_m|} e^{-\mathbf{z}^H \mathbf{\Lambda}_m{}^{-1} \mathbf{z}} \tag{B.57}$$

where,

$$\mathbf{\Lambda}_m = \overline{\mathbf{z}\mathbf{z}^H} \tag{B.58}$$

is the correlation matrix of the K-L coefficients over two symbol periods, $\mathbf{x}$ and $\mathbf{r}$, assuming that symbol m was transmitted, i.e. a relative phase shift of θ_m between symbols. For the case of equal energy symbols, the determinant of $\mathbf{\Lambda}_m$ is independent of m, and the maximum likelihood symbol is that for which,

$$\ell_m = \mathbf{z}^H \mathbf{\Lambda}_m{}^{-1} \mathbf{z} \tag{B.59}$$

is a minimum. In this case we have the correlations,

$$\begin{aligned}
\left.\begin{array}{c} \overline{x_i x_j^*} \\ \overline{r_i r_j^*} \end{array}\right\} &= (\lambda_i + \mathcal{N}_o)\,\delta_{ij} \\
\overline{x_i r_j^*} &= \rho e^{i\theta_m} \lambda_i \delta_{ij} \\
&\equiv s_m \lambda_i \delta_{ij}
\end{aligned} \tag{B.60}$$

For the case of $N = 3$ eigenvalues, say, we have the correlation matrix,

$$\mathbf{\Lambda}_m = \begin{bmatrix} x_1 \\ x_2 \\ x_3 \\ r_1 \\ r_2 \\ r_3 \end{bmatrix} \begin{bmatrix} x_1 & x_2 & x_3 & r_1 & r_2 & r_3 \end{bmatrix}^* \tag{B.61}$$

$$= \begin{bmatrix} \lambda_1+\mathcal{N}_o & 0 & 0 & s_m\lambda_1 & 0 & 0 \\ 0 & \lambda_2+\mathcal{N}_o & 0 & 0 & s_m\lambda_2 & 0 \\ 0 & 0 & \lambda_3+\mathcal{N}_o & 0 & 0 & s_m\lambda_3 \\ s_m^*\lambda_1 & 0 & 0 & \lambda_1+\mathcal{N}_o & 0 & 0 \\ 0 & s_m^*\lambda_2 & 0 & 0 & \lambda_2+\mathcal{N}_o & 0 \\ 0 & 0 & s_m^*\lambda_3 & 0 & 0 & \lambda_3+\mathcal{N}_o \end{bmatrix} \tag{B.62}$$

Inverting the matrix and defining $\sigma_i \equiv \lambda_i + \mathcal{N}_o$, we find,

$$\mathbf{\Lambda}_m^{-1} = \begin{bmatrix} \frac{\sigma_1}{\sigma_1{}^2-\rho^2\lambda_1{}^2} & 0 & 0 & \frac{-s_m\lambda_1}{\sigma_1{}^2-\rho^2\lambda_1{}^2} & 0 & 0 \\ 0 & \frac{\sigma_2}{\sigma_2{}^2-\rho^2\lambda_2{}^2} & 0 & 0 & \frac{-s_m\lambda_2}{\sigma_2{}^2-\rho^2\lambda_2{}^2} & 0 \\ 0 & 0 & \frac{\sigma_3}{\sigma_3{}^2-\rho^2\lambda_3{}^2} & 0 & 0 & \frac{-s_m\lambda_3}{\sigma_3{}^2-\rho^2\lambda_3{}^2} \\ \frac{-s_m^*\lambda_1}{\sigma_1{}^2-\rho^2\lambda_1{}^2} & 0 & 0 & \frac{\sigma_1}{\sigma_1{}^2-\rho^2\lambda_1{}^2} & 0 & 0 \\ 0 & \frac{-s_m^*\lambda_2}{\sigma_2{}^2-\rho^2\lambda_2{}^2} & 0 & 0 & \frac{\sigma_2}{\sigma_2{}^2-\rho^2\lambda_2{}^2} & 0 \\ 0 & 0 & \frac{-s_m^*\lambda_3}{\sigma_3{}^2-\rho^2\lambda_3{}^2} & 0 & 0 & \frac{\sigma_3}{\sigma_3{}^2-\rho^2\lambda_3{}^2} \end{bmatrix} \tag{B.63}$$

Expanding the decision variable expression in (B.59), and making the obvious generalization to N eigenvalues, gives the likelihood function,

$$\ell_m = \sum_{i=1}^{N} \frac{(\lambda_i+\mathcal{N}_o)(|x_i|^2+|r_i|^2) - \lambda_i(s_m^* x_i r_i^* + s_m x_i^* r_i)}{(\lambda_i+\mathcal{N}_o)^2 - \rho^2\lambda_i{}^2} \tag{B.64}$$

Subtracting the first term in the numerator since it is independent of the symbol, m, being considered, gives,

$$\ell_m = \sum_{i=1}^{N} \frac{-\lambda_i(s_m^* x_i r_i^* + s_m x_i^* r_i)}{(\lambda_i+\mathcal{N}_o)^2 - \rho^2\lambda_i{}^2} \tag{B.65}$$

as the optimum receiver's decision variable. To evaluate the asymptotic error performance, one lets $\mathcal{N}_o \to 0$, which gives,

$$\ell_m = -\sum_{i=1}^{N} \frac{s_m^* x_i r_i^* + s_m x_i^* r_i}{\lambda_i} \tag{B.66}$$

$$= -2\sum_{i=1}^{N} \frac{\mathcal{R}\{s_m^* x_i r_i^*\}}{\lambda_i} \tag{B.67}$$

Using the definitions,

$$\frac{x_i}{\sqrt{\lambda_i}} \to \tilde{x}_i \tag{B.68}$$

$$\frac{r_i}{\sqrt{\lambda_i}} \to \tilde{r}_i, \tag{B.69}$$

the decision variable which we are trying to minimize may be written in the form,

$$\ell_m = -2 \sum_{i=1}^{N} e^{-i\theta_m} \tilde{x}_i \tilde{r}_i^* + e^{i\theta_m} \tilde{x}_i^* \tilde{r}_i \tag{B.70}$$

where the constant ρ have been dropped, and we have the correlations,

$$\begin{aligned} \left.\begin{array}{l} \overline{\tilde{x}_i \tilde{x}_j^*} \\ \overline{\tilde{r}_i \tilde{r}_j^*} \end{array}\right\} &= 1 \\ \overline{\tilde{x}_i \tilde{r}_j^*} &= \rho e^{i\theta_m} \delta_{ij} \\ &\equiv s_m \delta_{ij} \end{aligned} \tag{B.71}$$

For the conventional DPSK receiver analyzed in the previous section, a decision variable Z was calculated from the received signal vector and "binned" into one of the four complex quadrants. For general M - ary signalling, this is done by forming the dot product of Z with the M message signals arranged uniformly around the unit circle, forming M separate decision variables. The chosen message is that which maximizes the decision variable. When two dimensional vectors are expressed as complex numbers, we have the real scalar identity,

$$\vec{u} \cdot \vec{v} = (\vec{u} \cdot \vec{v})^* \tag{B.72}$$

$$= \tilde{u}\tilde{v}^* + \tilde{u}^* \tilde{v} \tag{B.73}$$

So, for the conventional receiver we have the decision variables,

$$\ell_m^{std} = \vec{e^{i\theta_m}} \cdot \vec{Z} \tag{B.74}$$

$$= e^{i\theta_m} Z^* + e^{-i\theta_m} Z \tag{B.75}$$

$$= \sum_{i=1}^{N} e^{i\theta_m} x_i^* r_i + e^{-i\theta_m} x_i r_i^* \tag{B.76}$$

where we have the correlations given in (B.16).

Comparing this expression for the conventional receiver with (B.70) it is seen that the decision variables for the optimal receiver have an identical form with those of the conventional receiver. Moreover, the statistics of the random independent variables $\tilde{x}_i$ and $\tilde{r}_i$ of the optimal receiver, given in (B.71), corresponds to those of the conventional receiver given in (B.16), when all of the eigenvalues equal one. That is, the asymptotic error of the optimal receiver, independent of the actual eigenvalue spectrum, will have the same performance as a conventional receiver when all the eigenvalues are equal. The optimal receiver is seen to perform something of a whitening of the eigenvalue spectrum.

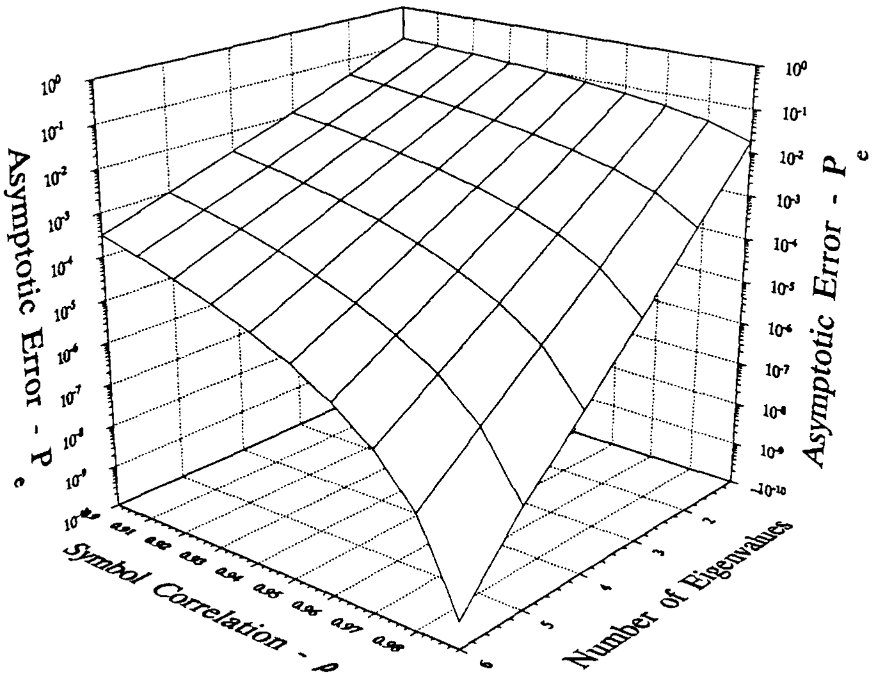

Figure B.9: Performance of the optimal receiver as a function of the number of channel eigenvalues and intersymbol correlation.

Equation (B.55) was numerically evaluated in the limit as all eigenvalues approach 1. The results are shown in Figure B.9 where the asymptotic error floor is given as a function of the number of eigenvalues, and the correlation parameter, ρ. It is seen that for a given channel correlation between symbols, the error floor decreases exponentially with the increasing number of eigenvalues. The magnitude of the exponent is also seen to increase as $\rho \to 1$, where the error floor disappears to zero as expected.

Bibliography

[1] J. M. Wozencraft and I. M. Jacobs, *Principles of Communication Engineering.* New York: John Wiley and Sons, 1965.

[2] H. L. Van Trees, *Detection, Estimation, and Modulation Theory, Part 1.* New York: John Wiley and Sons, 1968.

[3] R. S. Kennedy, *Fading Dispersive Communication Channels.* New York: John Wiley and Sons, 1969.

[4] W. C. Y. Lee, *Mobile Communications Engineering.* New York: McGraw-Hill, 1982.

[5] T. Hayes, "Beyond MSAT to personal communications via satellite," in *Wireless90 Workshop*, (Calgary, Alberta), Sponsered by the Alberta Telecommunications Research Center and the Telecommunications Research Institute of Ontario, 1990.

[6] A. G. Slekys, "Exploiting the digital radio wave of the 90's," in *Wireless90 Workshop*, (Calgary, Alberta), Sponsered by the Alberta Telecommunications Research Center and the Telecommunications Research Institute of Ontario, 1990.

[7] K. Brayer, "Introduction," in *Data Communications via Fading Channels* (K. Brayer, ed.), pp. 1–3, New York: IEEE Press, 1975.

[8] G. L. Grisdale, J. G. Morris, and D. S. Palmer, "Fading of long-distance radio signals and a comparison of space and polarization-diversity reception in the 6–18 Mc/s range," *Proceedings of the Institute of Electrical Engineers*, vol. 104B, pp. 39–51, January 1957.

[9] E. Arthurs and H. Dym, "On the optimum detection of digital signals in the presence of white Gaussian noise — a geometric interpretation and a study of three basic data

transmission systems," *IRE Transactions on Communication Systems*, pp. 386–372, December 1962.

[10] J. G. Proakis, *Digital Communications.* New York: McGraw-Hill, 1983.

[11] H. B. Voelcker, "Phase shift keying in fading channels," *Proceedings of the Institute of Electrical Engineers*, vol. 107B, pp. 31–38, January 1960.

[12] P. A. Bello and B. D. Nelin, "The influence of fading spectrum on the binary error probabilities of incoherent and differentially coherent matched filter receivers," *IRE Transactions on Communications Systems*, vol. CS-10, pp. 160–168, June 1962.

[13] W. C. Lindsey, "Error probabilities for rician fading multichannel reception of binary and N-ary signals," *IEEE Transactions on Information Theory*, vol. IT-10, pp. 339–350, October 1964.

[14] G. D. Hingorani, "Error rates for a class of binary receivers," *IEEE Transactions on Communications Technology*, vol. COM-15, pp. 209–215, April 1967.

[15] P. Bello, "Time-frequency duality," *IEEE Transactions on Information Theory*, vol. IT-10, pp. 18–33, January 1964.

[16] P. A. Bello and B. D. Nelin, "Optimization of subchannel data rate in FDM-SSB transmission over selectively fading media," *IEEE Transactions on Communications Systems*, vol. CS-12, pp. 46–53, March 1964.

[17] H. L. Van Trees, *Detection, Estimation, and Modulation Theory, Part 3.* New York: John Wiley and Sons, 1971.

[18] T. Kailath, "Correlation detection of signals perturbed by a random channel," *IRE Transactions on Information Theory*, vol. IT-6, pp. 361–366, June 1960.

[19] G. D. Hingorani and J. C. Hancock, "A transmitted reference system for communication in random or unknown channels," *IEEE Transactions on Communications Technology*, vol. COM-13, pp. 293–301, September 1965.

[20] C. K. Rushforth, "Transmitted-reference techniques for random or unknown channels," *IEEE Transactions on Information Theory*, vol. IT-9, pp. 39–42, January 1964.

[21] J. C. Hancock and P. A. Wintz, *Signal Detection Theory.* New York: McGraw-Hill Book Company, 1966.

[22] W. F. Walker, "The error performance of a class of binary communications systems in fading and noise," *IEEE Transactions on Communications Systems*, vol. CS-12, pp. 28–45, March 1964.

[23] C. W. Helstrom, *Statistical Theory of Signal Detection.* New York: Pergamon, 1960.

[24] J. H. Painter and S. C. Gupta, "Recursive ideal observer detection of known M-ary signals in multiplicative and additive Gaussian noise," *IEEE Transactions on Communications*, vol. COM-21, pp. 948–953, August 1973.

[25] J. H. Painter and L. R. Wilson, "Simulation results for the decision-directed map receiver for M-ary signals in multiplicative and additive Gaussian noise," *IEEE Transactions on Communications*, vol. COM-22, pp. 649–660, May 1974.

[26] L. Tziritas and G. Hakizimana, "Discrete realization for receivers detecting signals over random dispersive channels. Part I: Range-spread channel," *Signal Processing*, vol. 9, pp. 77–88, 1985.

[27] L. Andriot, L. Tziritas, and G. Jourdain, "Discrete realization for receivers detecting signals over random dispersive channels. Part II: Doppler-spread channel," *Signal Processing*, vol. 9, pp. 89–100, 1985.

[28] M. J. Barrett, "Error probability for optimal and suboptimal quadratic receivers in rapid Rayleigh fading channels," *IEEE Journal on Selected Areas in Communications*, vol. SAC-5, pp. 302–304, February 1987.

[29] J. H. Lodge and M. L. Moher, "Maximum likelihood sequence estimation of CPM signals transmitted over Rayleigh flat-fading channels," *IEEE Transactions on Communications*, vol. COM-38, pp. 787–794, June 1990.

[30] J. H. Lodge, "Maximum likelihood detection of CPM signals transmitted over Rayleigh flat-fading channels," in *Proceedings of the 14'th Biennial Symposium on Communications*, (Kingston, Ontario), pp. C.1.1–C.1.4, Queen's University, May 1988.

[31] S. L. Marple, *Digital Spectral Analysis with Applications.* Englewood Cliffs, New Jersey: Prentice Hall, Inc., 1987.

[32] A. Lee and P. J. McLane, "Convolutionally interleaved PSK and DPSK trellis codes for shadowed, fast fading mobile satellite communication channels," tech. rep., Queen's University, Kingston, Ontario, June 1988.

[33] W. D. Rummler, "A new selective fading model: Application to propogation data," *Bell Systems Technical Journal*, vol. 58, pp. 1037–1071, May/June 1979.

[34] P. Bello, "Characterization of randomly time-variant channels," *IEEE Transactions on Communications Systems*, vol. CS-11, pp. 360–393, December 1963.

[35] A. Saleh, A. J. Rustako, Jr., and R. S. Roman, "Distributed antennas for indoor radio communications," *IEEE Transactions on Communications*, vol. COM-35, pp. 1245–1251, December 1987.

[36] D. Middleton, *Introduction to Statistical Communications Theory.* New York: McGraw-Hill, 1960.

[37] S. Haykin, *Adaptive Filter Theory.* Englewood Cliffs, New Jersey: Prentice-Hall, 1986.

[38] K. S. Miller, *Complex Stochastic Processes.* New York: Addison-Wesley Publishing Company, 1974.

[39] R. A. Wooding, "The multivariate distribution of complex normal variables," *Biometrika*, vol. 43, pp. 212–215, 1956.

[40] F. R. Gantmacher, *The Theory of Matrices.* New York: Chelsea, 1977.

[41] J. P. Imhof, "Computing the distribution of quadratic forms in normal variables," *Biometrika*, vol. 48, no. 3 and 4, pp. 419–426, 1961.

[42] E. Snapper and R. J. Troyer, *Metric Affine Geometry.* New York: Dover Publications, Inc., 1971.

[43] P. Monsen, "Digital transmission performance on fading dispersive diversity channels," *IEEE Transactions on Communications*, vol. COM-21, pp. 33–39, January 1973.

[44] A. B. Baggeroer, *State Variables and Communications Theory.* Cambridge: MIT Press, 1970.

[45] S. T. Alexander, *Adaptive Signal Processing, Theory and Applications.* New York: Springer-Verlag, 1986.

[46] M. G. Bellanger, *Adaptive Digital Filters and Signal Analysis.* New York: Marcel Dekker, Inc., 1987.

[47] J. M. Cioffi, "Limited-precision effects in adaptive filtering," *IEEE Transactions on Circuits and Systems*, vol. CAS-34, pp. 821–833, July 1987.

[48] I. K. Proudler, J. G. McWhirter, and T. J. Shepard, "QRD-based lattice filter algorithms," in *Advanced Algorithms and Architectures for Signal Processing IV*, (San Diego, California), SPIE, 1989.

[49] S. Haykin, *Communication Systems.* New York: John Wiley and Sons, 2nd ed., 1983.

[50] G. A. Ybarra and S. T. Alexander, "Effects of ill-conditioned data on least squares adaptive filters," in *Proceedings of the IEEE International Conference on Acoustics, Speech, and Signal Processing*, (New York, NY), pp. 1387–1390, IEEE, 1988.

[51] C. Atkinson and A. F. S. Mitchell, "Rao's distance measure," *Sankhyā: The Indian Journal of Statistics*, vol. 43A, no. 3, pp. 345–365, 1981.

[52] S.-I. Amari, O. E. Barndorff-Nielsen, R. E. Kass, S. L. Lauritzen, and C. R. Rao, *Differential Geometry in Statistical Inference*, vol. 10 of *Lecture Notes — Monograph Series.* Hayward, California: Institute of Mathematical Statistics, 1987.

[53] G. Ungerboeck, "Channel coding with multilevel/phase signals," *IEEE Transactions on Information Theory*, vol. IT-28, pp. 55–67, January 1982.

[54] J. B. Thomas, *An Introduction to Communications Theory and Systems.* New York: Springer-Verlag, 1988.

[55] A. J. Jerri, *Introduction to Integral Equations with Applications.* New York: Dekker, 1985.

[56] R. G. Gallager, *Information Theory and Reliable Communications.* New York: Wiley, 1968.

[57] D. Divsalar and M. K. Simon, "Performance of trellis coded MDPSK on fast fading channels," in *Proceedings of the IEEE International Conference on Communications*, (Boston, MA), pp. 9.1.1–9.1.7, IEEE, 1989.